Modelling Distribution Network through Tensor Representation in the Presence of Power Electronic Devices

Muhammad Ramzan

A thesis presented for the degree of
Doctor of Philosophy
in
Electrical and Computer Engineering
at the
University of Canterbury,
Christchurch, New Zealand.

26 August 2021

ABSTRACT

The development in electronics technology in the last decade has greatly increased the use of power electronic-based non-linear loads. This power electronic equipment consists of power electronic loads, Renewable Energy Sources (RES) (wind, solar PV etc.) and new technologies such as heat-pumps, Electric Vehicles (EVs) and LED lightings. Their greatest harmonic impact is expected on Low-Voltage (LV) distribution networks. For this reason, it is essential to develop a robust analytical tool for the analysis of the performance of LV networks in the presence of non-linear power electronic equipment.

In this thesis, a modelling framework is developed to enable a more accurate representation of the distribution system. The tensor, commonly used in physics to characterize the invariant relationship of vectors in the coordinate axis, is a way to achieve this phase-dependency representation accurately. PSCAD/EMTDC is a time-domain analysis tool, which inherently models this phase-dependency; however, it is incapable of modelling a complete distribution system. For this reason, it is used as a benchmark for MATLAB program development in the frequency-domain. Frequency-domain approach using tensor analysis has the ability to model very large electrical networks accurately.

This work proposed and implemented two optimisation methods: Fourier Descriptors (FDs) and Average Admittance Locus (AAL) for the approximation of tensors. The region of linearity of non-linear devices around the operating point of the device is determined. Laboratory experiment was carried out for the validation of tensors.

A test feeder is modelled to compare the accuracy of tensor analysis against the harmonic Current Injection (CI) method and also through time-domain PSCAD/EMTDC simulations. This validation leads to the implementation of tensor analysis on different LV distribution systems, city and urban network. Different loading scenarios are investigated due to the inherent fluctuating nature of residential and commercial loads. The results of tensor analysis are compared against the CI approach. The results show the greater accuracy of tensor analysis over the fixed CI method particularly as the voltage distortion increases. The harmonic CI method does not consider the harmonic

interaction between non-linear devices and the a.c. system nor the interaction between multiple non-linear devices. Therefore, frequency-domain tensor analysis is expected to replace the CI method and time-domain methods for accurate harmonic studies of large electrical networks.

CONTENTS

LIST OF FIGURES

LIST OF TABLES

ACKNOWLEDGEMENT

I would like to express my sincere gratitude to my supervisor, Prof. Neville Watson for his continuous source of support, positive criticism and guidance throughout my PhD research. His intellectual and emotional contribution helped me all the time for fulfilling my research dreams. It was an honour for me to be his student and to work under his supervision. I'm also thankful to my co-supervisor Dr. Andrew Lapthan for his contribution and recommendations. Also sincere regards to staff of Computer and Electrical Engineering department. I would like to thank UC for providing me UC Doctoral Scholarship. I would also like to thank to Bruce C. Smith, no longer with us, but his research helped me a lot to achieve this goal.

I'm thankful to my parents, Safia and Muhammad Arshid, brothers and sisters for motivating and supporting me throughout this journey. Special thanks to my lovely wife, Azem for her continuous support and understanding while being busy in research. My heartiest gratitude to Soesi for being with us, especially with Azem, and made her stay in New Zealand so homely.

Assistance and advices provided by Prof. Sajid Iqbal from Pakistan was greatly appreciated. My acknowledgement to Usama Farooq for encouraging and motivating me throughout the PhD research. Thanks to Ali Othman for having great discussions and contribution till the end. Also, would like to extend my gratitude to all my friends and colleagues.

I dedicate this thesis to my family, and my late mother, Safia Bibi.

GLOSSARY

Abbreviations

RES	Renewable Energy Sources
EVs	Electric Vehicles
PV	Photovoltaic Arrays
LV	Low-Voltage
FD	Fourier Descriptor
AAL	Average Admittance Locus
CI	Current-Injection
DG	Distribution Generation
HVDC	High-Voltage Direct-Current
CSC	Current Source Converter
VSC	Voltage Source Converter
ATP	Alternative Transient Program
PSCAD	Power System Computer Aided Design
EMTP	Electromagnetic Transient Program
NIS	Numerical Integrator Substitution
ODEs	Ordinary Differential Equations
NR	Newton-Raphson
BF	Backward-Forward Sweep
THD	Total Harmonics Distortion
IHA	Iterative Harmonic Analysis
STATCOMS	Static Synchronous Compensator
SSSC	Static Synchronous Series Compensator
FCM	Frequency Coupling Matrix
DFT	Discrete Fourier Transform
GXP	Grid Exit Point
VSDs	Variable Speed Drives
LED	Light Emitting Diode

CFL	Compact Fluorescent Lamp
PC	Personal Computer
TV	Television
CRT	Cathode-ray Tube
ICP	Installation Control Point
HPF	Harmonic Power-Flow
DHD	Dynamic Harmonic Domain
CYMM	Couple Y Matrix Method

Symbols

Y	Admittance
I	Current
I_m	m^{th} order harmonic current
$I_{(m,pert)}$	m^{th} order harmonic current perturbation
I_{base}	Harmonic currents at the base case
ΔI_m	m^{th} order harmonic current variation
V	Voltage
V_n	n^{th} order harmonic voltage
$V_{(n,pert)}$	n^{th} order harmonic voltagte perturbation
V_{base}	Harmonic voltages at the base case
ΔV_n	n^{th} order harmonic voltage variation
$Y_{m,n}$	Coupling between ΔV_n and ΔI_m
$*$	Complex conjugate of
$\sum$	Summation operator
Y_T	Admittance tensor
$Y_{fd}[k]$	Fourier descriptor
$y(n_p)$	Admittances measures at ${n_p}^{th}$ voltage phase angle

Chapter 1

INTRODUCTION

1.1 RATIONAL

The widespread use of power electronic equipment is changing the nature of our electrical network [Watson et al. 2009a],[Sharifian et al. 2005],[Rawa et al. 2011]. Distributed Generation (DG) using Renewable Energy Resources (RES) is growing rapidly [Lins et al. 2014],[Ahmed et al. 2008] and these invariably use a power electronic interface. The nature of loads are also changing with many new non-linear, power electronic-based, residential, commercial, industrial and rural loads being deployed. Examples are LED lighting, heat-pumps (air-conditioners), Electric Vehicles (EVs) to name but a few. Moreover, there is an increasing use of power electronics in the transmission and distribution systems to overcome technical issues. For example, HVDC transmission, STATCOMs, SVCs and solid-state voltage regulators. All these power electronic devices generate harmonics and also respond to the harmonics from other devices.

There is an increasing need to be able to analyse the harmonic levels in a modern electrical power system due to the many non-linear devices (at load, generation and transmission/distribution levels) in order to ensure the levels are maintained within acceptable levels. At present the industry's standard analysis method is the direct Current Injection (CI) method, however, this assumes a fixed harmonic CI as shown in Figure 1.1a. This does not model the interaction between the non-linear devices and the a.c. system through the terminal distortion nor the interaction of multiple non-linear devices in a system. However, with different magnitudes and phase-angles of the supply voltage, the non-linear load's harmonic current injection will vary. This leads to the need to calculate the harmonic interaction with the a.c. network as shown in Figure 1.1b.

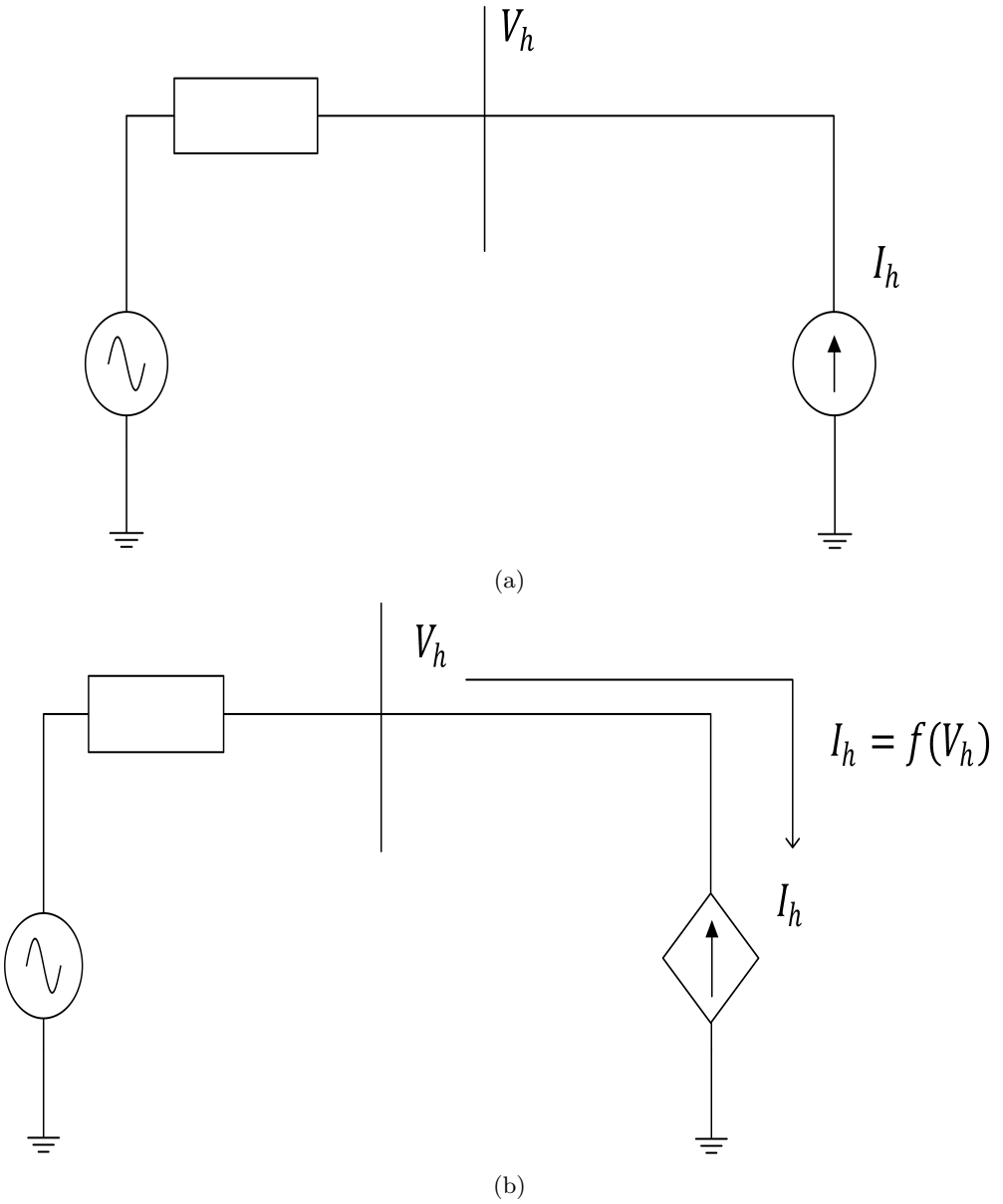

Figure 1.1 Harmonic Current Models (a) Fixed Harmonic Current (b) Harmonic Current Injection

It has been shown that the response of a power electronic converter is phase-dependent and can be modelled by a Norton circuit where the impedance is a tensor to model the phase-dependency [Smith 1996],[Smith et al. 1998b],[Hume et al. 1998],[Smith et al. 1998a],[Bathurst 1999],[Collins 2006],[Wei 2009],[Wei et al. 2008],[Frater 2015],[Gallo et al. 2017],[Gallo et al. 2018],[Langella et al. 2018]. Phase-dependency means that the apparent incremental impedance to a harmonic is a function of the harmonic voltage distortion.

The aim of the present work is to develop a modelling framework to enable

a more accurate representation of distribution systems containing power electronic devices. Previously, the tensor representation of High-Voltage Direct Current (HVDC) converters has been proposed in [Smith 1996]. Bruce Smith has proposed a 2^{nd} order tensor representation for nodal analysis of a network to incorporate phase-dependant admittances. The Line Commutated Converter (LCC) HVDC schemes are current stiff (as they use a Current Source Converter (CSC)) and this lends itself to tensor representation. The thrust of this work is to investigate using tensor analysis for modelling distribution networks. The question is how well tensor analysis can model such systems, particularly with the different types of typical loads. A 2×2 tensor matrix that represents the system is shown in Figure 1.2.

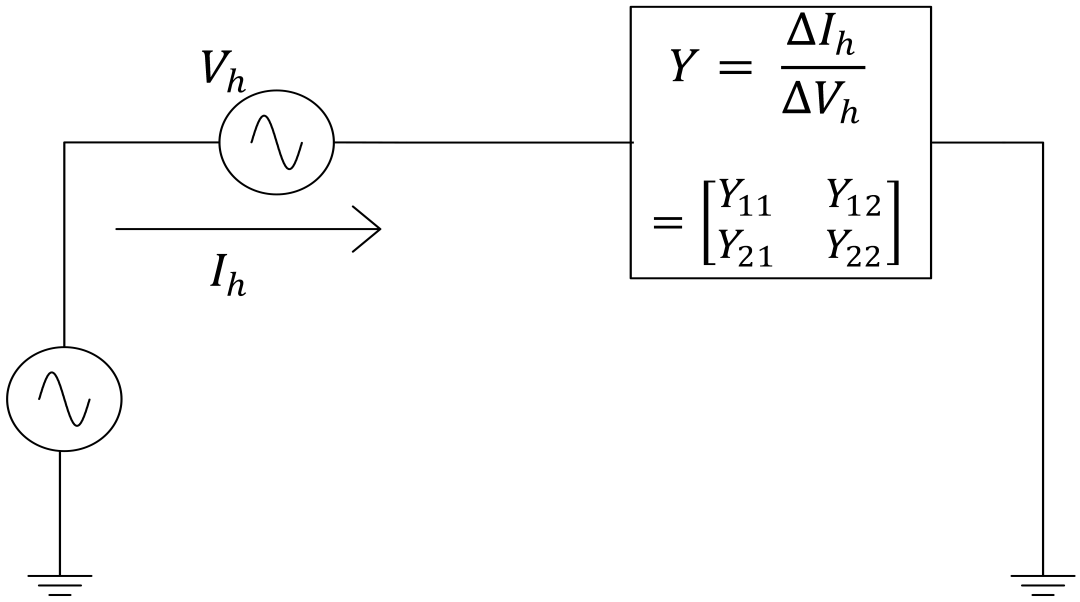

Figure 1.2 Tensor Representations of the System

A simple test feeder, shown in Figure 1.3, is a typical distribution network connected with different Installation Control Points (ICPs). The tensor representation of such networks considers the harmonic interaction with the AC electrical network. In this research, harmonic characterisation of non-linear devices is achieved using time-domain PSCAD/EMTDC tool. Time-domain is a powerful tool, as it inherently models the harmonic interactions. However, it is unable to represent large distribution networks; therefore, it is only used as the benchmark for the tensor analysis using MATLAB. Frequency-domain tensor analysis is used for the modelling of distribution networks. Tensor analysis has the ability to model large distribution networks using MATLAB.

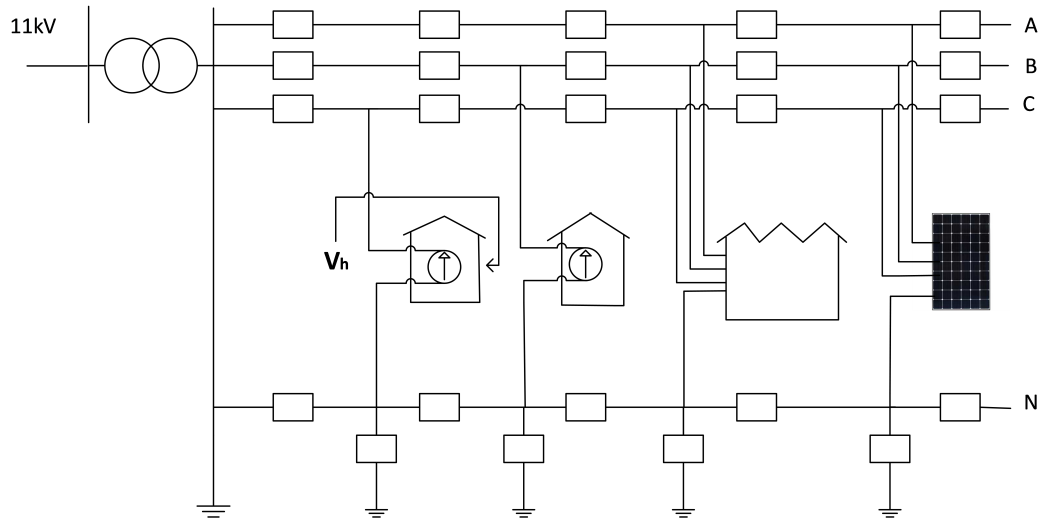

Figure 1.3 Electrical Power System Configration

In addition, non-linear devices are linearised around the operating point by perturbation analysis. It is evident from experimental results that CSCs have a larger linear region around their operating point than Voltage Source Converters (VSCs). Fourier Descriptors (FDs) and Averaging Admittance Locus (AAL) methods are used for determining the tensors from the loci obtained from the experiment. Moreover, these methods are not only used to find the tensors but also linearity region in the frequency-domain. These optimisation methods are used to determine whether the device is in its linear region and the limits to the tensor's validity.

1.2 MOTIVATION

The aim and objective of this work are to develop a comprehensive modelling framework, based on tensors, for a distribution network in the presence of power electronic devices.

In a distribution system, the non-linear behaviour of power electronic devices injects harmonic current into the network. In reality, this harmonic injection is a function of voltage at the device's terminals and the purpose of a tensor representation is to obtain a more accurate representation of this behaviour. Traditional frequency-domain analysis solves a set of equations, which does not give the harmonics' interaction between the power electronic loads and a.c. source or between multiple power electronic loads. However, the proposed tensor representation builds incremental admittance matrices of non-linear devices, which will model the harmonics interactions between the power electronic load and a.c. source or between multiple power electronic loads accurately.

1.3 THESIS CONTRIBUTION

This thesis contributions are as follow:

1. Investigated the phase-dependency of typical non-linear devices using perturbation analysis.
2. Investigated the linearity region in the frequency-domain of different non-linear devices.
3. Built a laboratory experiment for the validation of tensors.
4. Developed a library of tensors of household appliances, i.e. washing machine, fluorescent lamp, refrigerator, heat-pump, etc.
5. This work has shown the ability to combine the tensors for each non-linear appliance to form a overall tensor that represents the whole house without compromise in accuracy.
6. Obtained a tensor representation of a test feeder to compare and validate results against CI and PSCAD/EMTDC.
7. Showed how tensor analysis can be used to model typical distribution systems, as seen by applying to two New Zealand distribution systems i.e. city and urban systems.

1.4 THESIS OUTLINE

A roadmap for solving the problem:

Chapter 2: The basis of harmonic modelling of non-linear devices is presented in this chapter. The step-by-step building of tensors is carried out. Different optimisation techniques are presented and compared for the approximation of tensors and determine the region of linearity of devices around its operating point.

Chapter 3: A laboratory experiment is carried out for the validation of tensors. AAL and FDs methods are applied to the generated data obtained from the laboratory experiment and PSCAD/EMTDC. Tensors addition of different non-linear devices is proposed and evaluated to obtain resultant tensor matrix for all appliances in a house. In addition, a large number of simulations for different values of capacitors, and loads are performed to define the region of linearity.

Chapter 4: The first part of this chapter is the overview of non-linear devices such as lighting equipment, refrigerator, TV, oven, heat-pump, etc., using PSCAD/EMTDC. The second part introduces the harmonic representation of a distribution feeder using

both time-domain and frequency-domain simulations. For the first time, tensors of non-linear devices are combined to form a resultant tensor that represents the whole house without compromising accuracy. Tensor representation of the test feeder is obtained and compared with, and validated against, the CI and time-domain simulations.

Chapter 5: In this chapter, a modelling framework using tensors is developed to represent different distribution networks accurately. Due to residential and commercial devices' consumption fluctuation nature throughout the day, different loading scenarios and demand patterns are investigated. These investigations lead to a prediction of the potential impact of different load types on the LV feeders and, consequently, a proper network design of the networks.

Chapter 6: This chapter summarises the research described by this thesis. The future extension of this research is also discussed.

Chapter 2

BACKGROUND

2.1 CHAPTER OVERVIEW

Power system modelling is important for the planning and operation of electrical power systems. With the installation of more power electronic devices in the power network, there is a need to accurately model an electrical power system to ensure satisfactory performance.

In this chapter, an accurate tensor representation of an electrical distribution system is presented using both the time and frequency-domains. A single non-linear load is modelled to understand its characteristic in the presence of pre-existing distortion and to develop a tensor representation. The system is tested for different levels of harmonic distortion limits and the corresponding tensors are calculated for the approximation of admittance loci. FD and an AAL are presented for the approximation of tensors and to determine the linear region of the device around its operating point in the frequency-domain. Results from these two optimisation techniques showed robustness when compared with actual admittance and tensor obtained before applying optimisation techniques.

2.2 CHANGING DISTRIBUTION SYSTEM LOADS

The desire to transition to a low carbon electrical system which is more efficient and more controllable is causing the widespread deployment of power electronic based equipment, including in the Low Voltage (LV) level at customer premises. The essential voltage and current rating of different power electronic devices for different areas are well explained in [Tolbert et al. 2005]. The power electronic interfaced DG units and power electronic loads contribute to the harmonic distortion and there is a need to consider this when performing planning studies for a distribution system.

2.3 MODELLING OF AN ELECTRICAL POWER SYSTEM

Due to the many adverse effects of harmonic distortion [Arrillaga et al. 1997],[Acha and Madrigal 2001],[Arrillaga and Watson 2004] it is important to have adequate modelling tools to enable planning studies to be performed, as well as for investigating operational problems when they occur. Modelling tools can be classified as time-domain, frequency-domain or a hybrid of the two. Each has its advantages and disadvantages.

2.3.1 Time-Domain Modelling

Time-domain simulation is a mature method for analysing the power system transients. Time-domain models are based on the differential equations representing the power system components and are solved using numerical integration algorithms [Das 2002]. The time-domain approach includes Alternative Transient Program (ATP), PSCAD/EMTDC [Woodford et al. 1983], and Electromagnetic Transient Program (EMTP) [Dommel 1969] which all use the Numerical Integrator Substitution (NIS) method (also known as Dommel's method due to his classic paper and program that popularised it). These programs are used extensively for power system analysis. However, due to the computational effort and the need to run long enough to obtain an accurate steady-state, time-domain techniques are limited in the size of the system that can be modelled. The limitations of time-domain simulation can be seen while considering a wide range of power-quality issues that need frequency dependant equivalents for much of the system.

The NIS approach uses a numerical integrator to convert all the Ordinary Differential Equations (ODEs) representing each component into difference equations. The system equation is formed by using nodal equations to obtain a conductance matrix. The elements of the conductance matrix are functions of the time-step used [Watson et al. 2018],[Dommel 1986]. This results in a direct solution technique for each time-point rather than iterative. The computational decoupling of parts of the system separated by transmission lines or cables can also be used to increase computational efficiency [Semlyen and Iravani 1993]. The direct time-domain simulation also represents switches and non-linear elements in a very straightforward way. In this project PSCAD/EMTDC has been used to model a distribution network.

2.3.1.1 Electromagnetic Transient Analysis

The analysis of EMT is becoming a primary tool for understanding the performance of an electrical power system for finding component ratings, explaining equipment failures

or testing protection devices. EMT models are the most detailed type of power system models. For the planning and operation of the electrical system, EMT programs (such as EMTP and EMTDC) which are based on Numerical Integration Substitution (NIS) (Dommel's algorithm) are used to simulate transient disturbances of the system. This method superseded the more computational expensive state variable analysis technique [Watson 2010]. Applications of effective computational techniques to solve the EMT problems are well described in [Watson et al. 2018].

In order to obtain the voltage and current harmonics the steady-state must be obtained. The brute-force approach of running until the initialisation transient has finished may require a significant number of cycles to be simulated. This is especially true if there are some long time-constants in the circuit. The Fast Periodic Solution was designed to overcome the initialisation transient and reach the steady-state. It uses a Newton iterations-based method to iteratively refine the initial conditions to remove the transient [Aprille and Trick 1972]. In [Semlyen and Medina 1995], the convergence is improved in a time-domain based Newton methods. Fast periodic solution is difficult to use with converters and is difficult to setup.

2.3.2 Frequency-Domain Modelling

In frequency-domain modelling, ODEs are transformed to complex algebraic equations characterized by the complex phasor (in the rectangular or polar form) and it is easier to incorporate the behaviour of components. Frequency-domain is basically a linear methodology and the superposition principle is used which enables each harmonic frequency to be considered separately [Densem 1983].

Many frequency-domain models are already presented in the literature, which are divided into the CI method, linearised methods and iterative non-linear formulations. The time-variant converters, in the absence of commutation variation, possess linear harmonic transfer features [Smith 1996]. The benefits of both approaches are apparent, the linearised approaches taking benefit of the fixed operating point method to produce fast solutions while iterative non-linear approaches compromise solution speed to completely model minor operating point deviations and the related non-linearity.

Frequency-domain modelling is accurate for many power system applications and certainly it is much more efficient when compared with time-domain approaches. The frequency-domain is capable of accommodating frequency dependent components easily in the system admittance matrices. A range of frequency-domain correspondent already exists for normal system components. However, unlike time-domain techniques, the frequency-domain techniques do not possess modular control blocks.

2.3.2.1 Power-Flow

As an introduction to frequency-domain modelling the first task undertaken was investigating fundamental frequency power-flow analysis. A three-phase 3-wires and three-phase 4-wires system load-flow analysis were modelled using Newton-Raphson (NR), Backward-Forward (BF) Sweep and CI methods. The impact of grid-connected RES on power systems is analysed. A traditional three-phase power-flow approach generally considers a 3-wire configuration which assumes the system is balanced. However, a distribution system is three-phase 4-wire system as it must service single-phase loads. Hence, the distribution system may have a considerable levels of unbalance. A number of research has been presented on power-flow analysis using NR [Arrillaga and Callaghan 1989],[Nguyen 1997],[Zimmer et al. 2013], BF Sweep [Chang et al. 2007],[Samal and Ganguly 2015] and CI [Watson et al. 2016] methods.

Simulation results show that the CI method is robust in terms of computation time, and accuracy. In addition, it is able to explicitly include the neutral wire to precisely analyse impact of unbalance caused by RES and EVs on the distribution network.

2.3.2.2 Harmonic Analysis

Computationally, harmonic analysis in the frequency-domain has a number of advantages over time-domain simulation due to the ability to model large systems and computational efficiency. The harmonic domain is a subset of the frequency-domain modelling approach and various such harmonic models have been proposed and developed in accordance with the intended application [Arrillaga et al. 1995],[Smith et al. 1996],[Arrillaga et al. 1997],[Smith et al. 1997],[Fauri 1997],[Bathurst et al. 1998],[Smith and Arrillaga 1999],[BaSudan and Hegazy 2001],[Arrillaga and Watson 2004],[Medina et al. 2013]. Some of the frequency-domain harmonic analysis methods developed are:

- Direct method [Densem et al. 1984],[Hume 2002],[Larsen et al. 1989],[Wood 1993]
- Fixed-point techniques [Smith et al. 1998a],[Reeve and Baron 1971]
- Harmonic Domain [Smith 1996]
- Harmonic Power-Flow (HPF) methods [Bathurst et al. 1999]
- Dynamic Harmonic Domain (DHD) method [Arrillaga et al. 2004]
- Couple Y Matrix Method (CYMM) [Sun et al. 2007]

As mentioned previously, one of the main limitations of the frequency-domain approach has been the use of fixed current injection by the non-linear components. The first method to overcome this was the use of fixed-point iterative techniques (Iterative harmonic analysis and multiphase harmonic load-flow). Although Iterative harmonic analysis [Carbone et al. 1993],[Arrillaga and Callaghan 1989],[Arrillaga and Watson 2004] and multiphase harmonic load-flow [Dommel 1969],[Xu et al. 1991],[Watson et al. 2009b] are different algorithms they both use a fixed current injection for the AC system solution and a non-linear model which re-evaluated the current injection (based on terminal conditions) each iteration. Cross-coupling terms are not adequately represented and convergence is not robust. Many techniques were developed to improve convergence. A full linearisation of the non-linear device will more accurately model it while improving the convergence properties and this leads to the use of Norton equivalents and tensors.

2.4 TOTAL HARMONICS DISTORTION (THD)

Non-linear loads generate harmonic currents which result in harmonic voltage distortion throughout the power system. Extensive use of non-linear loads is becoming an important harmonic source. The quality of these non-linear devices has a significant influence on the V_{THD} throughout the power system.

THD is a measurement of the distorted harmonic in a signal. THD of current harmonics can be defined as follows:

$$THD_I = \frac{\sqrt{\sum_{h=2}^{\infty} I_h^2}}{I_1} \tag{2.1}$$

For voltage harmonics THD equation will be:

$$THD_u = \frac{\sqrt{\sum_{h=2}^{\infty} u_h^2}}{U_1} \tag{2.2}$$

Where I_h and u_h are the magnitude of the n^{th} harmonic.

2.5 TENSOR REPRESENTATION OF DISTRIBUTION SYSTEM

A Norton equivalent can alleviate the limitations of the frequency-domain approach, however, power electronic equipment is phase-dependent in its harmonic response. There are two possible ways to represent this phase-dependance. Using a positive and negative frequency coupled matrix or tensor representation using positive frequencies

only. The latter approach has been adopted for this work. Tensors have been used for HVDC converters, however, the present work is extending this to modelling distribution systems with a large number of non-linear devices. This means tensors of devices need to be combined to an overall tensor and the limits of the representation need to be determined and compared to realistic harmonic levels. The development of a tensor, as will be explained, involves linearisation around an operating point. It can be viewed as a Norton equivalent where the parallel admittance is a 2×2 tensor.

A harmonic domain model for solving harmonics in an AC system with an HVDC converter was first proposed by Smith [Hume et al. 1998, Smith et al. 1998a, b, Smith 1996]. Smith developed the tensor framework and demonstrated its use for modelling HVDC converters in rectification mode, considering the significant phase-dependence and frequency cross-coupling effects. Another noteworthy accomplishment was the analytic derivation of the harmonic Jacobian matrix. Later, Bathurst extended Smith's harmonic domain model to full HVDC link [Bathurst et al. 1999] for a fuller set of HVDC link configurations.

A number of harmonic domain models are presented by Collins in [Collins 2006] to calculate the steady-state performance of FACTS devices including a Static Synchronous Compensator (STATCOMs) and a Static Synchronous Series Compensator (SSSC). Collins adopted the tensor linearisation using positive frequency real-values decompositions and represented the phase dependency of the power electronics devices using tensor admittance. In this work, for the first time tensors were used for the voltage source converters. Frater has developed the Frequency Coupling Matrix (FCM) approach for the modelling of non-linear devices [Frater 2015]. A tensor representation is used to model the phase-dependent behaviour of CFLs, and a linear flourescent tube, where FDs is used for the approximation of tensor. In recent research Langella has also used Tensor representation and FD for the assessment of FCMs of Power Electronic Devices [Gallo et al. 2017],[Gallo et al. 2018],[Langella et al. 2018].

Wei has modelled the phase-dependency of CFL's to provide a better harmonic analysis [Wei 2009]. The CFLs linearisation for different percentage of voltage distortions was implemented and the admittance tensor was built. Two optimisation methods were used, namely AAL and averaging tensor to obtain tensor. AAL technique is considered in this research to get an accurate tensor representation of the distribution system.

2.6 BUILDING THE TENSOR STEP-BY-STEP

In order to represent a complete distribution system by tensors, a linearisation of the power electronic devices is achieved which is able to explain the phase-dependency

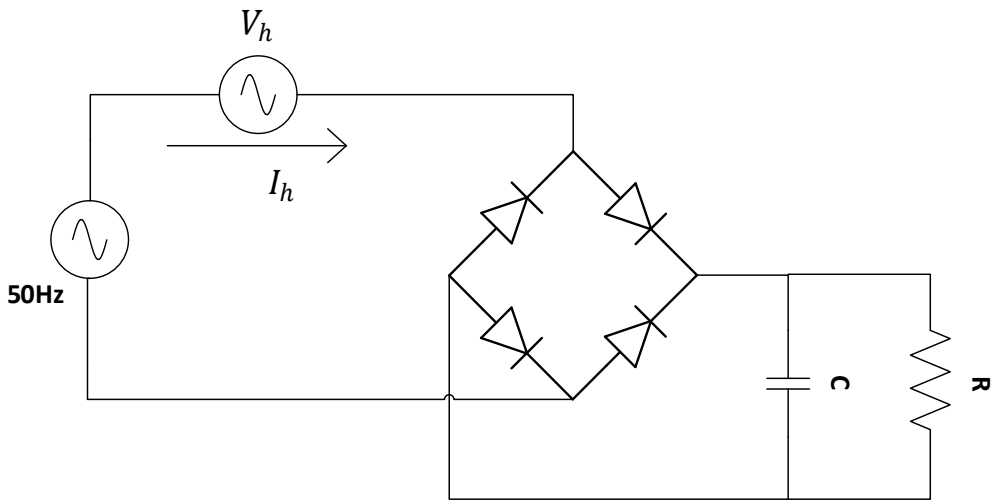

Figure 2.1 Non-linear Load PSCAD/EMTDC Model

for different harmonics. A single non-linear load is modelled in PSCAD/EMTDC to gain an understanding of how to build a resultant tensor matrix for different harmonic frequencies. The time-domain program PSCAD/EMTDC is a powerful tool but not able to model a large distribution system explicitly. Therefore, PSCAD/EMTDC simulations are only used as a benchmark to help generate tensors.

2.6.1 Perturbation Analysis

The linearisation of non-linear devices is obtained through perturbation analysis. The magnitude and phase-dependency relationship of a power electronic device is determined by injecting a small voltage distortion at the input terminal and the current response is observed. The response to the voltage distortion is phase-dependant. Any distortion at specific frequency produces current harmonics at different frequencies.

Figure 2.1 shows a simple system that is modelled in PSCAD/EMTDC. The FFT block in PSCAD/EMTDC is used to measure the harmonic voltages and currents in the system as a function of time. In order to determine the phase-dependency at a frequency, a voltage distortion is injected at different angles (0°, 10°, 20°,. . . , 360°) and the harmonic current response is observed. Four harmonic distortion levels are considered 25%, 50%, 75% and 100% of the AS/NZS61000.2.2:2003 limits [61000.2.2 2003]. For example, 100% of the distortion limit is 5% voltage distortion for the 3^{rd} harmonic. Other harmonics have different limits according to AS/NZS 61000.2.2 standards. Since the purpose is to calculate the harmonic voltage and current levels one tensor is needed to represent the device at all realistic distortion levels. The loci

of third harmonic voltages and currents for different phase angles and distortion levels are shown in Figure 2.2 and Figure 2.3 respectively.

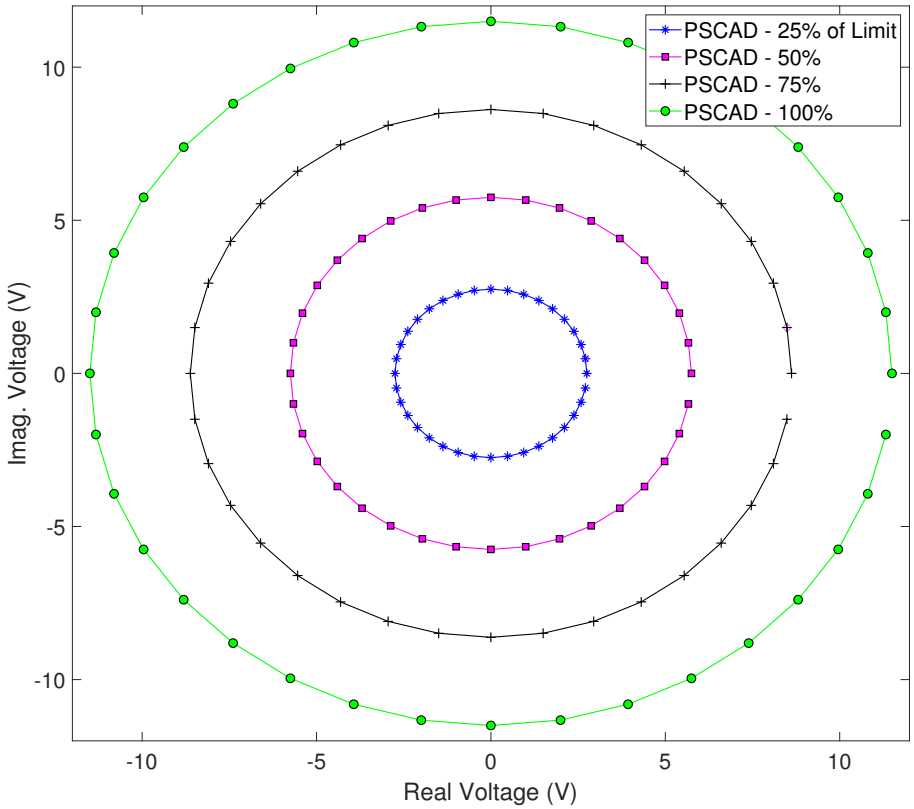

Figure 2.2 Loci of ΔV_3 for Different Distortions Limit

The incremental admittance of the system for all perturbation can be calculated by using Equation 2.3:

$$Y_{(m,n)} = \frac{I_{(m,pert)} - I_{(m,base)}}{V_{(n,pert)} - V_{(n,base)}} \tag{2.3}$$

Where m is the current harmonic order and n is the harmonic order of the voltage perturbation. For example, the value of 3^{rd} harmonic admittance:

$$Y_{(3,3)} = \frac{I_{(3,p)} - I_{(3,base)}}{V_{(3,p)} - V_{(3,base)}} \tag{2.4}$$

Admittance matrix for all the harmonics is expressed in Equation 2.5. Note the

cross-coupling between harmonic frequencies.

$$Y = \begin{bmatrix} \frac{\Delta I_1}{\Delta V_1} & \frac{\Delta I_1}{\Delta V_3} & \frac{\Delta I_1}{\Delta V_5} & \frac{\Delta I_1}{\Delta V_7} & \cdots & \frac{\Delta I_1}{\Delta V_m} & \cdots & \frac{\Delta I_1}{\Delta V_n} \\ \frac{\Delta I_3}{\Delta V_1} & \frac{\Delta I_3}{\Delta V_3} & \frac{\Delta I_3}{\Delta V_5} & \frac{\Delta I_3}{\Delta V_7} & \cdots & \frac{\Delta I_3}{\Delta V_m} & \cdots & \frac{\Delta I_3}{\Delta V_n} \\ \frac{\Delta I_5}{\Delta V_1} & \frac{\Delta I_5}{\Delta V_3} & \frac{\Delta I_5}{\Delta V_5} & \frac{\Delta I_5}{\Delta V_7} & \cdots & \frac{\Delta I_5}{\Delta V_m} & \cdots & \frac{\Delta I_5}{\Delta V_n} \\ \frac{\Delta I_7}{\Delta V_1} & \frac{\Delta I_7}{\Delta V_3} & \frac{\Delta I_7}{\Delta V_5} & \frac{\Delta I_7}{\Delta V_7} & \cdots & \frac{\Delta I_7}{\Delta V_m} & \cdots & \frac{\Delta I_7}{\Delta V_n} \\ \vdots & \vdots & \vdots & \vdots & \ddots & \vdots & \ddots & \vdots \\ \frac{\Delta I_m}{\Delta V_1} & \frac{\Delta I_m}{\Delta V_3} & \frac{\Delta I_m}{\Delta V_5} & \frac{\Delta I_m}{\Delta V_7} & \cdots & \frac{\Delta I_m}{\Delta V_m} & \cdots & \frac{\Delta I_m}{\Delta V_n} \\ \vdots & \vdots & \vdots & \vdots & \ddots & \vdots & \ddots & \vdots \\ \frac{\Delta I_n}{\Delta V_1} & \frac{\Delta I_n}{\Delta V_3} & \frac{\Delta I_n}{\Delta V_5} & \frac{\Delta I_n}{\Delta V_7} & \cdots & \frac{\Delta I_n}{\Delta V_m} & \cdots & \frac{\Delta I_n}{\Delta V_n} \end{bmatrix} \tag{2.5}$$

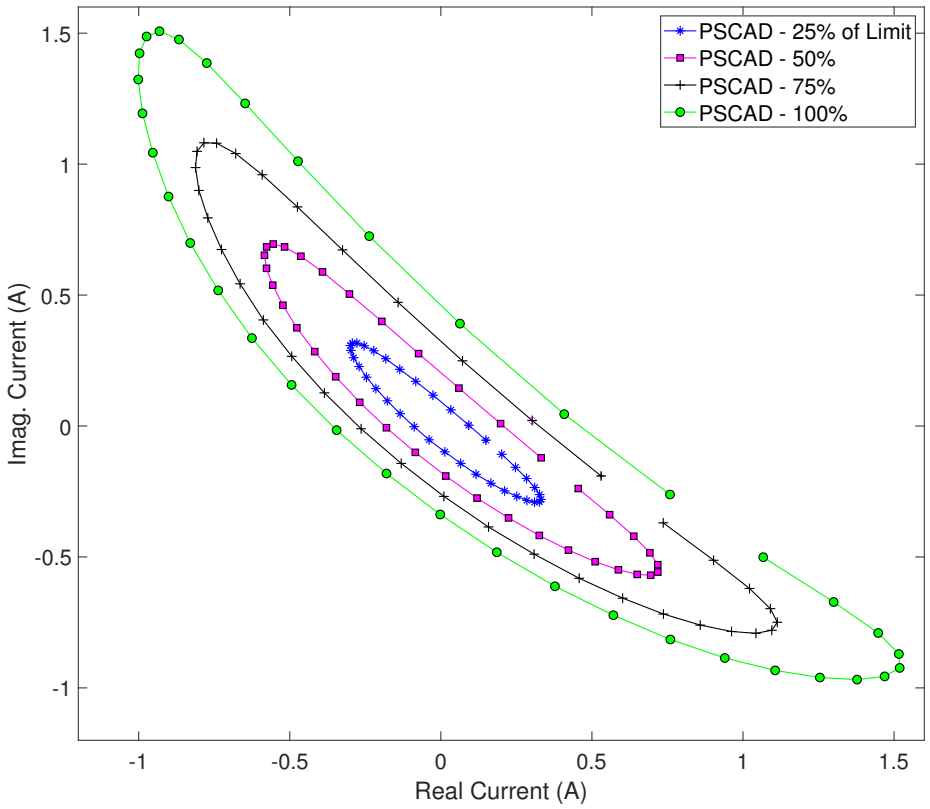

Figure 2.3 Loci of ΔI_3 for Different Distortions Limit

Based on this approach, the loci of the 3^{rd} harmonic admittances having voltage distortion magnitudes of 25%, 50%, 75% and 100% of the limit are shown in Figure 2.4 and Figure 2.5.

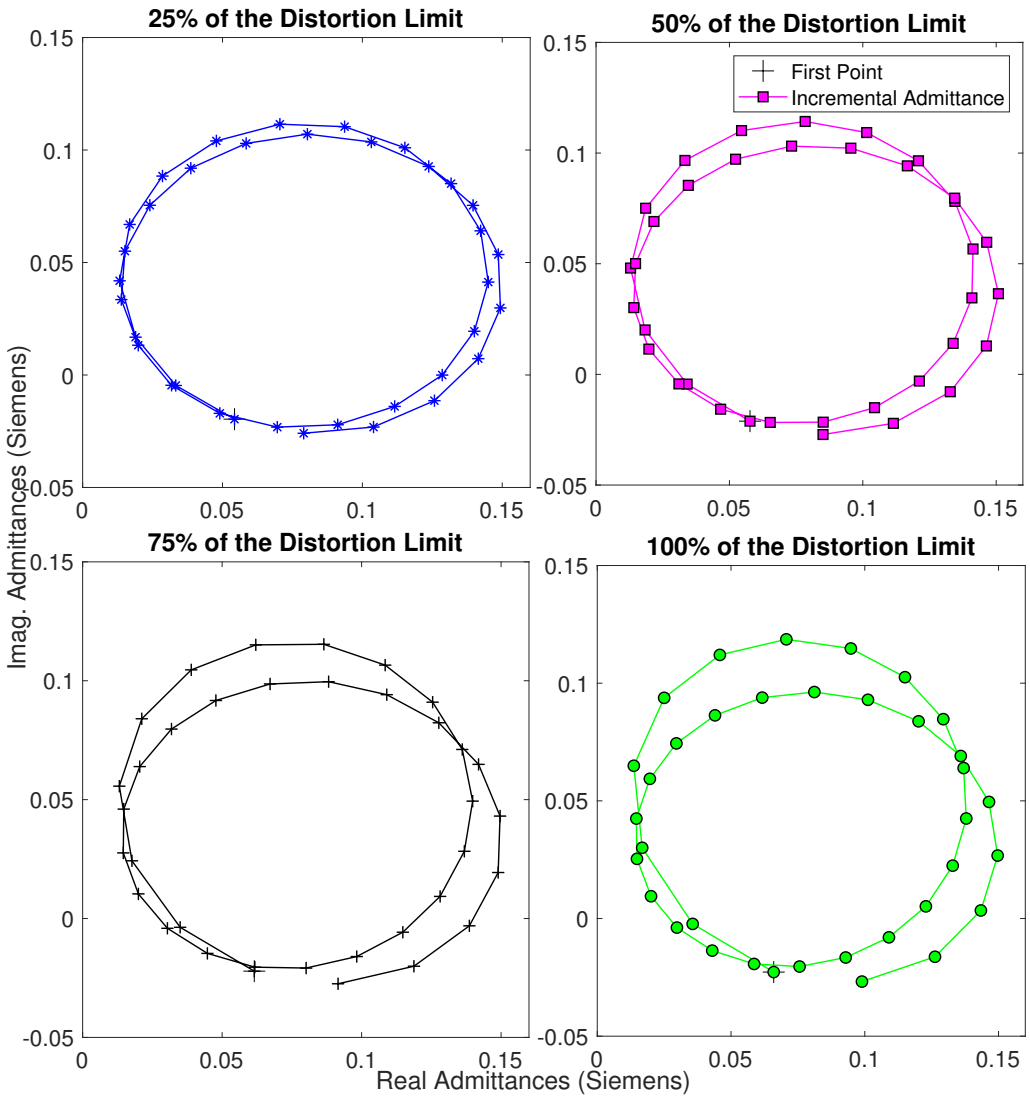

Figure 2.4 Loci of Admittance $Y_{(3,3)}$ for Different Distortions Levels (Separately)

2.6.2 Tensor Representation /Tensor Admittance

Smith established a framework to linearise the HVDC converter [Smith 1996]. He has used PSCAD/EMTDC for the modelling of an HVDC converter. He proposed a 2×2 tensor framework and demonstrated its use for modelling HVDC converters in rectification mode while considering the significant phase-dependence and frequency cross-coupling effects. In this work the same approach is used to investigate tensor analysis for the modelling of distribution systems. The relevant Equations (2.7 - 2.19) and Equations (2.23 - 2.26) provided by Smith [Smith 1996] are represented in this section, as it forms the basis for the work undertaken.

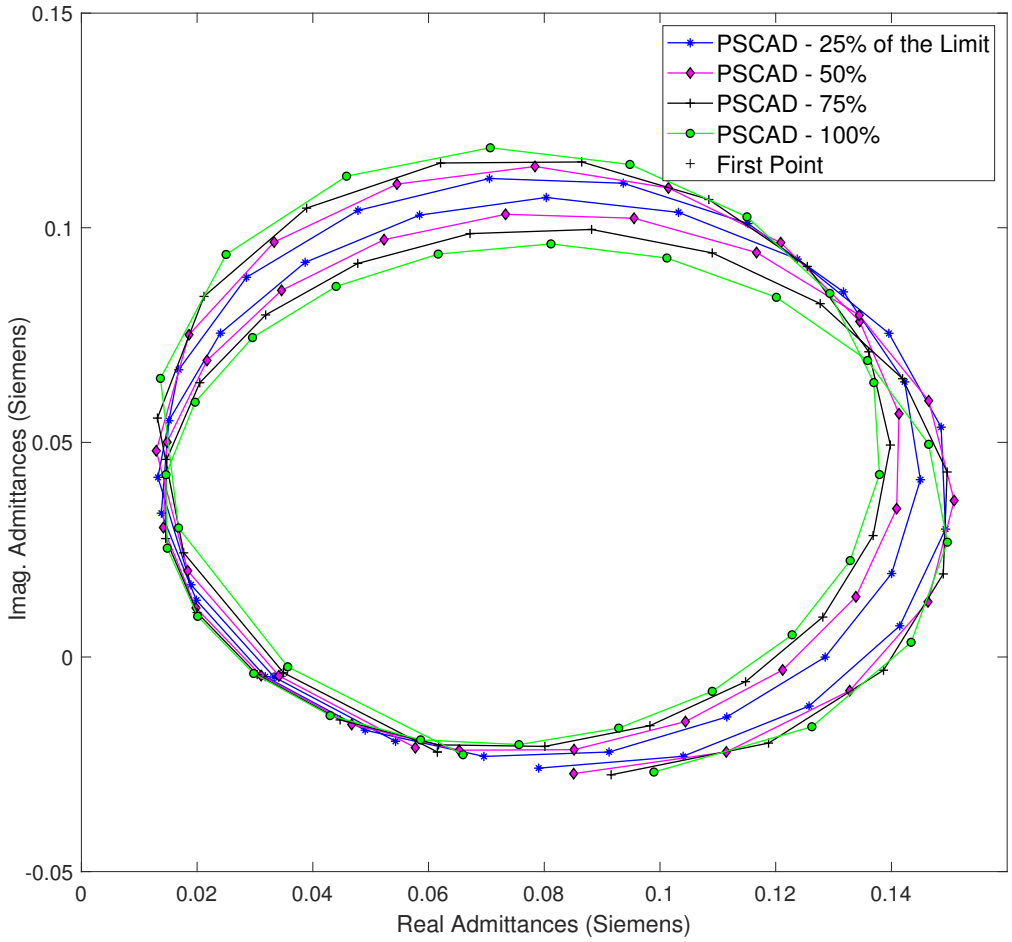

Figure 2.5 Loci of Admittance $Y_{(3,3)}$ for Different Distortions Levels (Together)

The voltage-current source representation of any power system component can be:

$$I = F(V) \tag{2.6}$$

In Equation 2.6, the complex vector function F can be non-linear. There can be a linear cross-coupling among harmonics for a linear function F, the cross-coupling and phase-dependence do not imply non-linearity in the frequency-domain. The linearisation of F can be calculated by:

$$\begin{bmatrix} \Delta I_R \\ \Delta I_I \end{bmatrix} = \begin{bmatrix} \frac{\delta F_R}{\delta V_R} & \frac{\delta F_R}{\delta V_I} \\ \frac{\delta F_I}{\delta V_R} & \frac{\delta F_I}{\delta V_I} \end{bmatrix} \begin{bmatrix} \Delta V_R \\ \Delta V_I \end{bmatrix} \tag{2.7}$$

Expanding F into its components gives

$$I_R + jI_I = F_R(V_R, V_I) + jF_I(V_R, V_I) \tag{2.8}$$

By applying Cauchy-Riemann conditions:

$$\frac{\delta F_R}{\delta V_R} = \frac{\delta F_I}{\delta V_I} \tag{2.9}$$

$$\frac{\delta F_I}{\delta V_R} = -\frac{\delta F_R}{\delta V_I} \tag{2.10}$$

The linearisation becomes:

$$\Delta I = \frac{\delta F}{\delta V}\Delta V \tag{2.11}$$

A linear and non-analytic injection be:

$$I = Y_1 V + Y_2 V^* \tag{2.12}$$

Complex admittance is therefore

$$Y = \frac{I}{V} \tag{2.13}$$

$$= \frac{Y_1 V + Y_2 V^*}{V} \tag{2.14}$$

$$= Y_1 + |Y_2|\angle(\angle Y_2 - 2\angle V) \tag{2.15}$$

Phase-dependence as an admittance coupling is:

$$\Delta I = Y_1 \Delta V + Y_2 \Delta V^* \tag{2.16}$$

Equation 2.16 expanded to its components as:

$$\begin{bmatrix} \Delta I_R \\ \Delta I_I \end{bmatrix} = \begin{bmatrix} Y_{1R} + Y_{2R} & Y_{2R} - Y_{1I} \\ Y_{1I} + Y_{2I} & Y_{1R} - Y_{2R} \end{bmatrix} \begin{bmatrix} \Delta V_R \\ \Delta V_I \end{bmatrix} \tag{2.17}$$

If conjugated quantities are considered as negative frequencies, then the linearised

admittance can be expressed as:

$$\begin{bmatrix} \Delta I \\ \Delta I^* \end{bmatrix} = \begin{bmatrix} Y_1 & Y_2 \\ {Y_2}^* & {Y_1}^* \end{bmatrix} \begin{bmatrix} \Delta V \\ \Delta V^* \end{bmatrix} \tag{2.18}$$

Alternatively, Equation 2.18 can be expressed in real and imaginary part as:

$$\begin{bmatrix} \Delta I_r \\ \Delta I_i \end{bmatrix} = \begin{bmatrix} Y_{11} & Y_{22} \\ Y_{21} & Y_{22} \end{bmatrix} \begin{bmatrix} \Delta V_r \\ \Delta V_i \end{bmatrix} \tag{2.19}$$

It has been shown that the response of a power electronic converter is phase-dependent and can be modelled by a Norton circuit where the admittance is a tensor, derived in Equation 2.18, to model the phase-dependency. Phase-dependency in Figure 2.6 shows apparent incremental admittance which is a function of the harmonic voltage distortion. Similarly, the voltage and current are represented by a 2×1 matrix with real and imaginary parts, as shown in Equation 2.19.

$$Y_{Tensor} = \begin{bmatrix} Y_{11} & Y_{22} \\ Y_{21} & Y_{22} \end{bmatrix} \tag{2.20}$$

The extended form of Equation 2.19 for all frequencies is:

$$\begin{bmatrix} \begin{bmatrix} \Delta I_r \\ \Delta I_i \end{bmatrix}_3 \\ \begin{bmatrix} \Delta I_r \\ \Delta I_i \end{bmatrix}_5 \\ \vdots \\ \begin{bmatrix} \Delta I_r \\ \Delta I_i \end{bmatrix}_n \end{bmatrix} = \begin{bmatrix} \begin{bmatrix} Y_{11} & Y_{12} \\ Y_{21} & Y_{22} \end{bmatrix}_{3,3} & \begin{bmatrix} Y_{11} & Y_{12} \\ Y_{21} & Y_{22} \end{bmatrix}_{3,5} & \cdots & \begin{bmatrix} Y_{11} & Y_{12} \\ Y_{21} & Y_{22} \end{bmatrix}_{3,m} \\ \begin{bmatrix} Y_{11} & Y_{12} \\ Y_{21} & Y_{22} \end{bmatrix}_{5,3} & \begin{bmatrix} Y_{11} & Y_{12} \\ Y_{21} & Y_{22} \end{bmatrix}_{5,5} & \cdots & \begin{bmatrix} Y_{11} & Y_{12} \\ Y_{21} & Y_{22} \end{bmatrix}_{5,m} \\ \vdots & \vdots & \ddots & \vdots \\ \begin{bmatrix} Y_{11} & Y_{12} \\ Y_{21} & Y_{22} \end{bmatrix}_{n,3} & \begin{bmatrix} Y_{11} & Y_{12} \\ Y_{21} & Y_{22} \end{bmatrix}_{n,5} & \cdots & \begin{bmatrix} Y_{11} & Y_{12} \\ Y_{21} & Y_{22} \end{bmatrix}_{n,m} \end{bmatrix} \begin{bmatrix} \begin{bmatrix} \Delta V_r \\ \Delta V_i \end{bmatrix}_3 \\ \begin{bmatrix} \Delta V_r \\ \Delta V_i \end{bmatrix}_5 \\ \vdots \\ \begin{bmatrix} \Delta V_r \\ \Delta V_i \end{bmatrix}_n \end{bmatrix} \tag{2.21}$$

For example the 3^{rd} harmonic current equation can be:

$$\begin{bmatrix} \Delta I_r \\ \Delta I_i \end{bmatrix}_3 = \begin{bmatrix} \Delta I_r \\ \Delta I_i \end{bmatrix}_3 + \begin{bmatrix} Y_{11} & Y_{12} \\ Y_{21} & Y_{22} \end{bmatrix}_{2,3} \begin{bmatrix} \Delta V_r \\ \Delta V_i \end{bmatrix}_3 + \begin{bmatrix} Y_{11} & Y_{12} \\ Y_{21} & Y_{22} \end{bmatrix}_{3,5} \begin{bmatrix} \Delta V_r \\ \Delta V_i \end{bmatrix}_5 \cdots + \begin{bmatrix} Y_{11} & Y_{12} \\ Y_{21} & Y_{22} \end{bmatrix}_{3,m} \begin{bmatrix} \Delta V_r \\ \Delta V_i \end{bmatrix}_m \tag{2.22}$$

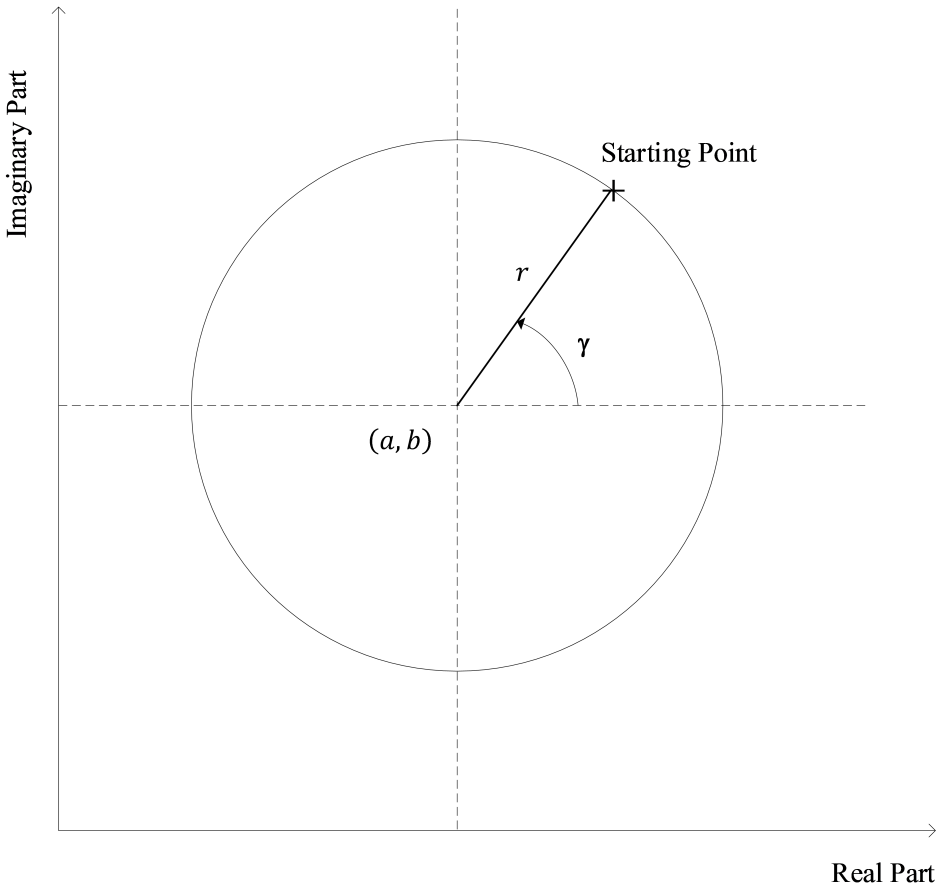

Figure 2.6 Phase-Dependent Admittance Locus for an Admittance Tensor

Admittances with no phase-dependency are expressed as a complex number which is a point in the real-imaginary plane. However, a tensor 2x2 expresses the phase-dependency in circular locus around a complex admittance point. A circular admittance of a tensor lies on the complex-plane having a radius r, with real-axis a, imaginary-axis b, and rotation γ is shown in Figure 2.6.

The parameters of circular admittance related to tensor components are determined by the following formulae:

$$a = \frac{1}{2}(Y_{11} + Y_{22}) \tag{2.23}$$

$$b = \frac{1}{2}(-Y_{12} + Y_{21}) \tag{2.24}$$

$$r = \frac{1}{2}\sqrt{(Y_{11} + Y_{22})^2 + (Y_{12} + {Y_{21}}^2)} \tag{2.25}$$

$$\gamma = \tan^{-1} \frac{Y_{12} + Y_{21}}{Y_{22} - Y_{11}} \tag{2.26}$$

The circular admittance tensor is a useful tool for calculating the phase-dependency and represents the limits of magnitude and phase angles of the admittance matrix that can be created at various harmonics. For tensor creation, different harmonic perturbations and the base case is used. Four unknowns Y_{11}, Y_{12}, Y_{21} and Y_{22} of 2nd rank tensor can be calculated by using Equation 2.27.

$$\begin{bmatrix} \Delta V_{r1} \\ \Delta V_{i1} \\ \Delta V_{r2} \\ \Delta V_{i2} \end{bmatrix} = \begin{bmatrix} \Delta I_{r1} & \Delta I_{i1} & 0 & 0 \\ 0 & 0 & \Delta I_{r1} & \Delta I_{i1} \\ \Delta I_{r2} & \Delta I_{i2} & 0 & 0 \\ 0 & 0 & \Delta I_{r2} & \Delta I_{i2} \end{bmatrix} \begin{bmatrix} Y_{11} \\ Y_{12} \\ Y_{21} \\ Y_{22} \end{bmatrix} \tag{2.27}$$

where,

$$\Delta V_1 = V_{perp1} - V_{base} \tag{2.28}$$

$$\Delta V_2 = V_{perp2} - V_{base} \tag{2.29}$$

$$\Delta I_1 = I_{perp1} - I_{base} \tag{2.30}$$

$$\Delta I_1 = I_{perp1} - I_{base} \tag{2.31}$$

Data gained from two perturbed solutions is sufficient to solve all the four components of the tensor. If the admittance is phase-dependant, then $Y_{11} \neq Y_{22}$ and $Y_{12} \neq -Y_{21}$, and tensor becomes a circular locus around the admittance point. The centre and radius of the circular locus of the tensor can be calculated using four real values of a 2nd rank tensor.

$$centre = \frac{1}{2}(Y_{11} + Y_{22}) + j\frac{1}{2}(Y_{21} - Y_{12}) \tag{2.32}$$

$$radius = \frac{1}{2}\sqrt{Y_{11} + Y_{22})^2 + (Y_{12} + {Y_{21}}^2)} \tag{2.33}$$

The loci of 3^{rd} harmonic admittances and the corresponding Actual Tensor(AT) (without approximation) obtained using voltage distortions magnitudes of 25%, 50%, 75% and 100% are shown in Figure 2.7. The admittance loci are a double traced circle for 25% of the limit and the AT is the good approximation to the admittance

loci. However, as the distortion level increases from 50% to 100% of the limit, the admittance loci shows deviation from a circular shape. The resulting AT shape does not fit the incremental admittance loci. Therefore, an approximation of the tensor is required to get an accurate tensor representation of power electronic devices.

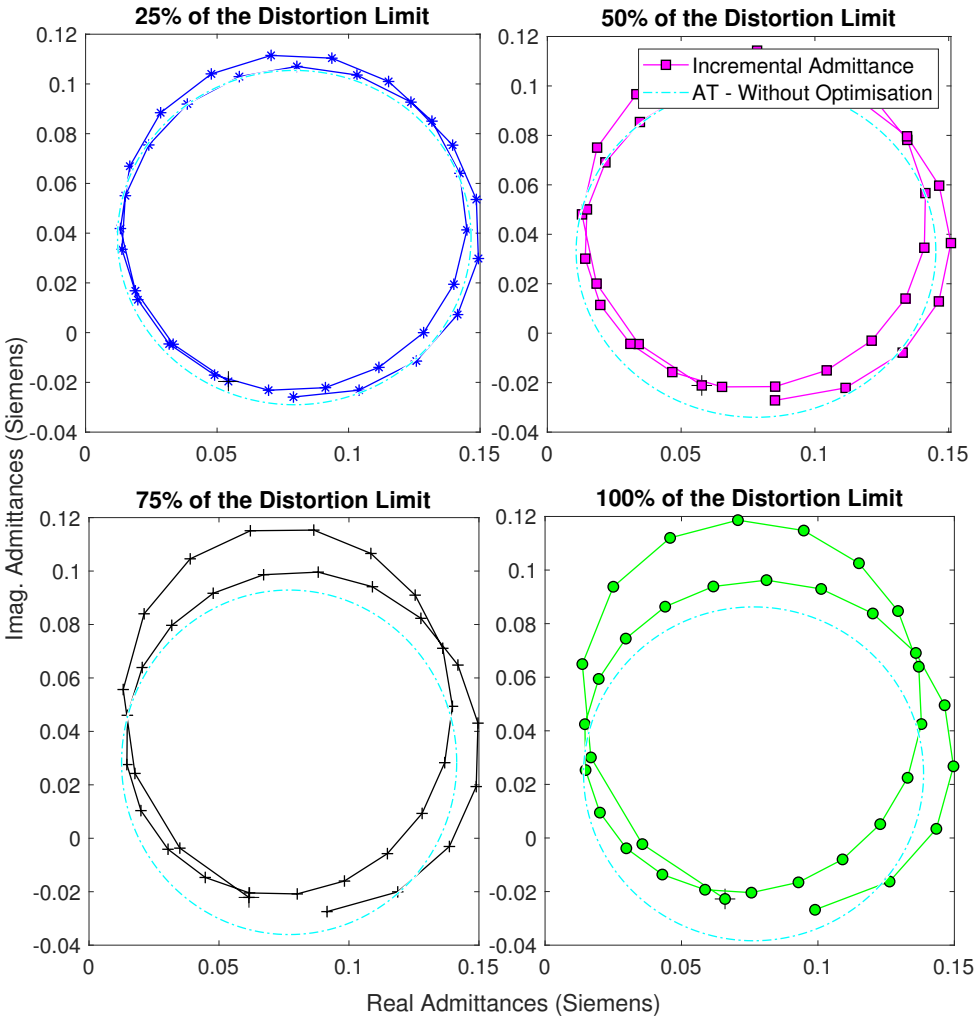

Figure 2.7 Admittance Loci and AT of $Y_{(3,3)}$ for Different Distortions Limit

2.7 TENSOR OPTIMISATION TECHNIQUES

Tensor accuracy is important for a wide range of applied voltage distortions. A certain level of distortion yields a linear double traced admittance loci, which have similar magnitudes. However, high distortion levels deviate from the double traced circles to partially overlapped circles. Besides the distortion level, the accuracy depends on the frequency of harmonics. For example, harmonics lower than the ninth harmonic are doubled traced circles which are better than higher harmonics in terms

of accuracy Appendix B. Therefore, it is evident from the experiment that if the load admittance loci are not doubled traced, the tensor representation will not be accurate. Each perturbation may produce different tensor shapes which are not accurate for high level distortions and higher harmonics. In order to get a more accurate tensor representations, two optimisation techniques are implemented and tested at different levels of distortion and harmonics.

2.7.1 Fourier Descriptors

The derived admittances at each phase angle (0 to 2π) of the voltage distortion are utilised to calculate the tensor. The derived admittance is vulnerable to experimental errors, and can have other higher complex non-linearities. Collins implemented FDs for the linearisation of the tensor and the representation of the phase-dependency of power electronic devices [Collins 2006]. This is an effective approach to enhance linearity region of power electronic devices. FDs are usually used in image processing to classify the closed loop objects [Zahn and Roskies 1972].

Locus of the tensor in Figure 2.6 is a closed loop in the complex plane which its FDs describes how the admittance changes with regards to the applied distortion angle. FDs are the discrete Fourier transform (DFT) of the admittance and follows as:

$$Y_{fd}[k] = \frac{1}{N_p} \sum_{n_p=0}^{N_p-1} y(n_p) e^{\frac{-j2\pi k n_p}{N_p}} \tag{2.34}$$

where, $y(n_p)$ represents there admittance measures at n_p^{th} voltage phase angle and $Y_{fd}[k]$ is a Fourier descriptor. Geometrically, the direct term of the tensor is equal to the offset of the admittance circle from x-axis and y-axis and relates to the zeroth FD. The direct and conjugate terms from the FDs can be obtained as follows.

$$y_{da} + jy_{db} = Y_{fd}(0) \tag{2.35}$$

$$y_{ca} + jy_{cb} = Y_{fd}(-2) \tag{2.36}$$

The admittance loci of $Y_{(3,3)}$ are calculated and represented in Figure 2.4. FDs are applied to the admittance loci of $Y_{(3,3)}$. The resulting current and double traced circular loci of FDs are shown in Figure 2.8. The third harmonic current is an elliptical shape for all percentages of voltage harmonic distortion. Also the tensor - FD is around the admittance loci.

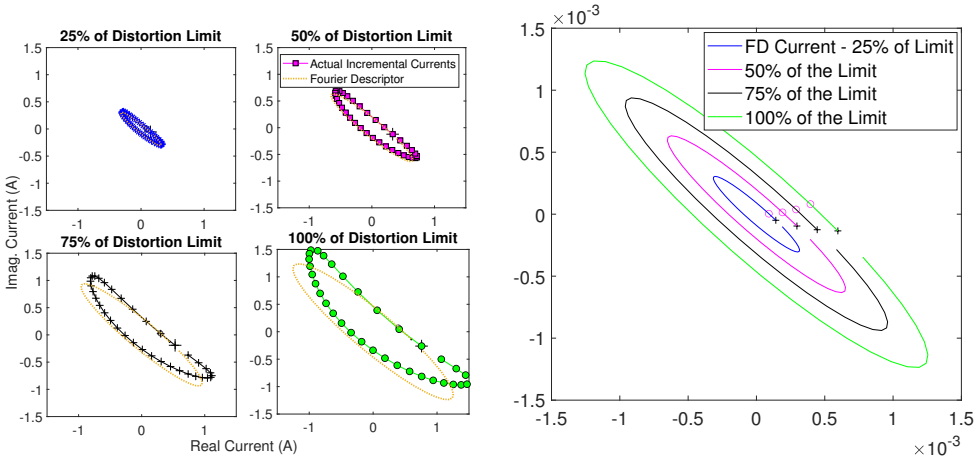

(a)

(b)

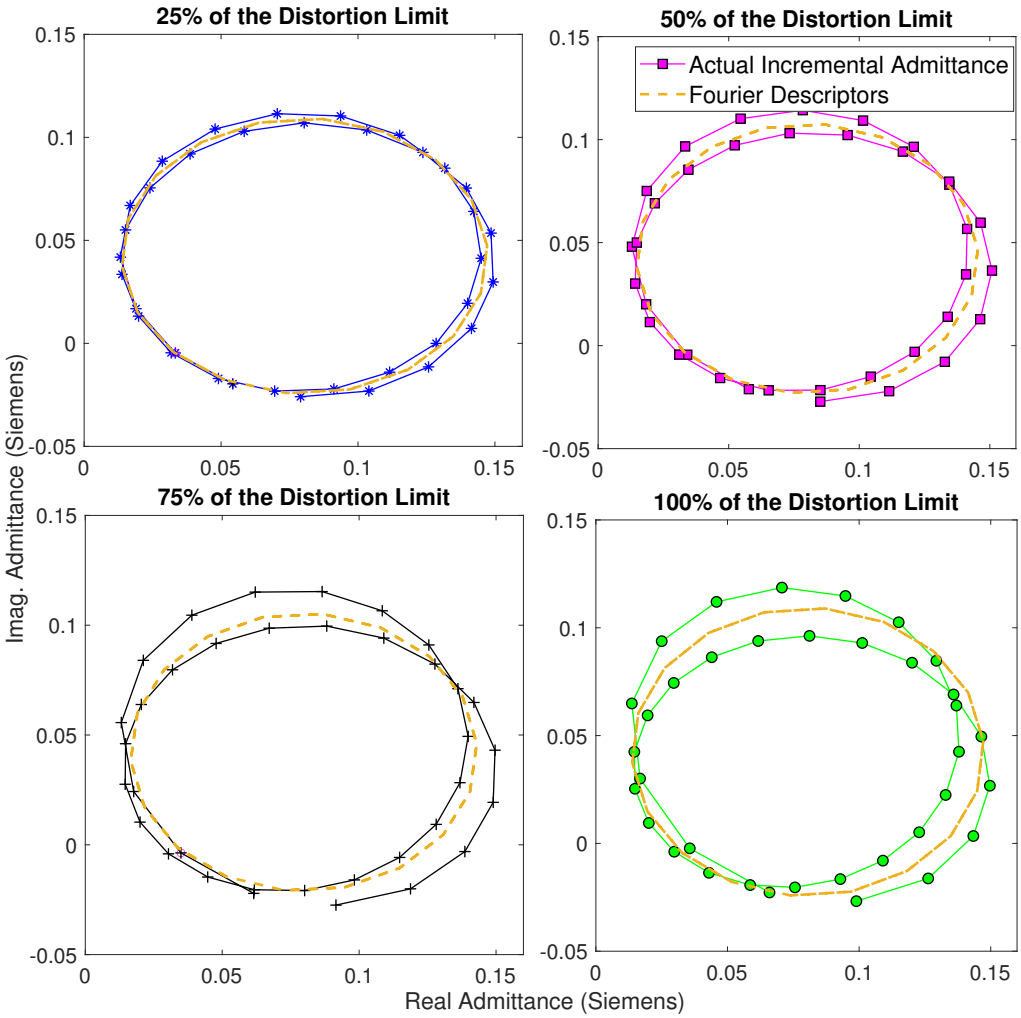

(c)

Figure 2.8 (a)Loci of Current ΔI_3- PSCAD/EMTDC and FDs (b) Loci of Current ΔI_3- FDs (c) Admittance Loci and Corresponding FD Tensors of $Y_{(3,3)}$ for Different Distortions Limit

2.7.2 Averaging Admittance Locus (AAL)

Another optimal solution is AAL which yields double traced circles [Wei 2009]. Rearranging Equations (2.23 - 2.26) gives the following.

if $-\frac{\pi}{2} < \beta < \frac{\pi}{2}$

$$Y_{11} = r \times \cos(\gamma) + ave(Y_{real}) \tag{2.37}$$

$$Y_{22} = -r \times \cos(\gamma) + ave(Y_{real}) \tag{2.38}$$

elsewhere,

$$Y_{11} = -r \times \cos(\gamma) + ave(Y_{real}) \tag{2.39}$$

$$Y_{22} = r \times \cos(\gamma) + ave(Y_{real}) \tag{2.40}$$

if $-0 < \beta < \pi$

$$Y_{12} = r \times \sin(\gamma) + -ave(Y_{imag}) \tag{2.41}$$

$$Y_{21} = r \times \sin(\gamma) + ave(Y_{imag}) \tag{2.42}$$

elsewhere,

$$Y_{12} = -r \times \sin(\gamma) - ave(Y_{imag}) \tag{2.43}$$

$$Y_{21} = -r \times \sin(\gamma) + ave(Y_{imag}) \tag{2.44}$$

With the help of the above mentioned equations, the AAL can be calculated resulting in a double-traced circle. The tensor of the average double-traced admittance circle is shown in Figure 2.9.

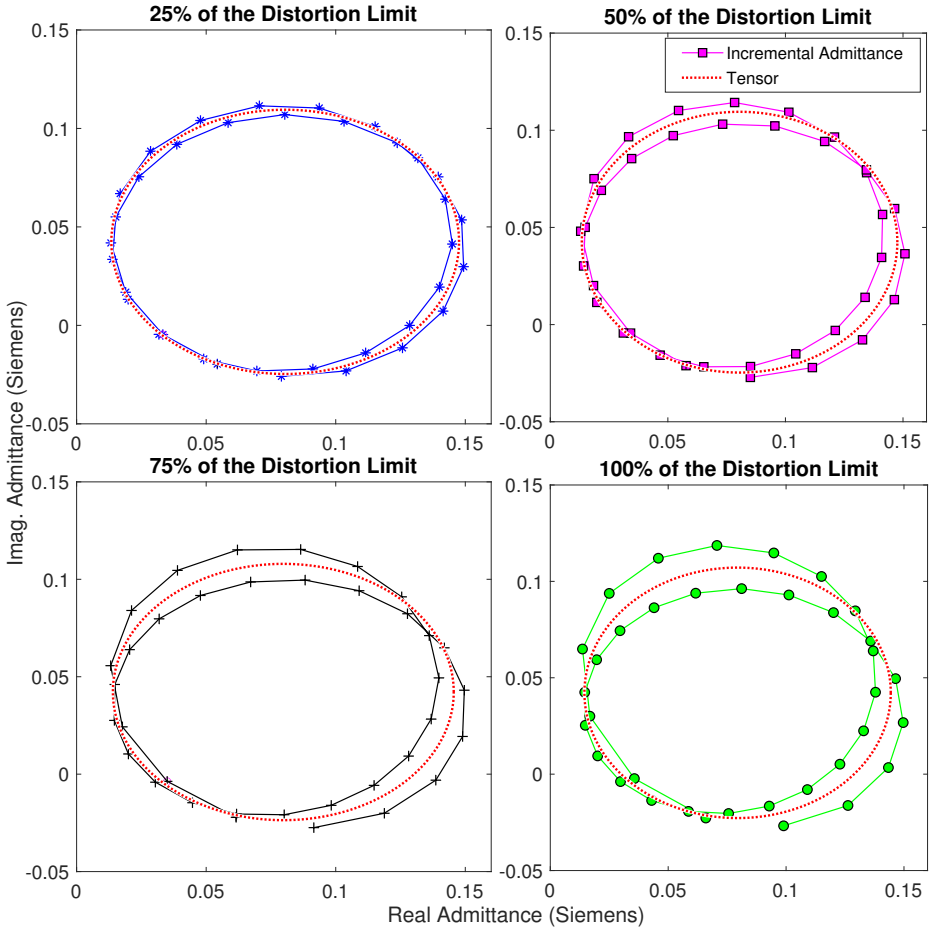

Figure 2.9 Admittance Loci and Corresponding AAL Tensors of $Y_{(3,3)}$ for Different Distortions Limit

Simulation for AAL and FDs are carried out for different percentage of voltages and for harmonics level. A great computational efficiency is seen for tensors obtained after applying both approaches. For 100% of the distortion limit the AT is a good approximation to the admittance loci in comparison with tensors obtained using FDs and AAL. AT and after optimisation methods of $Y_{(3,3)}$ is calculated as shown in Equations (2.45 - 2.47) and is showing in Figure 2.10. Both optimisation techniques produce a double traced circle and their tensors values are quite similar.

$$Y_{AT} = \begin{bmatrix} 0.001900 & -0.014828 \\ 0.014134 & 0.003300 \end{bmatrix} \tag{2.45}$$

$$Y_{AAL} = \begin{bmatrix} 0.002309 & -0.015189 \\ 0.014519 & 0.003055 \end{bmatrix} \tag{2.46}$$

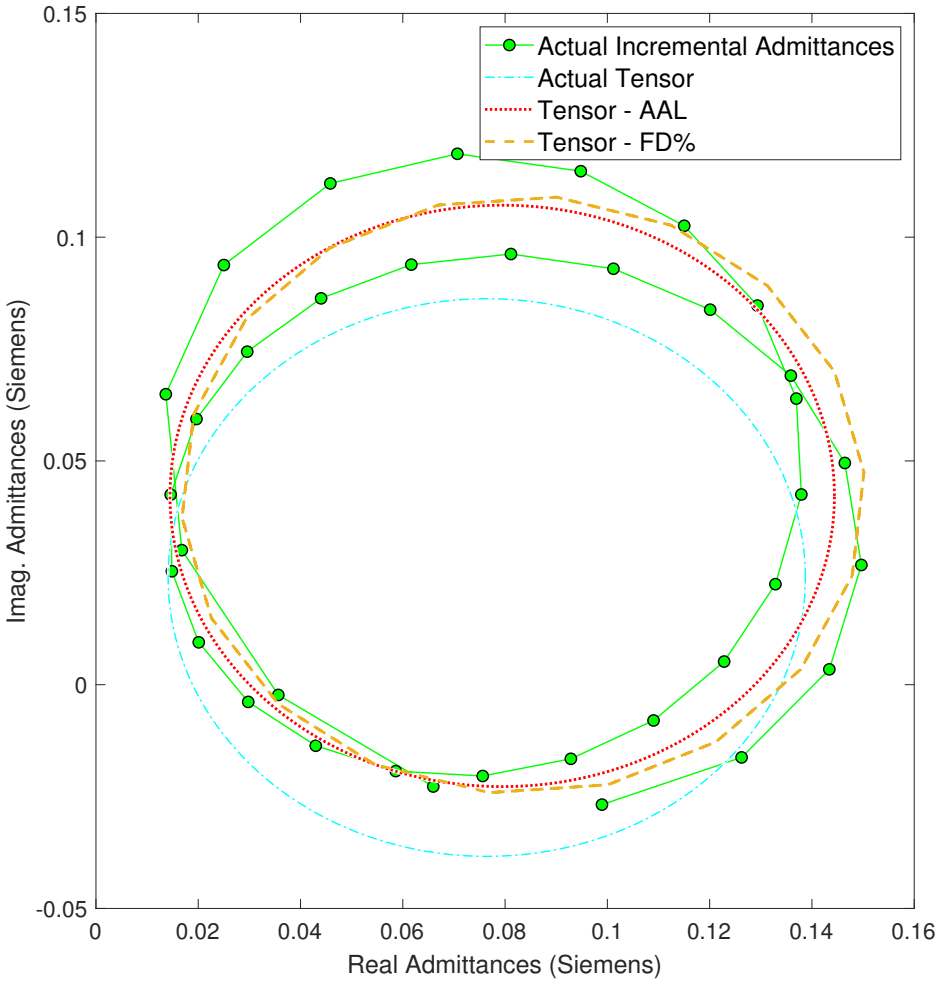

Figure 2.10 Admittance Loci, AT, AAL Tensors and FD Tensors for 100% of the Distortion Limit

$$Y_{FD} = \begin{bmatrix} 0.002335 & -0.015045 \\ 0.014663 & 0.003029 \end{bmatrix} \tag{2.47}$$

A comparison is carried out between FDs and AAL for 3^{rd} and 7^{th} harmonics as shown in Figure 2.11 and Figure 2.12, respectively. The purpose is to calculate one tensor which represent the device at all realistic distortions. Therefore, a tensor for low distortion at 0.01% of the limit is used for the comparison of displacement of the tensors obtained using voltage distortion magnitudes of 25%, 50%, 75%, and 100% for FDs and AAL techniques. In Figure 2.11, the double arrow shows the displacement in tensors for different levels of the distortion. It can be seen that the tensors displacement region is less for AAL when compared with FDs. Also, tensors obtained through

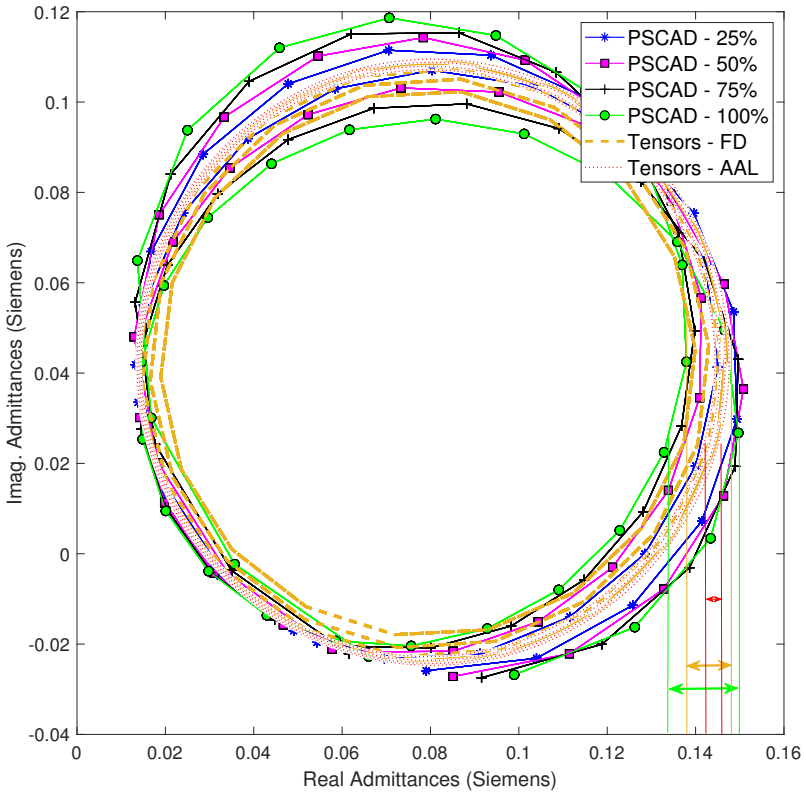

Figure 2.11 Admittance Loci, AAL Tensors and FD Tensors for 25%, 50%, 75% and 100% of the Distortion Limit for the 3_{rd} Harmonic

AAL are more closer at low distortion than FD by 26.5%. Therefore, throughout this research the AAL technique is considered because of its higher accuracy.

2.8 SUMMARY

In this chapter, the fundamentals of harmonic modelling of power electronic devices and distribution systems are explained. The existing time and frequency-domain techniques are reviewed. A test system is modelled and the admittance locus for each of the different levels of distortion is obtained. From these loci, an approximate admittance locus is derived and the corresponding tensor is calculated. Multiple optimisation techniques were investigated for an accurate approximation of tensors and determined the linear region of the device around its operating point in the frequency-domain. Comparison between optimisation techniques is carried out and found that AAL is more accurate and robust. Therefore, throughout this research AAL is used for the accurate representation.

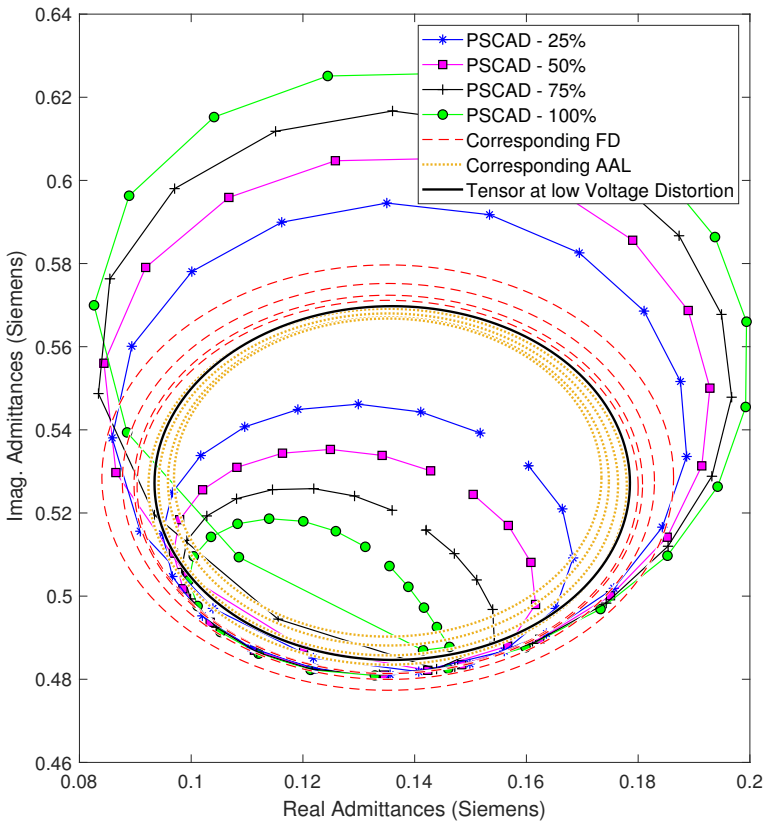

Figure 2.12 Admittance Loci, AAL Tensors and FD Tensors for 25%, 50%, 75% and 100% of the Distortion Limit for the 7_{th} Harmonic

Chapter 3

TENSORS VALIDATION

3.1 CHAPTER OVERVIEW

In this work, a large number of simulations were carried out using PSCAD/EMTDC and MATLAB. Therefore, it is important to validate tensors before moving to modelling distribution networks with different types of typical loads. A laboratory experiment was carried out using a Chroma programmable AC source and a Power Quality (PQ) analyser. The Chroma was used as a voltage source and for the injection of voltages distortion at different angles. The results generated from the laboratory experiments are compared with PSCAD/EMTDC and MATLAB simulations.

In addition, the AAL and FDs methods are implemented on the data obtained from the laboratory tests and PSCAD/EMTDC simulations. Having verified the tensor, in the next step tensors of several non-linear devices are added. This validation leads to a tensor representation of a distribution feeder (Described in Chapter 4). The linearity region of different components is calculated by carrying out a large number of simulations for different smoothing capacitors, inductors and loads. The linearity region is defined as a region where the tensor is linear and accurate for different levels of voltage distortion. For example, if the tensor is only valid for 2% distortion of the fundamental voltage then there is a need to re-linearise the system around another operating point.

3.2 TEST SYSTEM

In order to model distribution networks using tensors, there is a need to get an accurate validation of the tensor. This validation is achieved by the comparison of the software-based simulations and laboratory experiment. To illustrate this, a simple test system comprised of a full-bridge rectifier consisting of a capacitor of 23.74 µF and resistance of 4700 Ω is considered, as shown in Figure 3.1.

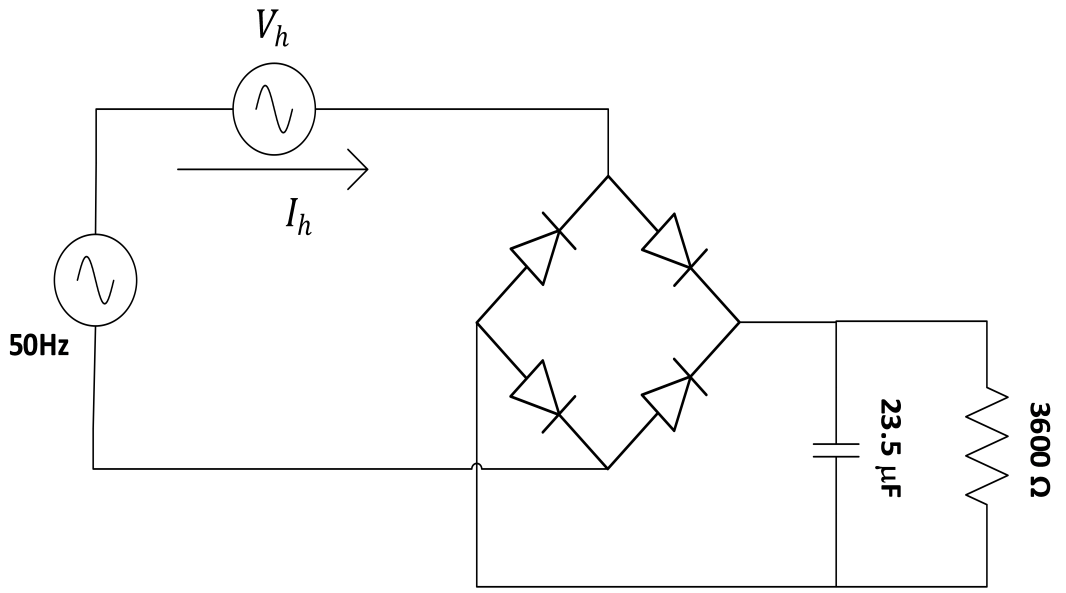

Figure 3.1 Non-linear Load PSCAD/EMTDC Model

3.2.1 Computer Simulations

For the computer-based simulations, a time-domain PSCAD/EMTDC tool and frequency-domain MATLAB simulations are used to get tensor representation of Figure 3.1. The data obtained from the PSCAD/EMTDC is imported in MATLAB simulations to obtain the incremental admittances and their tensors.

3.2.1.1 PSCAD/EMTDC

A time-domain simulation using PSCAD/EMTDC is carried out. The run time of the simulation is taken as 0.5 s and the solution time-step is set to 50 μs. Figure 3.2 displays the voltage and current waveforms and the harmonics that are the evident in the current waveform. There are considerable harmonics. A FFT block in PSCAD/EMTDC is used to get a bar-chart of the harmonics magnitudes, as displayed in Figure 3.3.

The results are obtained after 37 runs of PSCAD/EMTDC, in which the first run is used as a base case. The FFT block in PSCAD/EMTDC is used to measure the number of runs, HarmAngle, Imag, Iphase, Vmag, and Vphase for different distortion limits. The results at 100% of the distortion limit for 3^{rd} harmonics are given in Table 3.1.

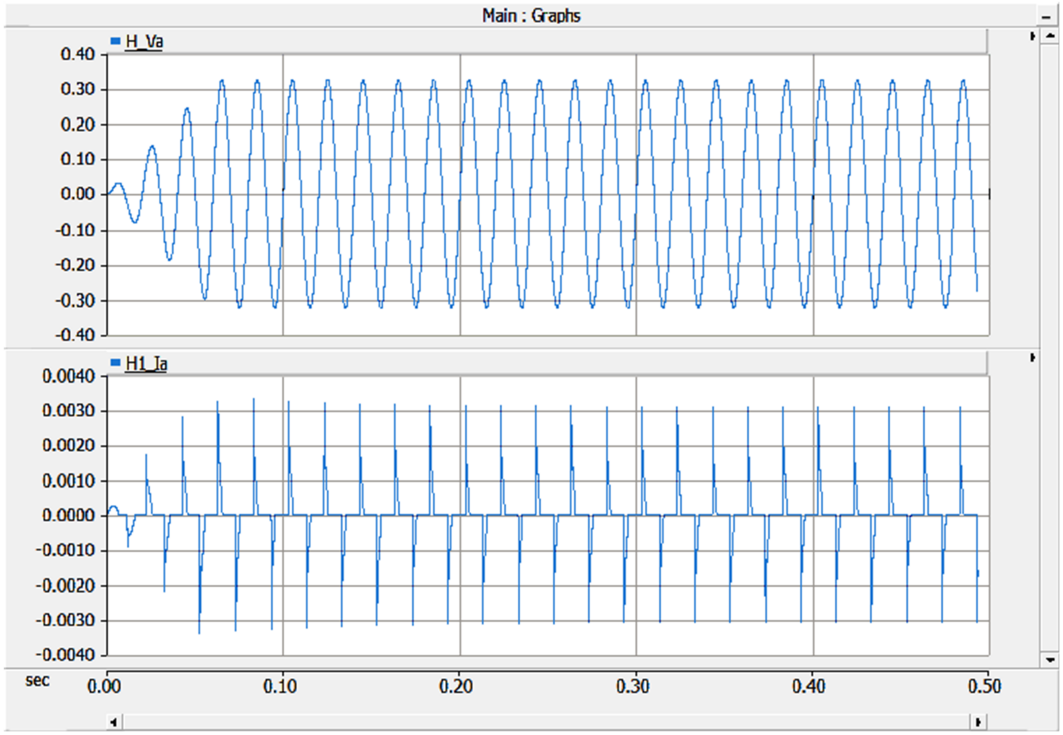

Figure 3.2 The Voltage and Current Waveforms PSCAD/EMTDC

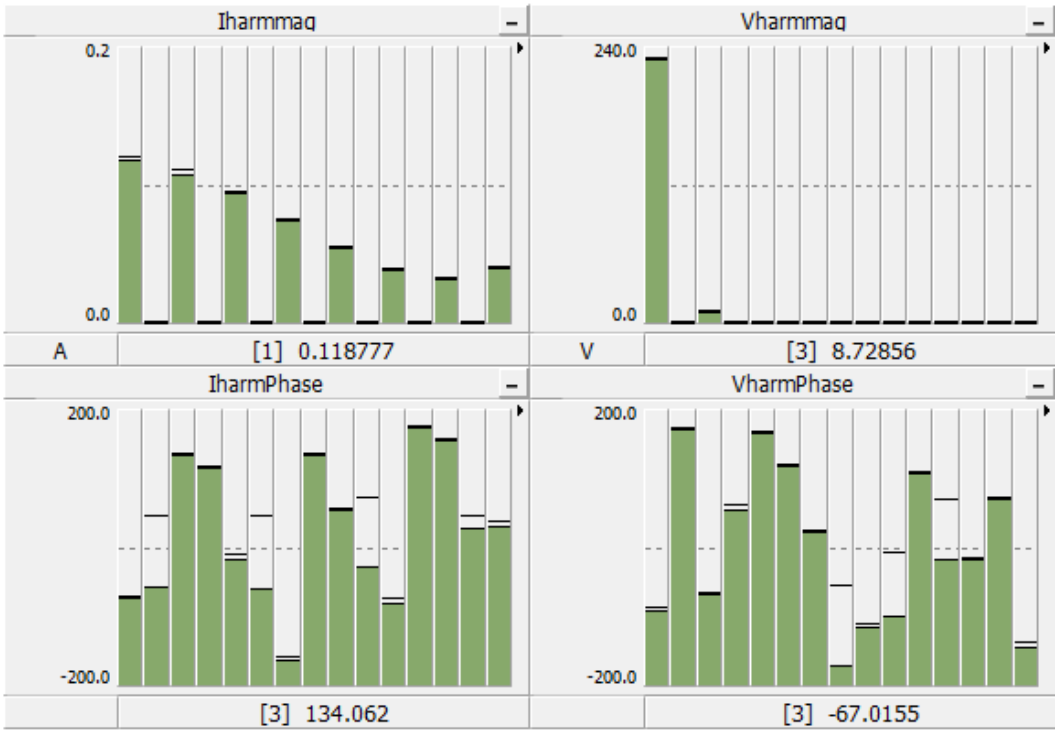

Figure 3.3 The Harmonic Voltage and the Current Magnitude and Corresponding Phases PSCAD/EMTDC

Table 3.1 Output Results from PSCAD/EMTDC Multi-run Simulations for 3^{rd} Harmonic

No. of Runs	HarmAngle	Imag	Iphase	Vmag	Vphase
1	0.0	0.1059	60.51	0.4934	-31.35
2	10.0	0.1017	56.87	0.1088	-60.24
3	20.0	0.1021	54.10	0.1127	-55.31
4	30.0	0.1026	51.70	0.1154	-50.28
5	40.0	0.1032	49.76	0.1168	-45.15
6	50.0	0.1039	48.34	0.1172	-39.82
7	60.0	0.1047	47.42	0.1163	-34.35
8	70.0	0.1054	47.00	0.1147	-28.66
9	80.0	0.1061	47.02	0.1122	-22.79
10	90.0	0.1068	47.43	0.1090	-16.74
11	100.0	0.1075	48.19	0.1053	-10.52
12	110.0	0.1081	49.24	0.1010	-4.140
13	120.0	0.1086	50.53	0.9625	2.391
14	130.0	0.1090	52.02	0.9088	9.132
15	140.0	0.1094	53.67	0.8523	16.02
16	150.0	0.1096	55.44	0.7917	23.13
17	160.0	0.1098	57.30	0.7276	30.50
18	170.0	0.1099	59.21	0.6596	38.28
19	180.0	0.1099	61.13	0.5910	46.37
20	190.0	0.1099	63.05	0.5189	55.28
21	200.0	0.1097	64.92	0.4466	65.07
22	210.0	0.1095	66.71	0.3740	76.61
23	220.0	0.1091	68.40	0.3047	90.73
24	230.0	0.1087	69.94	0.2433	109.7
25	240.0	0.1082	71.29	0.2000	135.7
26	250.0	0.1076	72.43	0.1925	168.5
27	260.0	0.1070	73.30	0.2257	-161.6
28	270.0	0.1063	73.85	0.2888	-139.9
29	280.0	0.1056	74.05	0.3670	-124.4
30	290.0	0.1049	73.85	0.4526	-112.6
31	300.0	0.1041	73.19	0.5431	-103.1
32	310.0	0.1034	72.05	0.6347	-95.13
33	320.0	0.1027	70.41	0.7255	-88.04
34	330.0	0.1022	68.28	0.8134	-81.60
35	340.0	0.1018	65.73	0.8957	-75.82
36	350.0	0.1015	62.87	0.9706	-70.38
37	360.0	0.1015	59.85	0.1035	-65.24

The data from PSCAD/EMTDC is used as a benchmark to obtained admittances in the MATLAB simulation. The results obtained from the computer simulation are compared with laboratory experiment in next section.

3.3 LABORATORY EXPERIMENT

A load with the same parameters as modelled in PSCAD/EMTDC, is tested in the laboratory shown in Figure 3.4. The Chroma Programmable AC Source is used for injecting distortions with different angles. The Programmable AC Source has advanced DSP technology, which can generate harmonics and interharmonics waveforms. Therefore, this device is used to introduce periodic harmonics to the waveform. A PQ analyser is used for measurements.

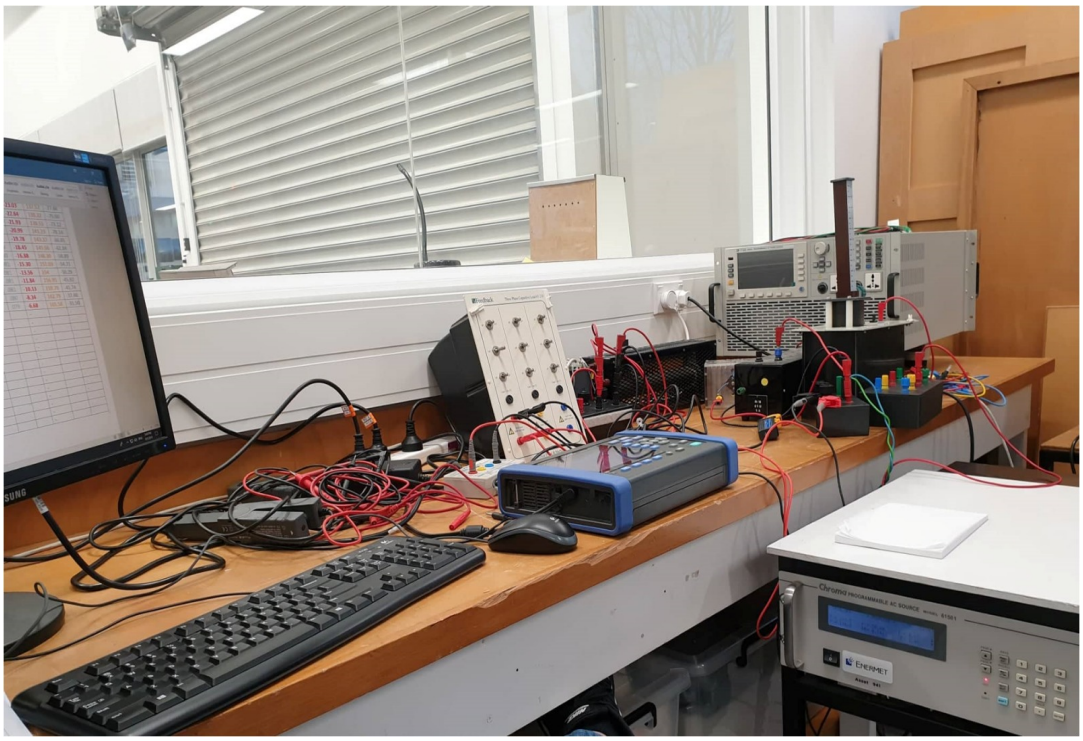

Figure 3.4 Lab Experiment for the Validation of Tensors

The harmonic voltages and currents are recorded while changing the voltage angle from 0 to 360 degrees with a step size of 10 degrees. This testing is done for two different levels of distortion. The first experiment is performed for 25% of the distortion limit and the second is for 100%. The distortions are injected at 3^{rd}, 5^{th} and 7^{th} harmonics and the harmonic current magnitudes and angles were measured. Table 3.2 and Table 3.3 presents the readings for 25% and 100% of the voltage distortion limits, respectively.

Table 3.2 Lab Experiment: Harmonic Current magnitude and Phase Angle Readings when 25% Harmonic Distortion Limit Injected

Angle	Current Magnitude			Current Phases		
	I_3	I_5	I_7	I_3	I_5	I_7
0	0.111	0.085	0.042	-24.76	136.55	-64.73
10	0.111	0.085	0.042	-25.54	137.92	-67.14
20	0.111	0.085	0.043	-26.31	139.25	-69.52
30	0.111	0.085	0.044	-27.07	140.55	-71.81
40	0.111	0.085	0.045	-27.73	141.89	-73.67
50	0.112	0.084	0.046	-28.28	142.95	-75.19
60	0.112	0.084	0.047	-28.72	143.96	-76.30
70	0.112	0.083	0.048	-29.03	144.78	-76.95
80	0.112	0.083	0.049	-29.17	145.35	-77.25
90	0.113	0.082	0.050	-29.26	145.78	-77.10
100	0.113	0.082	0.051	-29.18	145.95	-76.71
110	0.113	0.081	0.052	-28.91	145.78	-76.03
120	0.113	0.080	0.053	-28.6	145.28	-74.96
130	0.113	0.080	0.053	-28.17	144.58	-73.74
140	0.114	0.079	0.054	-27.64	143.60	-72.19
150	0.114	0.079	0.054	-27.02	142.38	-70.57
160	0.114	0.078	0.054	-26.38	140.81	-68.91
170	0.114	0.078	0.054	-25.74	139.19	-67.06
180	0.114	0.078	0.054	-25	137.44	-65.20
190	0.114	0.078	0.054	-24.27	135.62	-63.47
200	0.114	0.079	0.054	-23.64	133.72	-61.71
210	0.114	0.079	0.053	-22.95	132.28	-59.92
220	0.114	0.079	0.053	-22.37	130.70	-58.33
230	0.113	0.080	0.052	-21.84	129.56	-56.87
240	0.113	0.081	0.051	-21.32	128.74	-55.53
250	0.113	0.081	0.051	-20.97	127.89	-54.41
260	0.113	0.082	0.050	-20.66	127.66	-53.77
270	0.113	0.083	0.049	-20.59	127.55	-53.15
280	0.112	0.083	0.048	-20.54	127.90	-53.03
290	0.112	0.084	0.047	-20.64	128.37	-53.24
300	0.112	0.084	0.046	-20.94	129.09	-53.85
310	0.112	0.084	0.045	-21.36	130.01	-54.59
320	0.111	0.085	0.044	-21.84	131.09	-56.17
330	0.111	0.085	0.043	-22.45	132.28	-57.63
340	0.111	0.085	0.042	-23.19	133.64	-59.75
350	0.111	0.085	0.042	-23.98	134.94	-62.08
360	0.111	0.085	0.042	-24.69	136.28	-64.31

Table 3.3 Lab Experiment: Harmonic Current magnitude and Phase Angle Readings when 100% Harmonic Distortion Limit Injected

Angle	Current Magnitude			Current Phases		
	I_3	I_5	I_7	I_3	I_5	I_7
0	0.333	0.204	0.115	86.37	-26.15	-113.60
10	0.333	0.199	0.111	84.26	-28.963	-114.85
20	0.331	0.195	0.106	81.71	-33.07	-118.82
30	0.331	0.193	0.102	79.01	-37.70	-124.05
40	0.333	0.193	0.099	76.54	-42.27	-130.15
50	0.333	0.195	0.097	73.91	-47.41	-137.27
60	0.336	0.199	0.097	72.34	-50.56	-144.06
70	0.343	0.205	0.098	70.68	-54.07	-151.23
80	0.347	0.211	0.101	69.46	-56.79	-157.56
90	0.352	0.218	0.105	68.58	-58.80	-163.03
100	0.356	0.225	0.111	68.16	-60.01	-167.10
110	0.360	0.231	0.116	68.10	-60.55	-169.97
120	0.365	0.238	0.122	68.33	-60.54	-171.77
130	0.368	0.244	0.128	68.90	-59.82	-172.28
140	0.371	0.250	0.134	69.76	-58.65	-171.93
150	0.374	0.254	0.139	70.86	-57.03	-170.68
160	0.376	0.259	0.144	72.18	-54.98	-168.71
170	0.378	0.263	0.148	73.62	-52.74	-166.16
180	0.377	0.65	0.153	75.01	-50.04	-162.99
190	0.380	0.268	0.156	76.95	-47.27	-159.54
200	0.381	0.270	0.158	78.69	-44.45	-155.84
210	0.381	0.270	0.160	80.56	-41.32	-151.56
220	0.380	0.271	0.161	82.36	-38.35	-147.46
230	0.379	0.270	0.162	84.17	-35.20	-143.01
240	0.378	0.269	0.162	85.89	-32.29	-138.70
250	0.376	0.267	0.160	87.54	-29.42	-134.32
260	0.373	0.265	0.159	89.03	-26.74	-130.16
270	0.371	0.262	0.157	90.33	-24.27	-136.00
280	0.368	0.258	0.154	91.42	-22.21	-122.37
290	0.364	0.253	0.150	92.25	-20.50	-118.96
300	0.360	0.247	0.146	92.76	-19.19	-115.94
310	0.356	0.341	0.141	92.88	-18.54	-113.46
320	0.352	0.234	0.136	92.59	-18.37	-111.43
330	0.347	0.227	0.131	91.82	-18.97	-110.18
340	0.343	0.219	0.126	90.54	-20.31	-109.72
350	0.339	0.212	0.121	88.83	-22.41	-110.31
360	0.335	0.205	0.116	86.89	-25.04	-111.77

These data are used to obtain the admittance loci of the harmonics for the laboratory experiment and PSCAD/EMTDC data. Figure 3.5 and Figure 3.6 show the comparison between the computer simulation and the laboratory generated data.

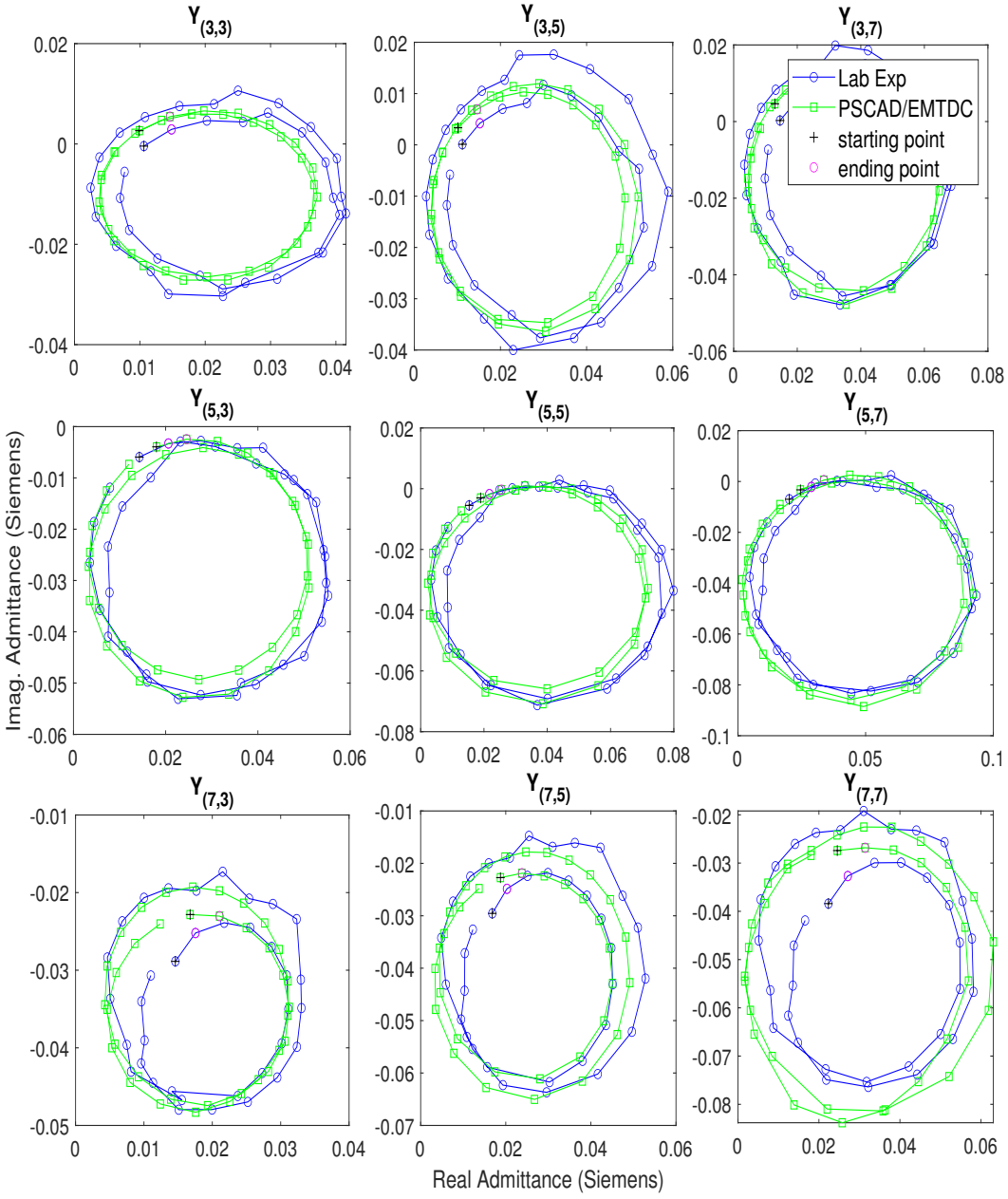

Figure 3.5 Incremental Admittance Loci for 25% of Harmonic Distortion Limit - Simulation vs Lab Experiment

The PSCAD/EMTDC and the laboratory experimental results verify that the admittance loci for all frequencies follow double traced circles with the same magnitudes. The starting and ending points are close to each other and the rotation of circles for

both simulation and experimental results agree. Therefore, this validation suggests that the tensor representations of non-linear appliances can be used for harmonic modelling of the distribution system.

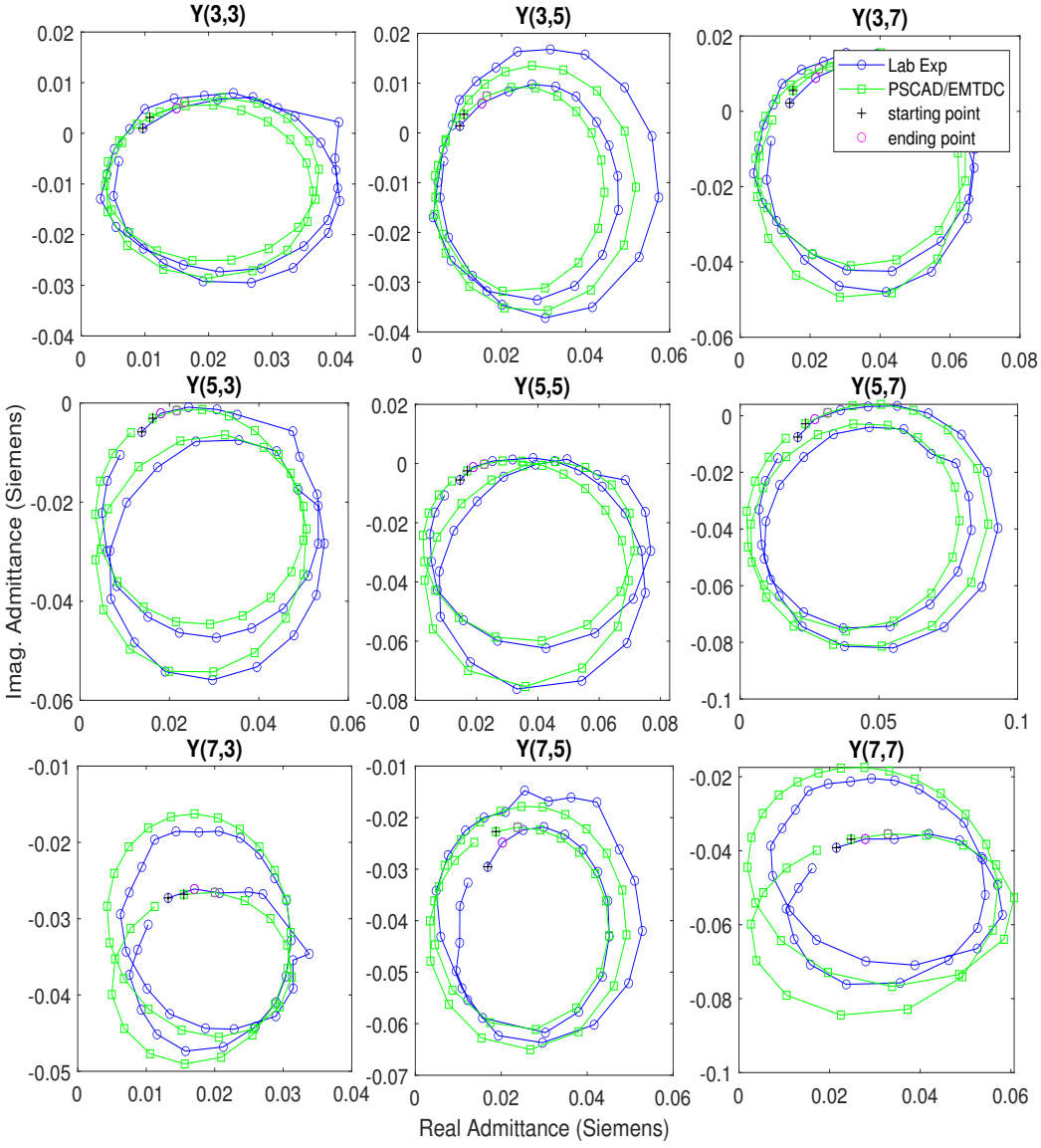

Figure 3.6 Incremental Admittance Loci for 100% of Harmonic Distortion Limit - Simulation vs Lab Experiment

In addition, optimisation methods are applied to the PSCAD/EMTDC and laboratory generated data. The incremental admittances loci, AT, AAL and FDs for three different harmonics are shown in Figure 3.7. For $Y_{(3,3)}$, the AT, which is before optimisation, match the tensors obtained using AAL and FDs. However, the incremental admittance loci of $Y_{(3,5)}$ and $Y_{(7,7)}$ shows deviation from double-traced

circular shape. Therefore, the AT shape does not fit the incremental admittance loci. On the other hand, tensor approximation using AAL and FDs shows a great computational efficiency. As a result, tensors obtained using AAL and FDs are robust in comparison with AT.

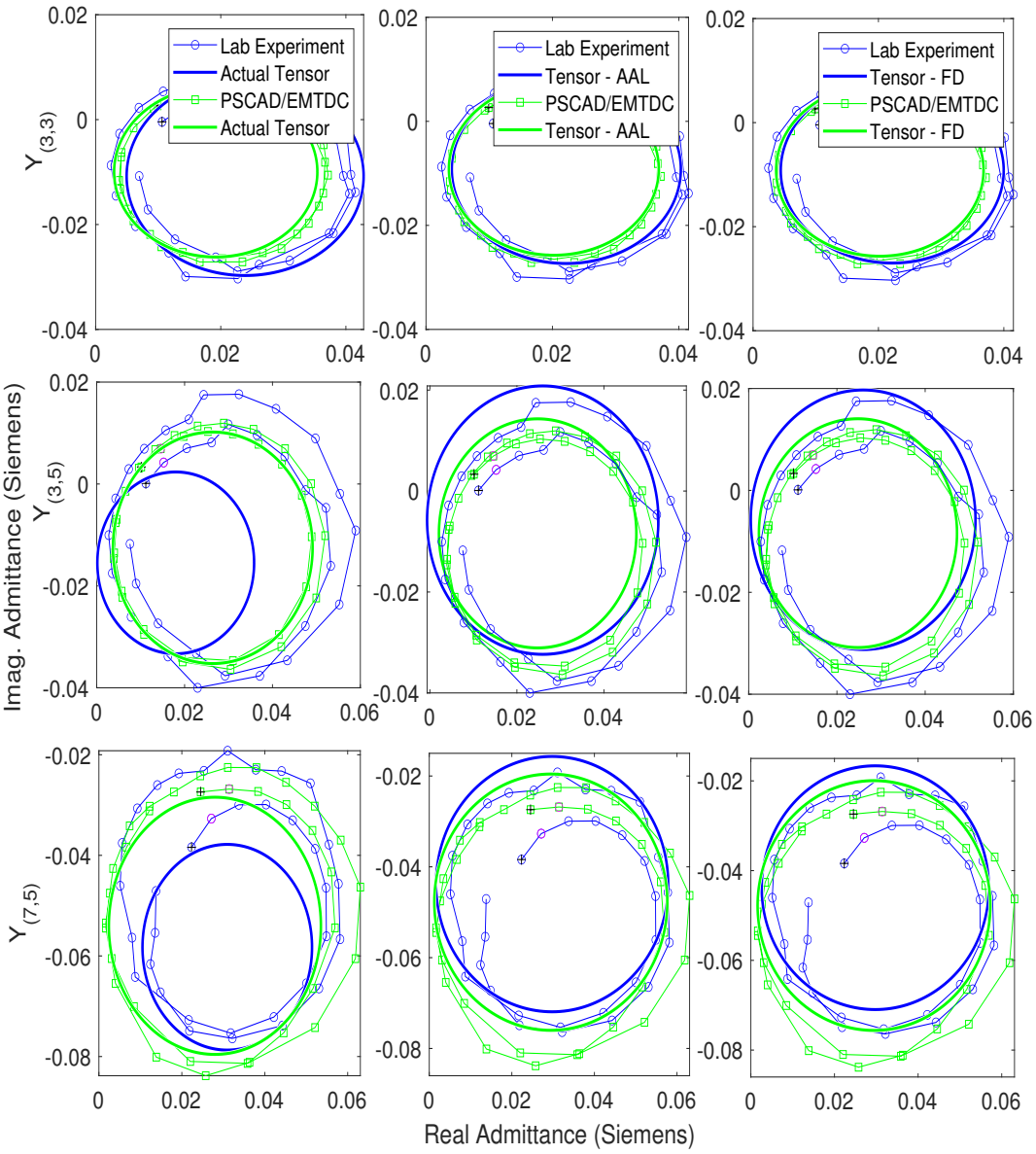

Figure 3.7 Incremental Admittance Loci, Actual Tensors, and FDs for 100% of Harmonic Voltage Distortion Limit - Simulation vs Lab Experiment

3.4 ADDITION OF TENSORS

For modelling the distribution system, a library of tensors for different non-linear devices is required. Adding tensors of different household appliances is important

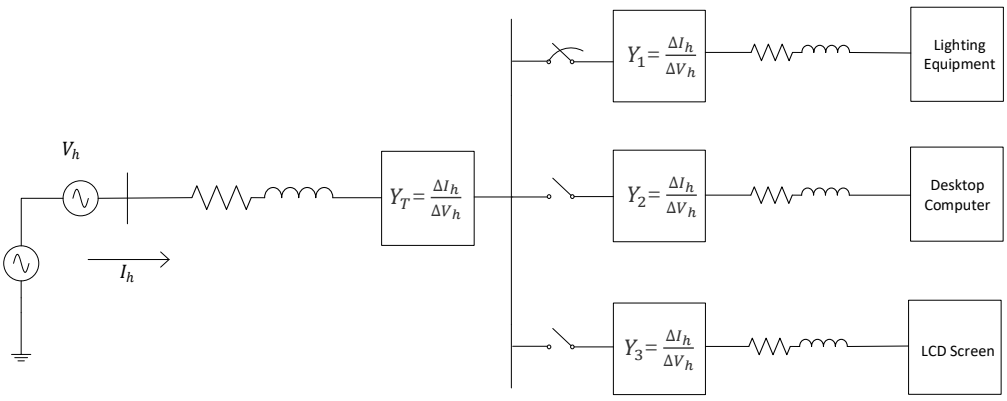

Figure 3.8 Three Loads Electrical Power Model for the Addition of Tensors

to get a resulting tensor matrix for each house. In this section, three non-linear household appliances lighting equipment, desktop computer and TV are modelled in PSCAD/EMTDC, as shown in Figure 3.8. In this research, circuit-based representation consisting of a full bridge rectifier, standard smoothing capacitors and loads rating is considered.

In the first step, only Load 1 is connected at a time and the tensor matrix Y_1 of the first 8^{th} harmonics is calculated. The same simulations are repeated for Load 2 and Load 3 to get corresponding tensors Y_2 and Y_3. Those three tensors are added up to get an resultant tensor. In next step all the three loads are connected and tensors of Y_T is calculated. The sum of the tensors Y_1, Y_2, and Y_3 is found to be equal to the tensor Y_T that is computed when all the loads are connected as shown in Figure 3.9. In the nodal analysis, the resulting current ΔI_T is given as:

$$\Delta I = [Y]\Delta V \tag{3.1}$$

$$\Delta I_T = \Delta I_{T1} + \Delta I_{T2} + \Delta I_{T3} \tag{3.2}$$

$$= [Y_1]\Delta V + [Y_2]\Delta V + [Y_3]\Delta V \tag{3.3}$$

$$= ([Y_1] + [Y_2] + [Y_3])\Delta V \tag{3.4}$$

$$= Y_T \Delta V \tag{3.5}$$

Table 3.4 shows values for resultant tensors, estimated tensor and the difference between them. A difference of 10^{-8} Siemens shows that the addition of multiple

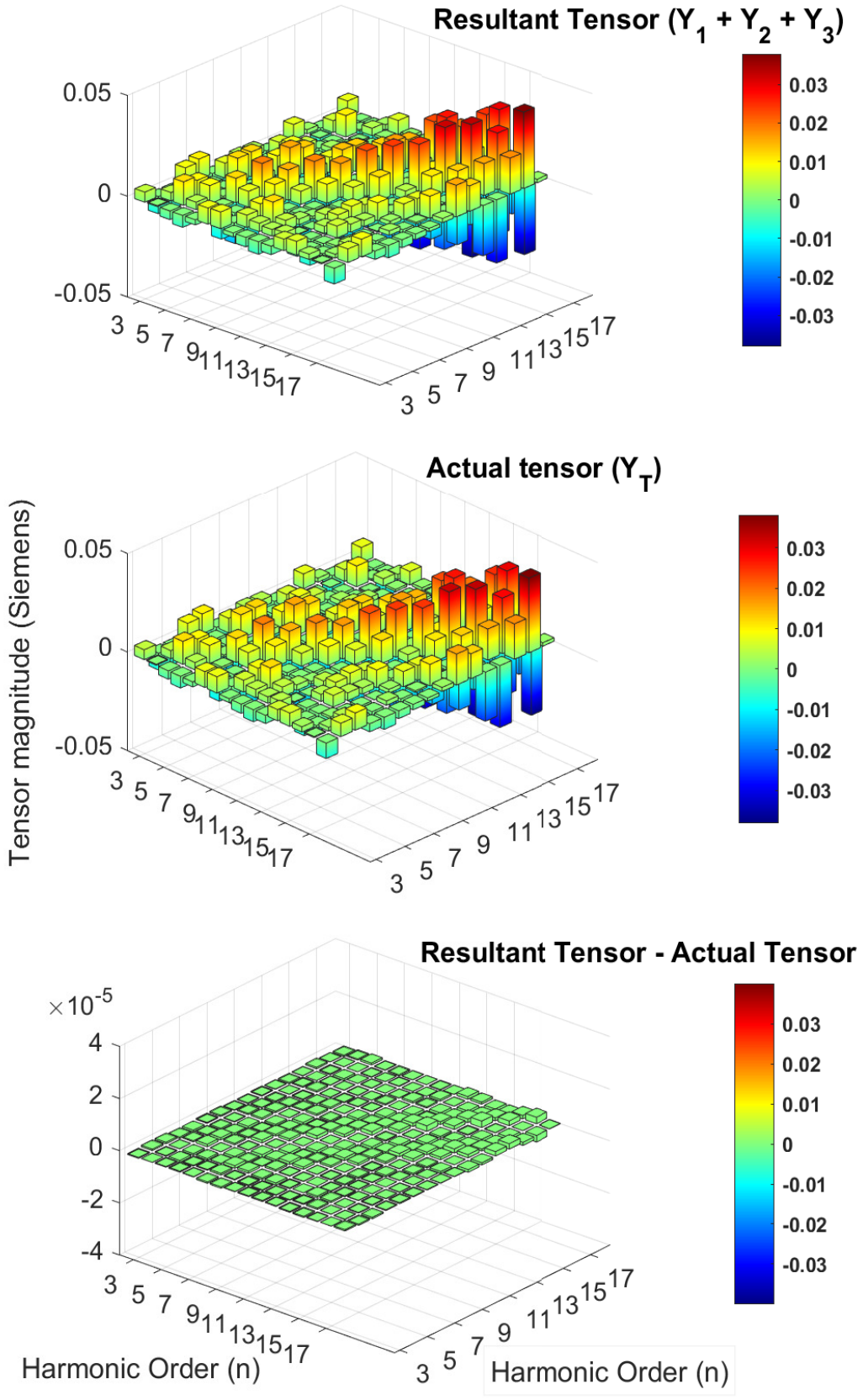

Figure 3.9 (a) Tensors Additions of Three Single-Phase Load (b) Actual Tensors When All the Loads are Connected (c) Difference of Estimated Tensors and Actual Tensors

Table 3.4 Resultant Tensor, Actual Tensor and Difference of Estimated Tensors and Actual

	Y_3	Y_5
Resultant Tensor - (Y_1 + Y_2 + Y_3)		
Y_3	**0.6163 -0.1874** **-0.2433 0.2827**	0.9796 -0.0625 -0.5060 0.3765
Y_5	0.6164 -0.1874 -0.2434 0.2828	**0.9800 -0.0627** **-0.5066 0.3764**
Actual Tensors - (Y_T)		
Y_3	**0.6163 -0.1874** **-0.2433 0.2827**	0.9796 -0.0625 -0.5060 0.3765
Y_5	0.6164 -0.1874 -0.2434 0.2828	**0.9800 -0.0627** **-0.5066 0.3764**
Difference = Resultant Tensor - Actual Tensor		
Y_3	**-2.895e-08 1.157e-07** **1.197e-07 -5.948e-08**	3.114e-08 1.7775e-07 2.119e-07 -1.703e-07
Y_5	-3.679e-08 2.825e-08 5.4332e-08 -4.058e-08	**-1.298e-07 7.489e-08** **1.9701e-07 -8.209e-08**

appliances is applicable.

For a three-phase system, the Y_{Tensor} can be expressed as in Equation 3.6. The addition of a tensor of a single-phase load connected at phase-a will be added with $[Y_T]_{V_a,I_a}$ of Y_{Tensor}.

$$\begin{bmatrix} \begin{bmatrix} Y_{1,1} & Y_{1,3} & \cdots & Y_{1,n} \\ Y_{3,1} & Y_{3,3} & \cdots & Y_{3,n} \\ \vdots & \vdots & \ddots & \vdots \\ Y_{m,1} & Y_{m,3} & \cdots & Y_{m,n} \end{bmatrix}_{V_a,Ia} & \begin{bmatrix} Y_{1,1} & Y_{1,3} & \cdots & Y_{1,n} \\ Y_{3,1} & Y_{3,3} & \cdots & Y_{3,n} \\ \vdots & \vdots & \ddots & \vdots \\ Y_{m,1} & Y_{m,3} & \cdots & Y_{m,n} \end{bmatrix}_{V_a,Ib} & \begin{bmatrix} Y_{1,1} & Y_{1,3} & \cdots & Y_{1,n} \\ Y_{3,1} & Y_{3,3} & \cdots & Y_{3,n} \\ \vdots & \vdots & \ddots & \vdots \\ Y_{m,1} & Y_{m,3} & \cdots & Y_{m,n} \end{bmatrix}_{V_a,Ic} \\ \begin{bmatrix} Y_{1,1} & Y_{1,3} & \cdots & Y_{1,n} \\ Y_{3,1} & Y_{3,3} & \cdots & Y_{3,n} \\ \vdots & \vdots & \ddots & \vdots \\ Y_{m,1} & Y_{m,3} & \cdots & Y_{m,n} \end{bmatrix}_{V_b,Ia} & \begin{bmatrix} Y_{1,1} & Y_{1,3} & \cdots & Y_{1,n} \\ Y_{3,1} & Y_{3,3} & \cdots & Y_{3,n} \\ \vdots & \vdots & \ddots & \vdots \\ Y_{m,1} & Y_{m,3} & \cdots & Y_{m,n} \end{bmatrix}_{V_b,Ib} & \begin{bmatrix} Y_{1,1} & Y_{1,3} & \cdots & Y_{1,n} \\ Y_{3,1} & Y_{3,3} & \cdots & Y_{3,n} \\ \vdots & \vdots & \ddots & \vdots \\ Y_{m,1} & Y_{m,3} & \cdots & Y_{m,n} \end{bmatrix}_{V_b,Ic} \\ \begin{bmatrix} Y_{1,1} & Y_{1,3} & \cdots & Y_{1,n} \\ Y_{3,1} & Y_{3,3} & \cdots & Y_{3,n} \\ \vdots & \vdots & \ddots & \vdots \\ Y_{m,1} & Y_{m,3} & \cdots & Y_{m,n} \end{bmatrix}_{V_c,Ia} & \begin{bmatrix} Y_{1,1} & Y_{1,3} & \cdots & Y_{1,n} \\ Y_{3,1} & Y_{3,3} & \cdots & Y_{3,n} \\ \vdots & \vdots & \ddots & \vdots \\ Y_{m,1} & Y_{m,3} & \cdots & Y_{m,n} \end{bmatrix}_{V_c,Ib} & \begin{bmatrix} Y_{1,1} & Y_{1,3} & \cdots & Y_{1,n} \\ Y_{3,1} & Y_{3,3} & \cdots & Y_{3,n} \\ \vdots & \vdots & \ddots & \vdots \\ Y_{m,1} & Y_{m,3} & \cdots & Y_{m,n} \end{bmatrix}_{V_c,Ic} \end{bmatrix} \tag{3.6}$$

3.5 LINEARITY REGION

For the tensor representation, the non-linear devices were linearised around an operating point by perturbation analysis. It is evident from the experimental testing that

employing large perturbations on a current source converter still results in a linear response. Whereas, for voltage source converter, the linear region is much smaller.

To find the region of linearity, a test system was developed in PSCAD/EMTDC, as shown in Figure 3.1. Different capacitor and load values were varied to find the limits for where the system is linear and where it is not. Different percentage of voltage distortions were injected at different frequencies, and the current response was observed. The region of linearity for four harmonic distortions levels 25%, 50%, 75% and 100% was calculated, as shown in Figure 3.10.

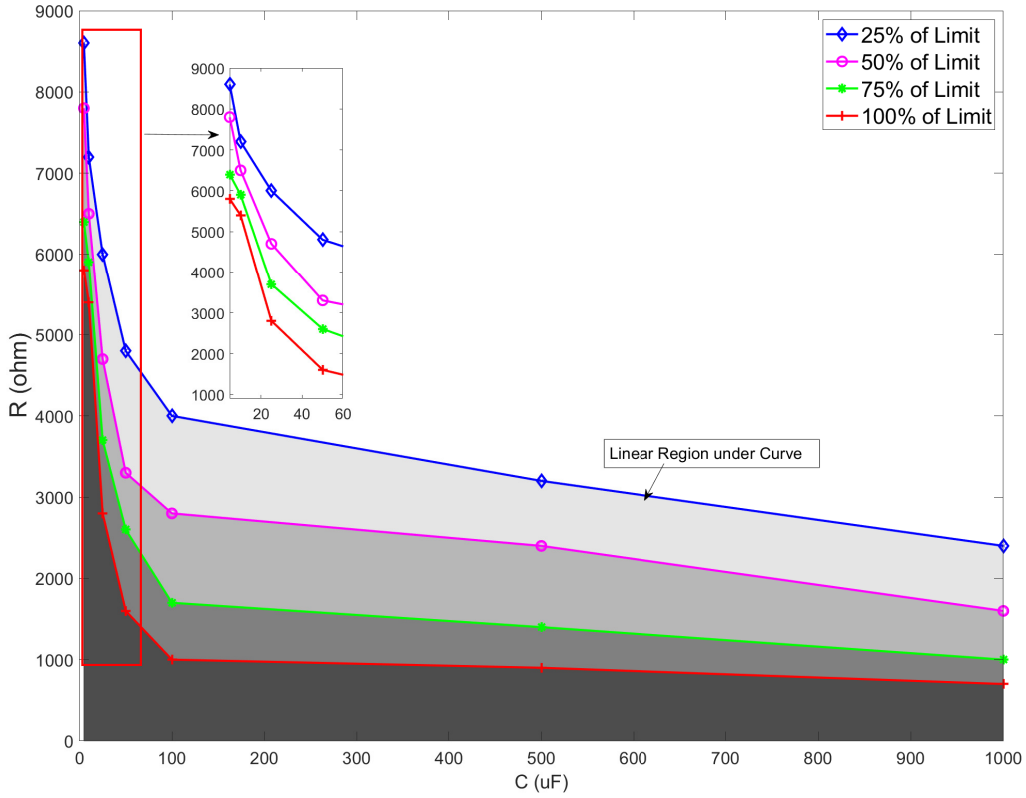

Figure 3.10 Linearity Region of Single-Phase Rectifier for Different Percentage of Harmonic Voltage Distortion Limit

A large region of linearity can be seen for 25% of the limit, and the linearity region decreased as the distortion level increased to 100% of the limit. Circuits with a smaller smoothing capacitor had a larger region of linearity. The linearity region rapidly decreased as the capacitor value increased from $1\mu F$ to $50\mu F$. Moreover, after a specific capacitor value, even doubling the capacitor value it has not make a significant difference in the region of linearity. Therefore, for small values of capacitors, the linearity region was more dependent on the value of resistors than the capacitors.

In order to define the limits of linearity, the first eight harmonics were tested. The

region of linearity for 7^{th} harmonic was smaller than the rest of harmonics. Therefore, the nearest distortion level was considered which produces a linear circular locus for 7^{th} harmonics.

3.6 SUMMARY

For the validation of tensors, this chapter successfully compared the results generated from the laboratory experiment and the computer simulations. Laboratory testing was performed using a Programmable AC Source and PQ analyser. For the first time the tensors of different non-linear devices are added to form a resultant tensor that illustrates the whole house without compromise in accuracy. Also, the region of linearity is defined for different harmonic distortions levels.

Chapter 4

TENSOR REPRESENTATIONS OF AN ELECTRICAL DISTRIBUTION FEEDER AND VALIDATION

4.1 CHAPTER OVERVIEW

Modelling of LV distribution networks has been challenging due to the size of the system and the deployment of a large number of different power electronic devices. Moreover, there are other factors that make this analysis complex, such as network topology, levels of voltage distortion, and the time-varying nature of loads.

A number of publications have been presented to explore the harmonic behaviour of different non-linear devices [Watson et al. 2009a],[Sharifian et al. 2005],[Rawa et al. 2011],[Doroshin and Neri 2014],[Kazibwe et al. 1990]. However, most of these examined the impact of one or a few home appliances on the distribution network. Therefore, it is essential to consider the combined effect of non-linear devices for better assessment. To date, the CI method has been considered for modelling. This modelling does not evaluate the interaction between non-linear devices and the a.c. system nor the interaction between multiple non-linear devices. Typically, traditional frequency-domain analysis solves a set of equations without considering these interactions. However, tensor representation forms an incremental admittance matrix, which models the interaction between non-linear devices and the a.c. system or between multiple non-linear devices accurately.

The first part of this chapter provides an overview of non-linear devices such as CFL, refrigerator, TV, oven, heat-pump, etc. PSCAD/EMTDC is used as a benchmark to build a library of tensors of non-linear devices.

The second part of this chapter introduces the harmonic representation of a distribution feeder using both time-domain and frequency-domain simulations. Time-domain simulation is exclusively used to model the test feeder as a benchmark to compare with other simulation algorithms. MATLAB simulation is used for the tensor representation of the distribution test system. Multiple houses, with various non-linear devices, have been connected with a test a.c. system. This chapter shows for the first

time how the tensors for each non-linear device can be combined to form a resultant tensor that represents the whole house without a compromise in accuracy. The tensor representation of the test system is compared with, and validated against, the CI and time-domain simulations. Once validated, the tensor-based simulation will replace CI and time-domain simulations for modelling large distribution networks.

4.2 HARMONIC CHARACTERISATION OF POWER ELECTRONIC DEVICES USING PSCAD/EMTDC

The use of modern power electronic-based loads is increasing dramatically due to their advantages. One key advantage is their energy efficiency. Power electronic converters in these devices can be categorised into three groups, namely:

- **Small-sized** converters are used in residential appliances, i.e., TV, PC, battery charges, printers, and lightings.
- **Medium-sized** converters are being used for industrial purposes to control motor speed, such as Variable Speed Drives (VSDs).
- **Large-sized** converters are installed in the transmission and distribution systems to overcome technical issues — for example, HVDC transmission, STATCOMs, SVCs, and solid-state voltage regulators.

In this thesis only small-sized converters are considered. These power electronic devices produce harmonic currents which in turn cause voltage distortion which can adversely affect equipment (cause maloperation, shorten lifetime, or even destroy) and increase losses [Hardie and Watson 2010],[Grady and Santoso 2001].

4.2.1 Non-Linear Loads

The deployment of non-linear loads is expected to increase with the installation of modern Televisions (TVs), PVs, advanced air conditioning systems, plug-in EVs, lighting equipment (LED and CFLs), VSDs systems, and appliances with VSDs such as fridges and freezers, as well as other standard residential and commercial loads. By installing more power electronic equipment, an increase in harmonic currents injected into the system will result [Watson et al. 2009a],[Sharifian et al. 2005],[Rawa et al. 2011]. Harmonic currents interact with the impedance of the power system to generate the voltage distortion that affects power system equipment and the connected loads. The overall impact of these harmonic currents depends on the number of non-linear devices and their harmonic diversity. The harmonic diversity depends on the type of

loads and their operating condition as this determines the phase angle of the harmonic currents and hence whether they reinforce or reduce the overall harmonic voltage magnitude [Sharifian et al. 2005].

Table 4.1 Electronic Devices and their Ratings

Devices	Power Ratings (W)	I_{rms} (A)
Lighting Equipment	25	0.1023
Refrigerator	480	0.6118
Laptop Charger	250	0.310
Microwave	1200	6.035
TV	150	0.428
Induction Cooker	2000	4.474
PC	800	0.838
Heat-Pump	1350	5.400
Vacuum Cleaner	1450	6.808
Washing Machine	500	2.950

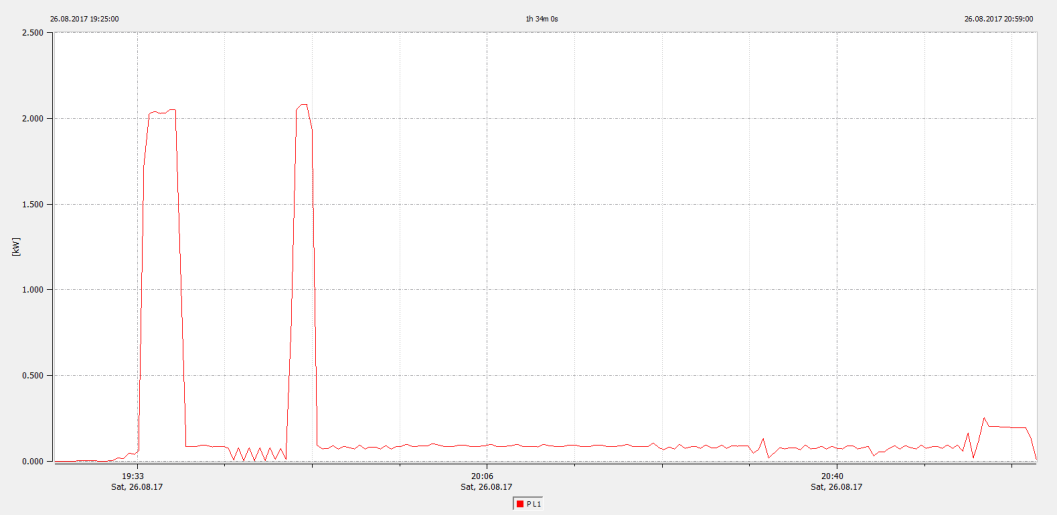

Figure 4.1 Washing Machine Power Demand Waveform for a Complete Cycle

Different devices, shown in Table 4.1, as a circuit-based were modelled in PSCAD/EMTDC. These are not the maximum appliance's ratings but these are assumed operating point. Some appliances basically change their demands during their cycles. For example testing of washing machine is shown in Figure 4.1. Mostly, the demand was jumping around 0.8A. However, it jumped to 2.2 kW (around 10A) only when washing machine was heating water and which was mainly resistive. Therefore, when simulating loads, the lower power level were considered rather than the maximum.

4.2.1.1 Lighting Equipment

Energy-efficient lighting technologies are being introduced on a large scale, which are cost-competitive and have an increased lifespan. Electric lights have extensive usage throughout the day to provide safer working conditions and comfortable living environments. The total energy demand for lighting in residential and business areas is considerable as shown in Figure 4.2 [European Commission 2010].

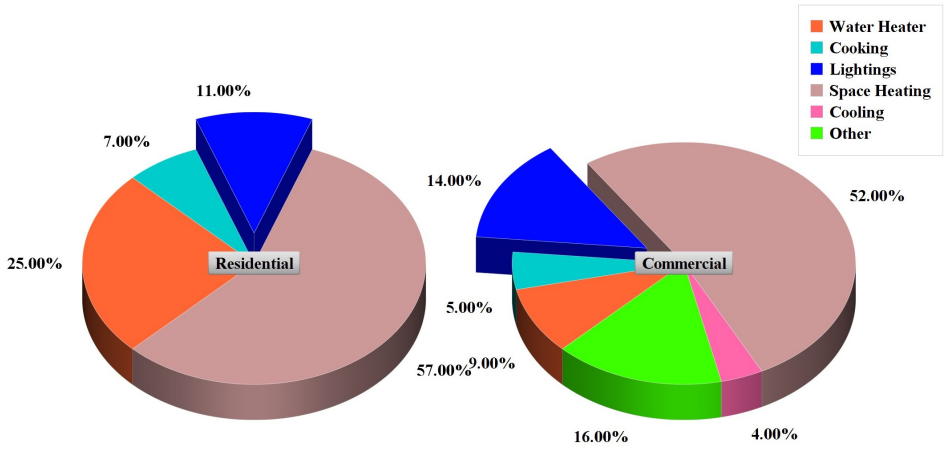

Figure 4.2 EU building energy consumption for residential and commercial buildings [European Commission 2010]

Recently, LEDs and CFLs have emerged as energy-efficient alternatives to conventional incandescent lamps and have quickly replaced them. CFLs are still commonly used for residential and commercial purposes because of their low energy consumption and long lifetime compared with incandescent bulbs. However, because of their non-linearity, they inject harmonics into the system. The harmonic effect of individual luminaries on the power network is very low because of their small power rating, however their collective can become significant.

In this research, lighting equipment of different power ratings are modelled in PSCAD/EMTDC. LEDs and CFLs have quite similar cross-coupling and effects because they convert from AC to DC. The cross-coupling tensor admittance matrix is calculated for the first eight harmonics of lighting equipment. Figure 4.3 depicts the tensor matrix obtained using AAL (were calculated as per Section 2.7.2) for all the cross-couplings up to the 8th harmonic. Note that the negative magnitudes means a different sign on the incremental currents for the incremental change of voltage. Also, note that there are significant off-diagonal entries showing coupling between the harmonics orders. The significance of large or small tensor magnitudes can be explained while looking at the currents flowing through the admittance in the Norton equivalent circuit (Figure 1.1b). A very low magnitude of tensors means that there

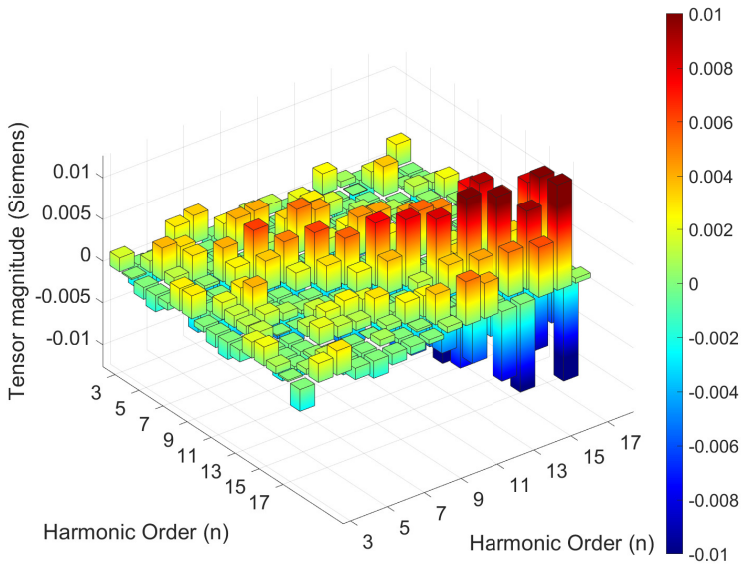

Figure 4.3 Lighting Equipment Tensor Matrix for All Harmonics

will be low change in current ΔI for the change in voltage ΔV, which indicates a stable relation. However, with a large magnitude of tensors, there will be a significant change in current ΔI and possesses high variability.

The magnitude and phase angle of the harmonic currents of lighting equipment obtained using tensor representation are compared with PSCAD/EMTDC in Figure 4.4. These show a very good agreement. Similarly, different tensor matrices for lighting equipment of different ratings were built and stored in the tensors library.

4.2.1.2 Microwave

Microwaves are one of the commonly used appliances in both domestic and commercial food serving kitchens. Microwave ovens are frequently used for heating foods, however, several surveys showed that these are increasingly being used for cooking and defrosting for a long-duration. Therefore, harmonic studies of the microwave are becoming an important research area in recent years. The harmonic effect of a microwave oven is much higher than the lighting equipment. The THD in the current waveform is measured to be approximately 32.6%.

Cross-coupling admittances for all frequencies are shown in Figure 4.5. The magnitude of tensors of all diagonal terms are high and equal, however, off-diagonal terms are very low indicating little cross-coupling between harmonics of different orders. Comparison of harmonics current obtained using tensors, and PSCAD/EMTDC is

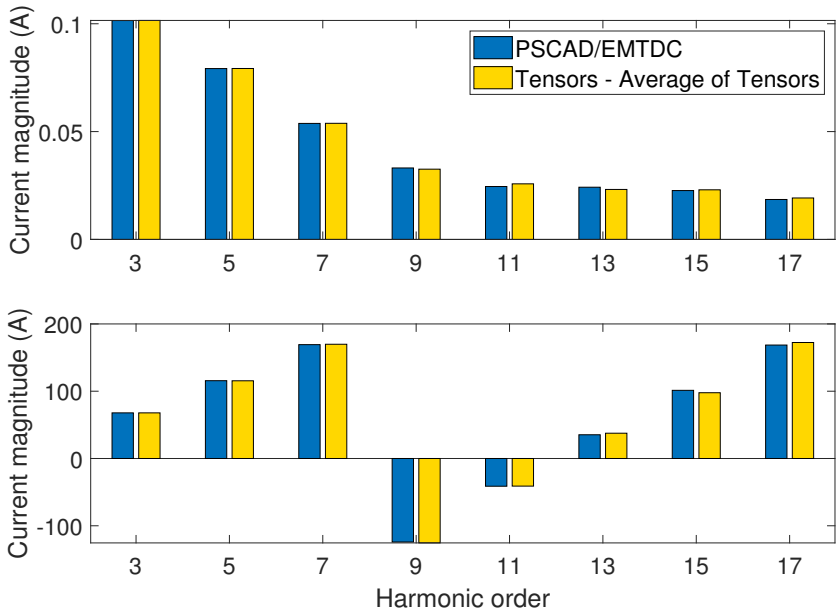

Figure 4.4 Lighting Equipment Comparison of Tensors and PSCAD/EMTDC

presented in Figure 4.6. and again good agreement is obtained.

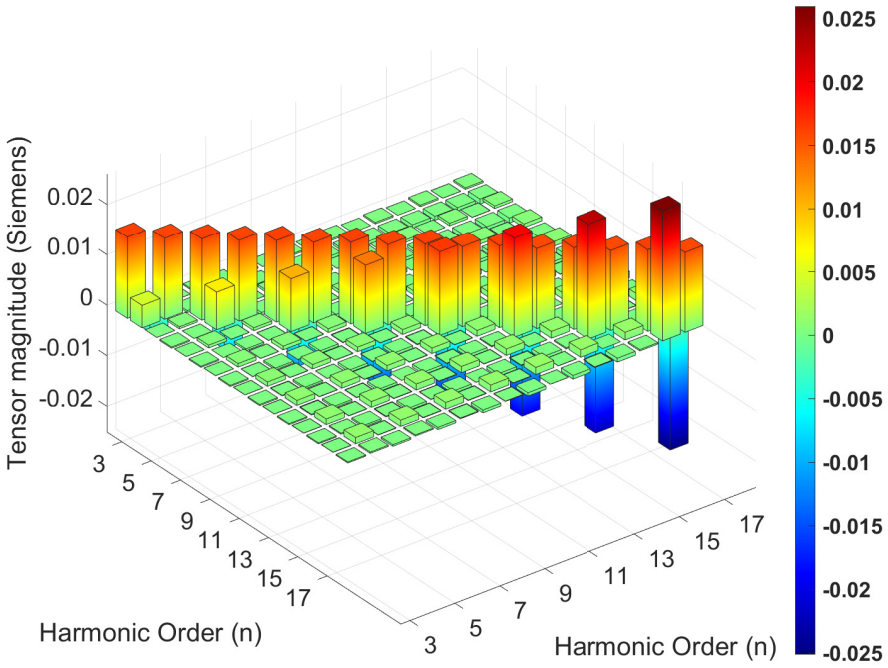

Figure 4.5 Microwave Tensor Matrix for All Harmonics

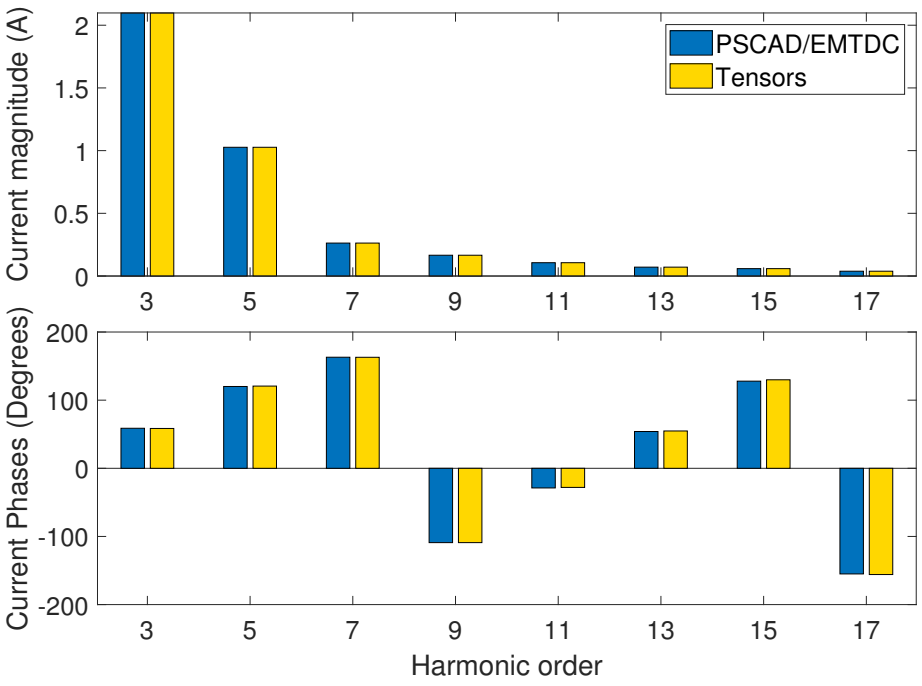

Figure 4.6 Microwave Comparison of Tensors and PSCAD/EMTDC

4.2.1.3 Refrigerator

A VSD based refrigerator is an example of periodic a non-linear load that injects harmonics into the distribution networks. Considering refrigerators work throughout the day, their harmonic components are becoming more important.

Rectifier circuit was modelled in PSCAD/EMTDC to represent the front end of a modern fridge-freezer. There is not much cross-coupling at the off-diagonal values. There is only cross-coupling at the mediate. The THD of the refrigerator is small relatively when compared with other appliances. Figure 4.7 displays the 3D bar representation of the tensor matrix of a refrigerator.

The comparison of the current harmonic spectrum using PSCAD/EMTDC and tensors representation is shown in Figure 4.8. The third harmonic current is dominant compared to other harmonics, which is 15% of the fundamental component. I THD is calculated, to be 27% of the fundamental current.

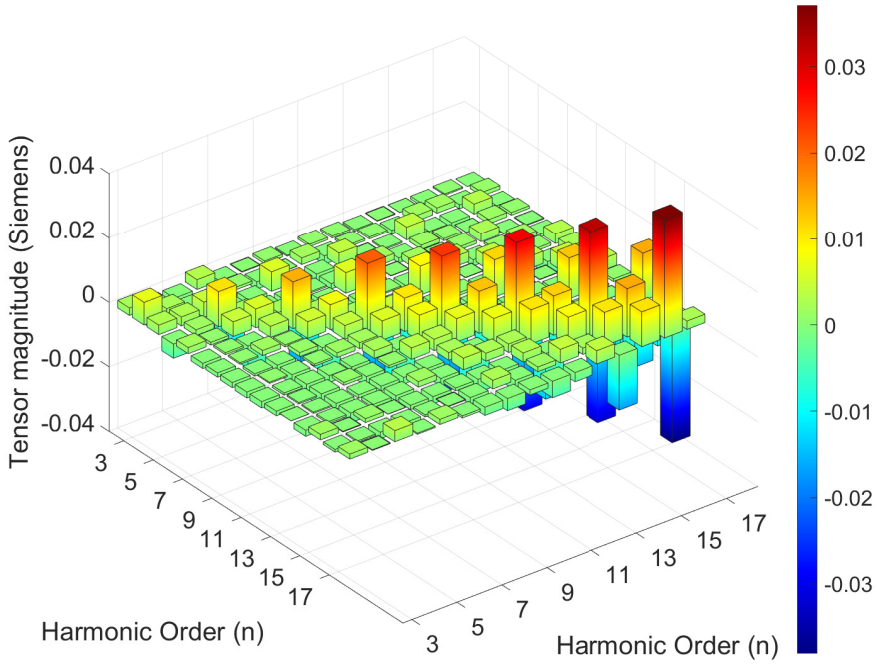

Figure 4.7 Refrigerator Tensor Matrix for All Harmonics

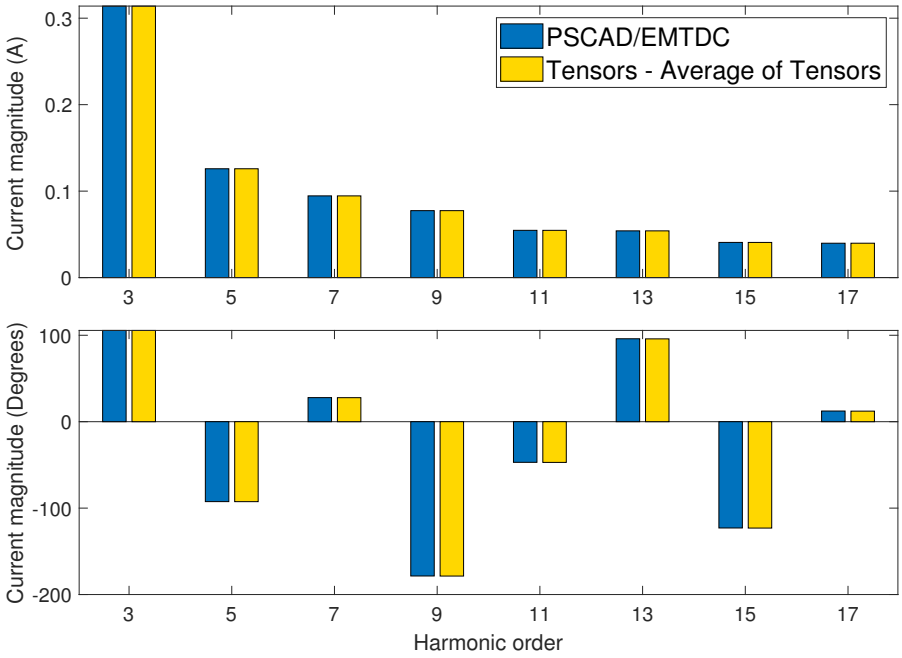

Figure 4.8 Refrigerator Comparison of Tensors and PSCAD/EMTDC

4.2.1.4 Laptop Charger

Nowadays, a large number of people own laptops. Most of the time, laptops chargers are continuously connected to the power supply and produce harmonic currents that are being injected into the electrical networks. It is observed that harmonics from laptops are notable up to 50^{th} harmonics.

Figure 4.9 show the cross-coupling between harmonics. Same as the refrigerator, there is a low cross-coupling at the off-diagonals. A significant agreement can be seen between tensors and PSCAD/EMTDC as shown in Figure 4.10.

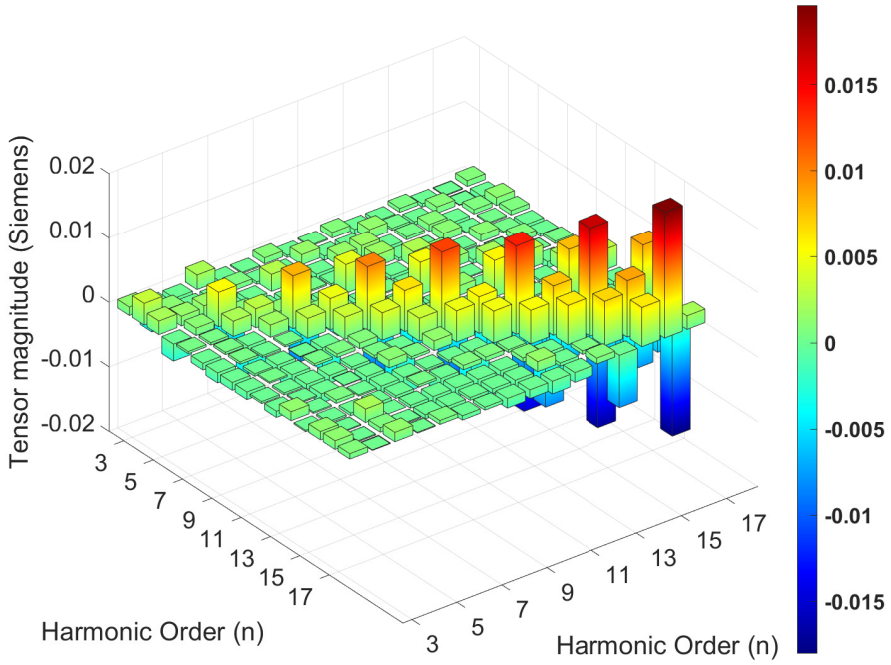

Figure 4.9 Laptop Tensor Matrix for All Harmonics

4.2.1.5 TV and PC

A large number of Personal Computers (PCs) and Televisions (TVs) are presented in a distribution network and cause harmonic distortion. The Liquid Crystal Display (LCD) technologies, which replace Cathode-ray Tube (CRT) screens, are injecting higher current harmonics into the network. Moreover, extensive research showed that a significant amount of harmonic distortion cause in the distribution network during different sporting events [Leitão et al. 2007],[Browne et al. 2007].

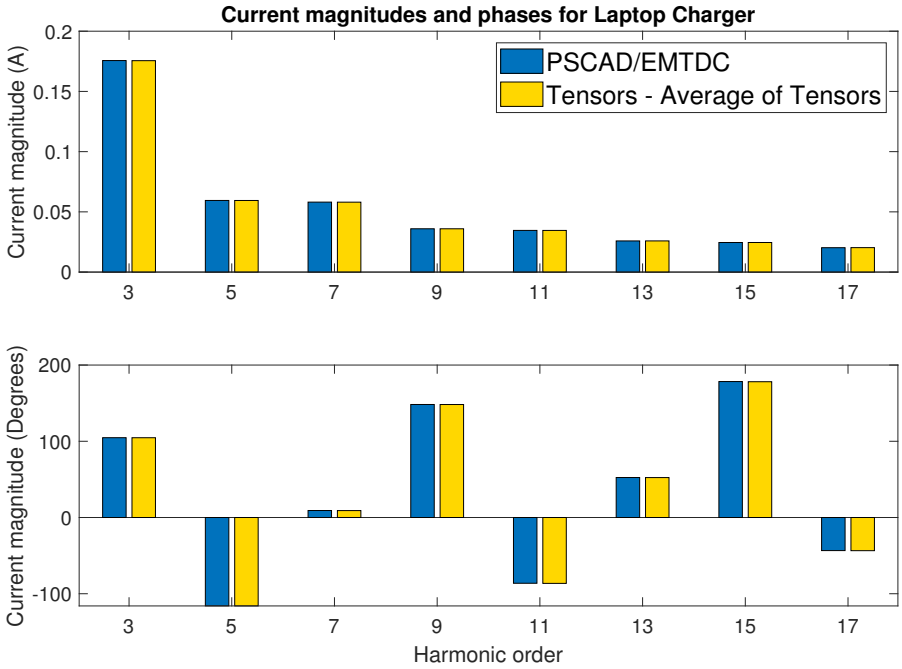

Figure 4.10 Laptop Charger Comparison of Tensors and PSCAD/EMTDC

Personal usage of PCs is decreasing, therefore, the effect of the harmonic component generated is rarely seen in the residential networks. However, these PCs do cause quality issues when many are used in the same location as in some educational and commercial facilities. This is because the concentration of a large number of these devices in a single Installation Control Point (ICP) will lead to injecting high harmonic currents. Therefore, accurate modelling is necessary to deal with this situation.

In this research, a PC rating of 800 W is modelled. Similar to other devices, the cross-coupling of a PC increases from lower to higher harmonics, as shown in Figure 4.11. A significant cross-coupling is present at the off-diagonals.

The harmonic spectrum of the current obtained using PSCAD/EMTDC and tensor analysis is shown in Figure 4.12. Note that the current spectrum is relatively high for all the harmonics unlike other devices previously mentioned in this chapter.

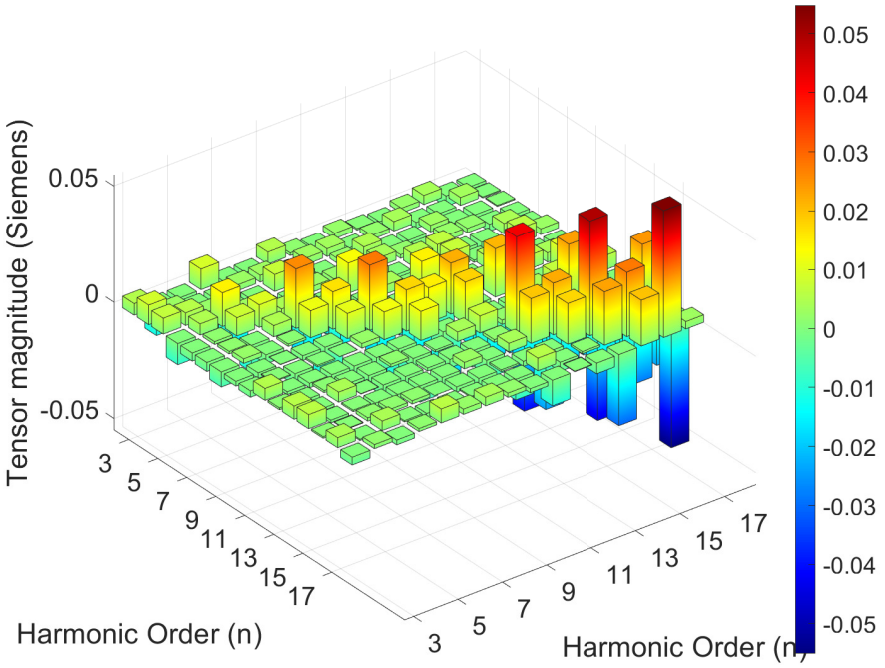

Figure 4.11 PC Tensor Matrix for All Harmonics

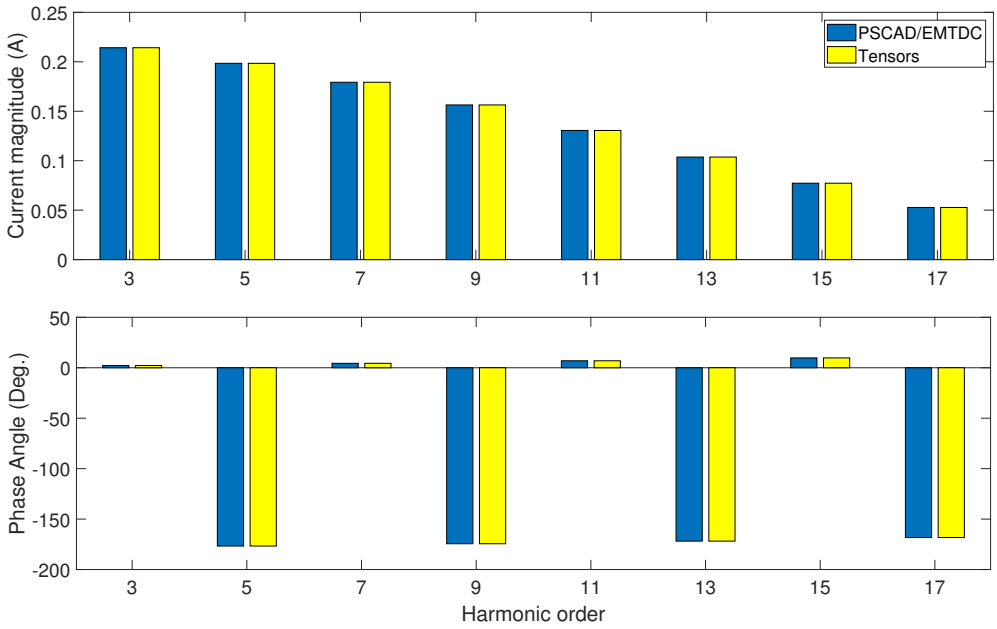

Figure 4.12 TV Comparison of Tensors and PSCAD/EMTDC

Table 4.2 Selection of Tensors of Different Devices for all Houses

	Library of Tensors of multiple devices	House 1	House 2	House 3	House 4
1	Lighting Equipment	X	X	X	XX
2	Refrigerator	X	X	X	X
3	Laptop Charger			X	X
4	Microwave	X	X		X
5	Washing Machine				X
6	TV	X			
7	Induction Cooker	X	X	X	X
8	PC		X		

4.3 MODEL IMPLEMENTATION - TENSOR REPRESENTATION OF A DISTRIBUTION FEEDER

In this section, a tensor representation of a distribution feeder is obtained for harmonic analysis. This harmonic analysis included multiple non-linear devices in different houses to simulate the condition of an actual feeder. Relying on the tensors for individual devices obtained using PSCAD/EMTDC in the previous section, the tensor presentation is expanded to obtain a tensor incorporating all devices in each house. Moreover, this section discusses the process of including the service-main impedance and its effect on the tensor matrix. After obtaining a tensor representation of the distribution feeder in the frequency-domain, the results were compared with the CI method and PSCAD/EMTDC.

A simple feeder of a distribution network supplied by 150kVA delta/wye transformer with impedance Z_{sc} of 5%, as shown in Figure 4.13, was taken as the test feeder. The feeder is modelled using series resistance of 0.297 ohm/km and inductance of 0.0295 ohm/km as a line impedance [Elphick 2011]. It is connected to four houses via a service-main line. This service-main line is assumed to be 20 metres for all houses which is an average length of a service mains. Each house contains several random non-linear households (between 5 to 8 devices) as shown in Table 4.2 and a linear load of 3 kW in some cases.

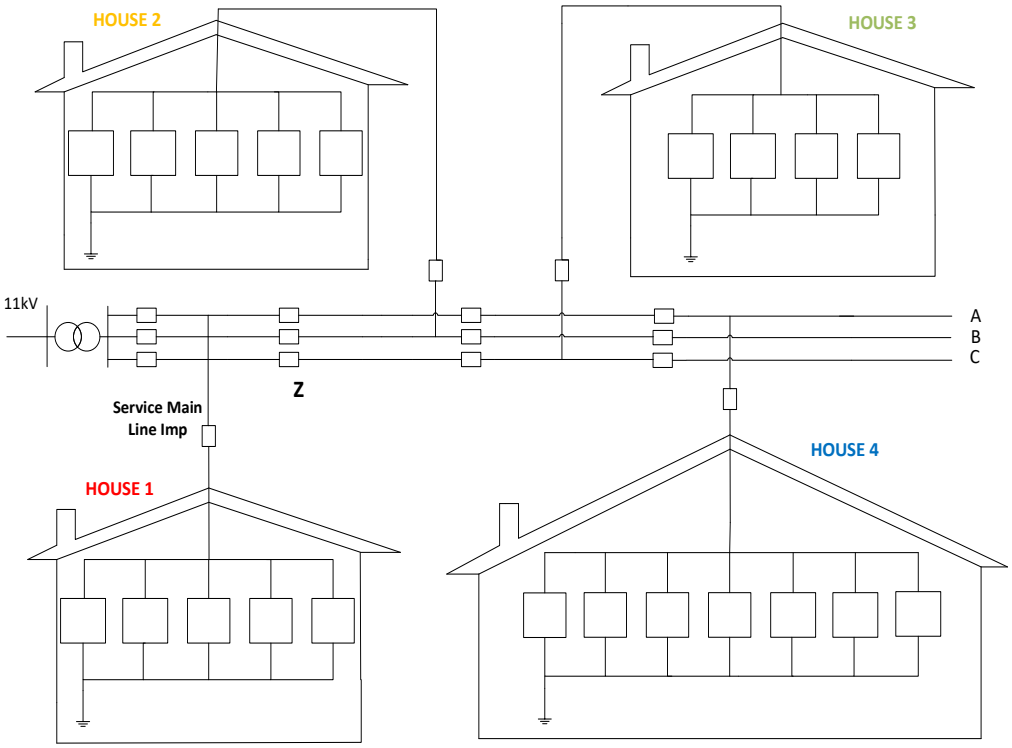

Figure 4.13 Modelling of One Feeder

4.3.1 Time-Domain Modelling

In order to validate the tensor approach, time-domain PSCAD/EMTDC simulation is used as a benchmark because it inherently integrates the operating point of the system and any corresponding distortion in the system. However, as already mentioned, this tool is not able to model large distribution networks completely. Moreover, this approach requires a long simulation time to obtain steady-state solutions.

The test feeder, shown in Figure 4.13, is modelled in PSCAD/EMTDC which involves both linear and non-linear loads. PSCAD/EMTDC simulation with a time-step of $50\mu s$ and a simulation period of $0.5s$ is performed to obtain the current waveforms for aggregated house loads, as shown in Figure 4.14. The magnitudes of the aggregated house currents varied from house to house depending on the number and type of its loads. As it can be seen that the house 4 has the highest current magnitude of about $20A$ as it has eight devices connected. On the other hand house 3 has the lowest magnitude, about $10A$, as only four devices are connected. Also, the distortion in each waveform differs as will be evident when the harmonics components are inspected later.

For the frequency analysis, a three-phase FFT block in PSCAD/EMTDC is used to measure the magnitude and phase angle of the harmonic currents, as shown in Figure 4.15. As can be seen, the higher-order harmonic magnitude is noticeable in house 2 and 4 because of the presence of the PC device (as it was shown in Section 4.2.1.5). These results are used for the verification of the tensor approach to harmonic analysis of a system.

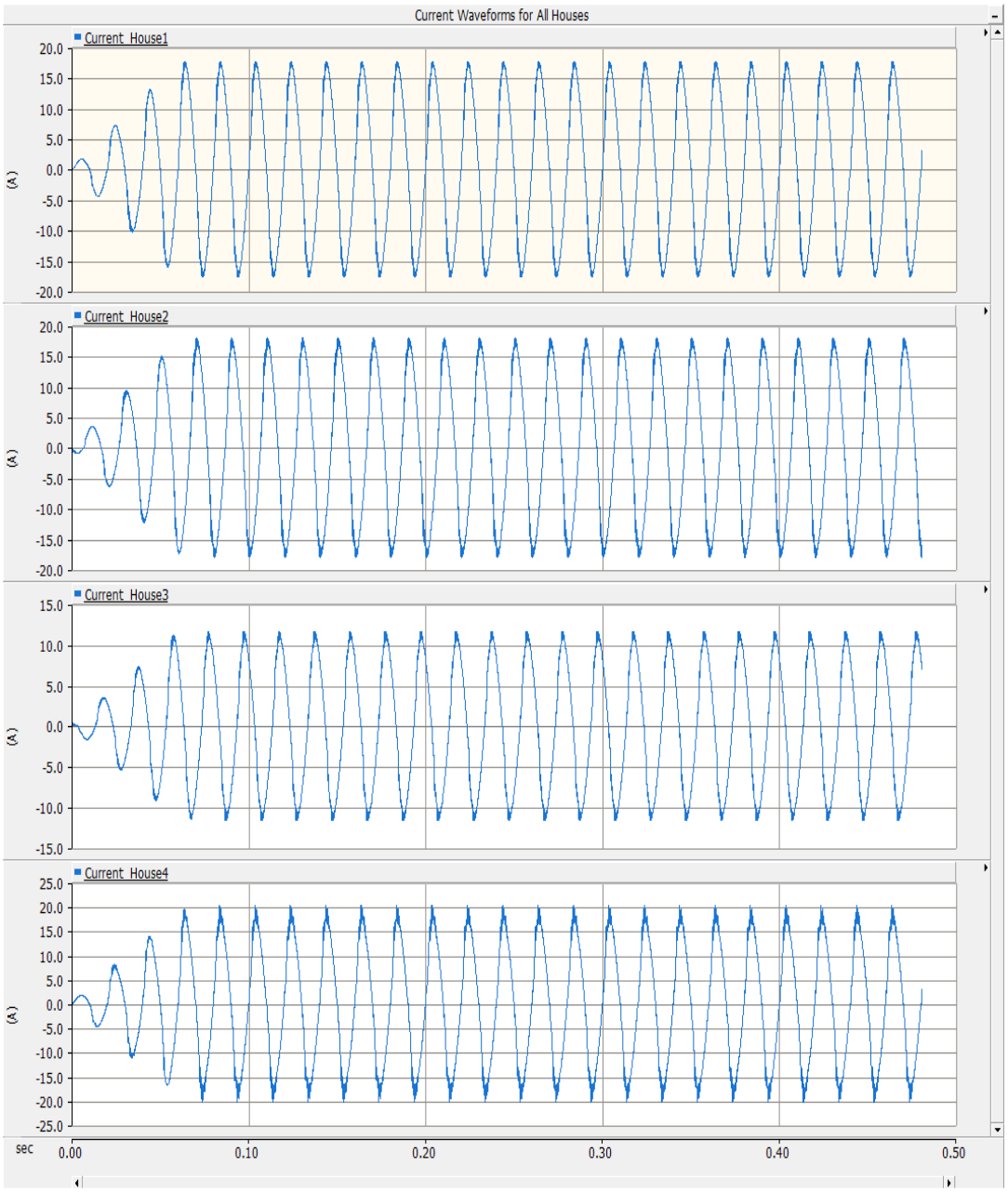

Figure 4.14 PSCAD/EMTDC - The current Waveforms for All Houses

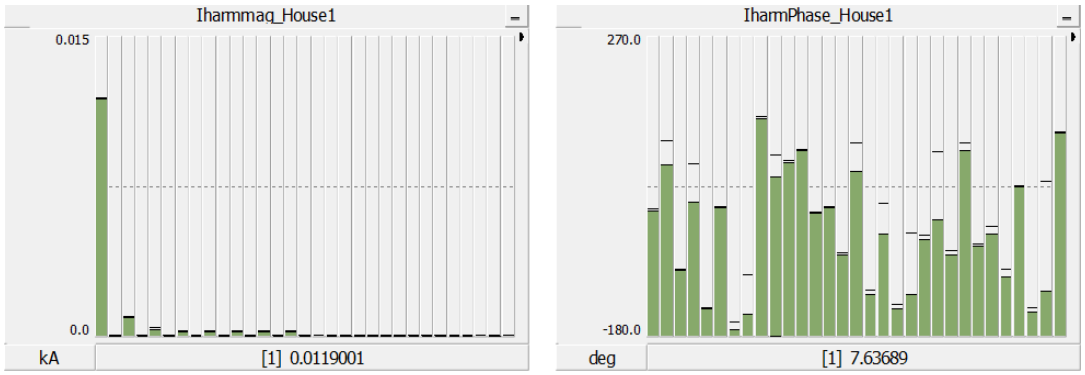

(a)

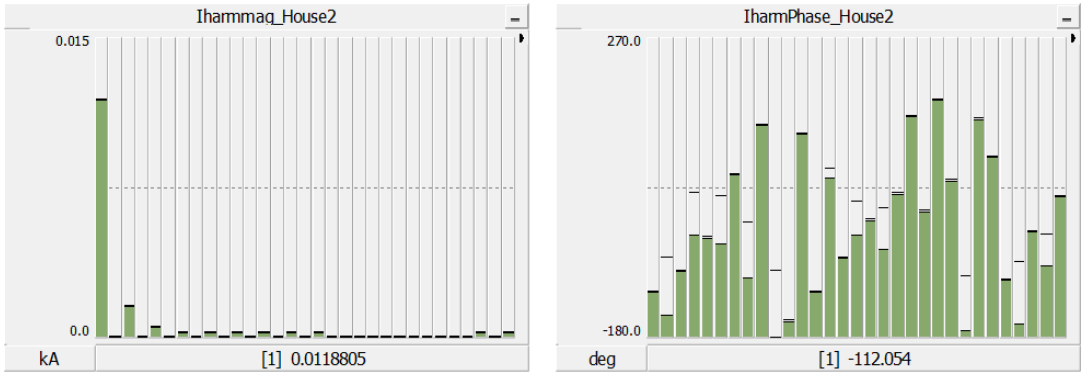

(b)

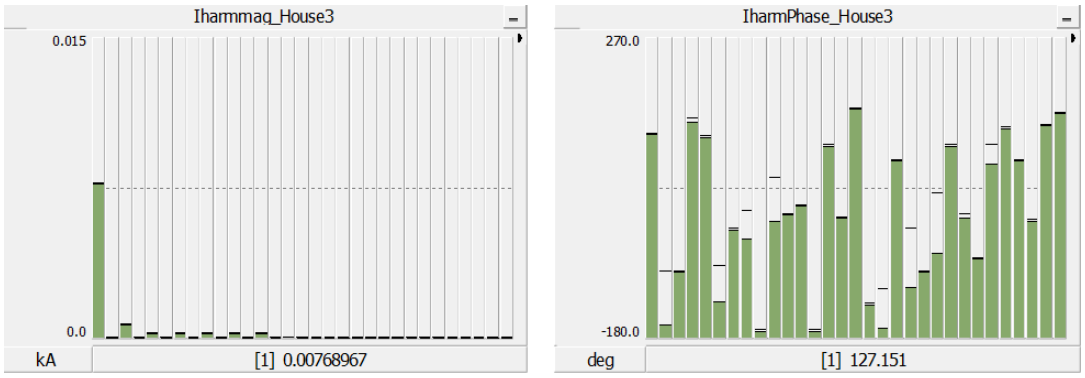

(c)

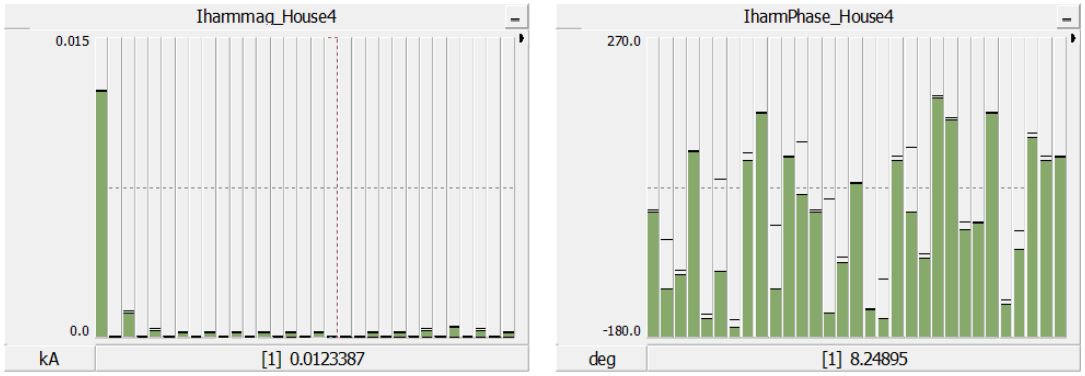

(d)

Figure 4.15 Harmonic Currents Magnitudes and Phases (a) House 1 (b) House 2 (c) House 3 (d) House 4

4.3.2 Frequency-Domain(Tensor Representation)

MATLAB was used to obtain a tensor representation of the test feeder. Frequency-domain models have a short simulation time compared to time-domain PSCAD/EMTDC.

In this research, the harmonic modelling of the distribution network using tensors is divided into three stages: creating tensor matrices, tensors addition, and solving the system equations iteratively as shown in Figure 4.16.

Stage 1: The tensor matrices of multiple non-linear devices were obtained using PSCAD/EMTDC. The resulting tensor matrices were saved as a tensor library.

Stage 2: This stage is summarised in Figure 4.17. In the transition 1, multiple tensors of the non-linear devices are aggregated to represent the resultant house tensor, as shown in Equation 4.1. Each of the admittances in Equation 4.1 is incremental admittances representing the incremental admittances in the Norton equivalent circuit shown in Figure 1.1b (Section 1.1). After aggregation, the service-main impedance is added to have a more accurate representation of a house as seen from the feeder Equation 4.2.

$$Y_{T_{House_2}} = Y_{T_{InductionStove}} + Y_{T_{CFL}} + ... + Y_{T_{TV}} + Y_{T_{Microwave}} \tag{4.1}$$

$$Z_{T_{House_2.Node}} = \frac{1}{Z_{T_{House_2}}} + \frac{1}{Z_{servicemain}} \tag{4.2}$$

Stage 3: The nodal system admittance matrix Y_{sys} is built using MATLAB depending on the parameters of the networks. Then the current injection from the base operation point I_{base} are calculated using PSCAD/EMTDC that is without distortion. V_{Nodes} are calculated based on the Y_{sys} matrix and I_{base} vector. Multiplying V_{Nodes} by the $Y_{Tensors}$ the harmonic current injection I_{Nodes} are calculated as shown in Equation 4.4. As a result, the actual harmonic currents at all nodes are determined.

$$V_{Nodes} = inv(Y_{sys})I_{base} \tag{4.3}$$

$$I_{Nodes} = (Y_{Tensors})V_{base} \tag{4.4}$$

$$I_{Nodes} = I_{base} - I_{Nodes} \tag{4.5}$$

The previous three stages are applied to the test feeder in Figure 4.13 to obtain the magnitude and phase angle for current harmonics in the frequency-domain. The resultant tensor matrices of the houses are calculated using Equation 4.1 and

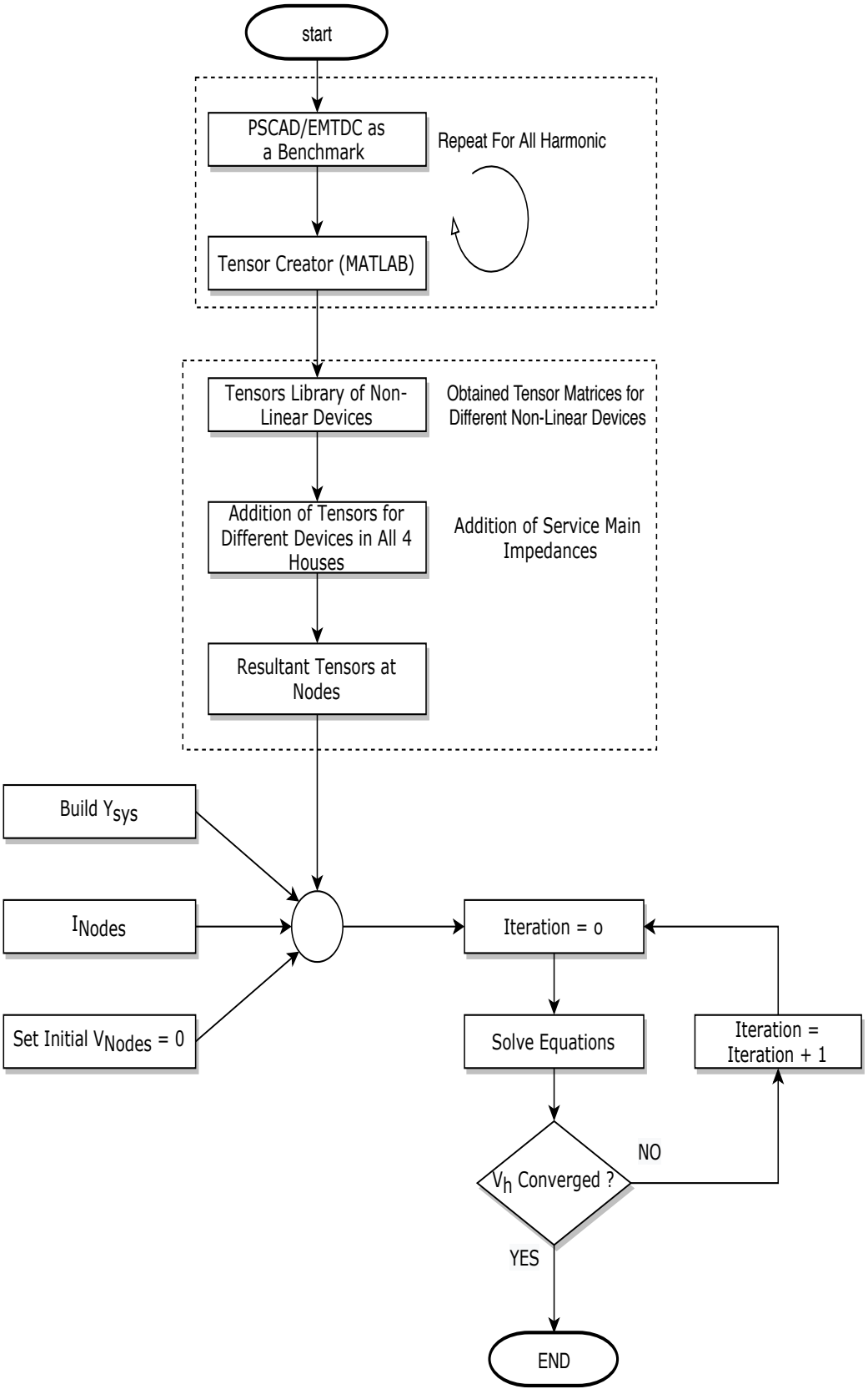

Figure 4.16 Flowchart of the Harmonic Modelling of Distribution System using Tensors

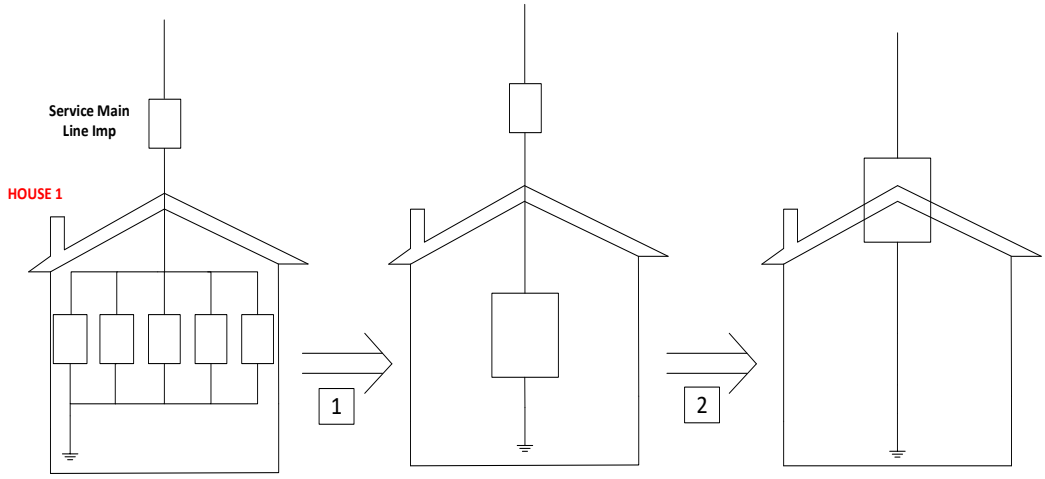

Figure 4.17 Detailed Combined Load and service-main

Equation 4.2. A visual representation of the admittance tensor matrix can be seen in Figure 4.18. It is evident that all the magnitude of tensors increases diagonally. However, house 2 shows less increase due to the nature of devices in it, especially the harmonics generated by the microwave (Figure 4.5).

Finally, Equation 4.3 to Equation 4.5 in stage 3 are solved iteratively to obtain the solution. The number of iterations to obtain convergence was three in this case, however, it could vary depending on the complexity of the system. Generally, this complexity is associated with the structure of the network and the type of devices. The magnitude and phase angle of the current harmonics were calculated to be as shown in Figure 4.19.

The nodal system admittance matrix Y_{sys} and I_{base} were calculated. In the last stage, the system was iterative until it converged. The proposed method was converged reliably, and the solution of the system was achieved. Different scenarios were analysed by considering the different number of devices for each house. The convergence rate was different for different cases, but it was computational in-expensive. The number of iterations depends on the types of devices and how many devices are being considered into the system. In this model, it took three iterations to converge the system. The different harmonic currents and the phases of all the houses are calculated, as shown in Figure 4.19.

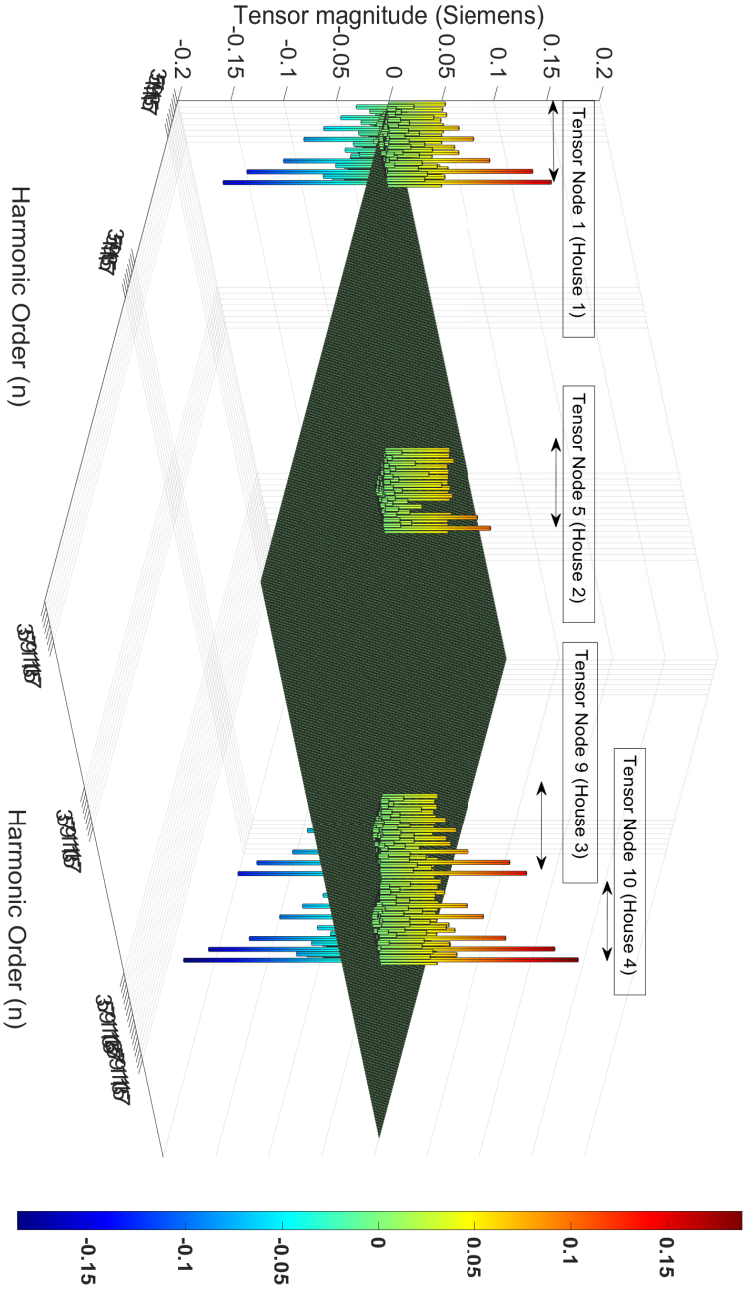

Figure 4.18 Admittance Tensor Matrix of a Feeder

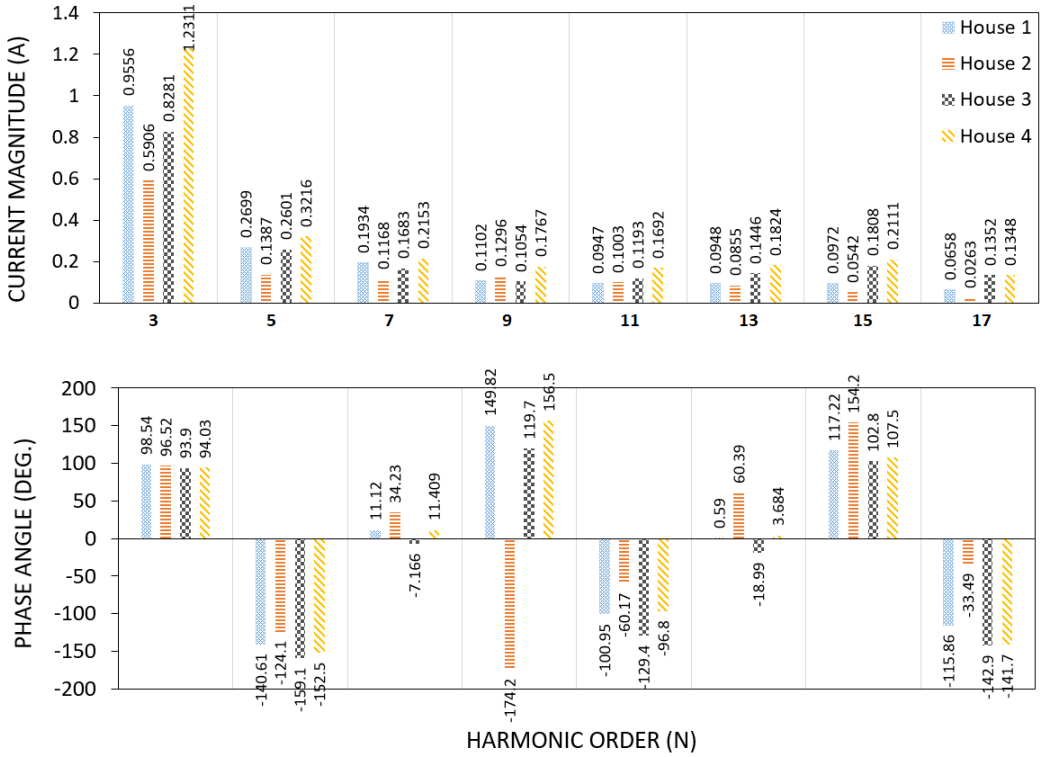

Figure 4.19 Current Magnitude and Phases of All Four Houses

4.4 SIMULATION RESULTS - VALIDATIONS

In this section, the time-domain and the frequency-domain results were compared for the test feeder. In both domains, the results obtained from tensors and PSCAD/EMTDC showed high similarity.

The tensor analysis results are converted to time-domain waveforms and are compared to the PSCAD/EMTDC waveforms to demonstrate the accuracy, as shown in Figure 4.20 to Figure 4.23. There is a significant similarity between tensors and PSCAD/EMTDC. However, the slight differences in the current waveforms for houses 3 and 4 are due to truncation of the harmonic spectra used in the tensor analysis.

The results for tensor analysis, CI and PSCAD/EMTDC are compared in the frequency-domain as shown in Figure 4.24 to Figure 4.27. The obtained results demonstrated better accuracy for the tensor and PSCAD/EMTDC compared to CI. For most of the harmonic frequencies the harmonic current from tensors and PSCAD/EMTDC are almost identical.

For house 1, the results for tensors, CI and PSCAD/EMTDC for all harmonics are almost equal. This is because house 1 is at the start of the feeder and hence the voltage distortion is the smallest and hence the smallest contribution of harmonic current through (equivalent circuit Figure 1.1b.. The voltage distortion increases for

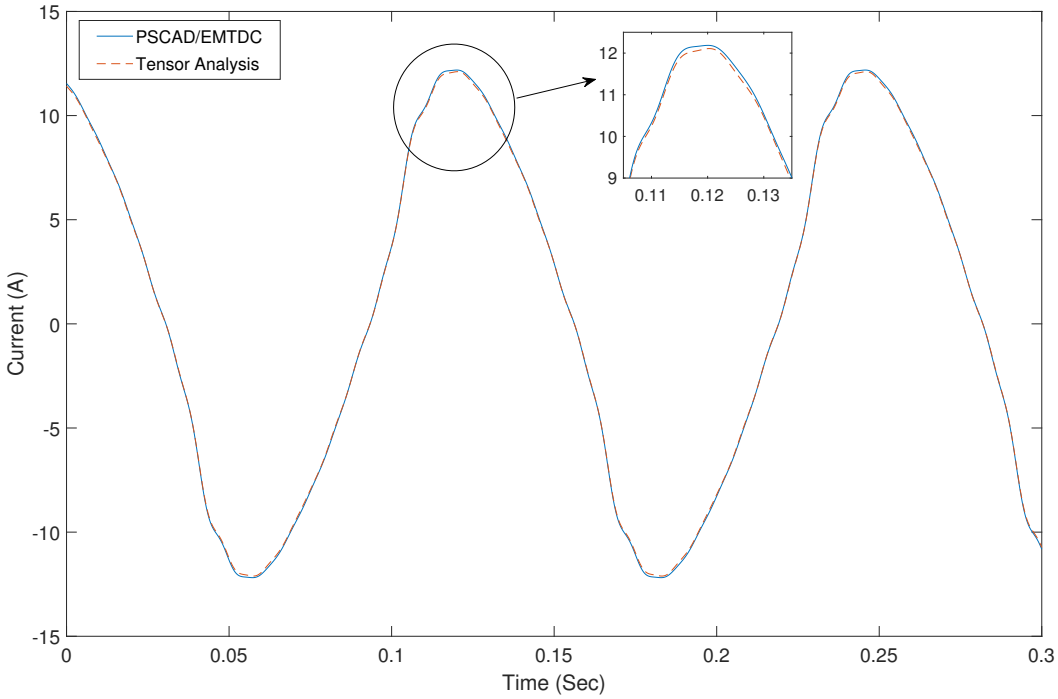

Figure 4.20 Tensors and Time-domain comparison for House 1

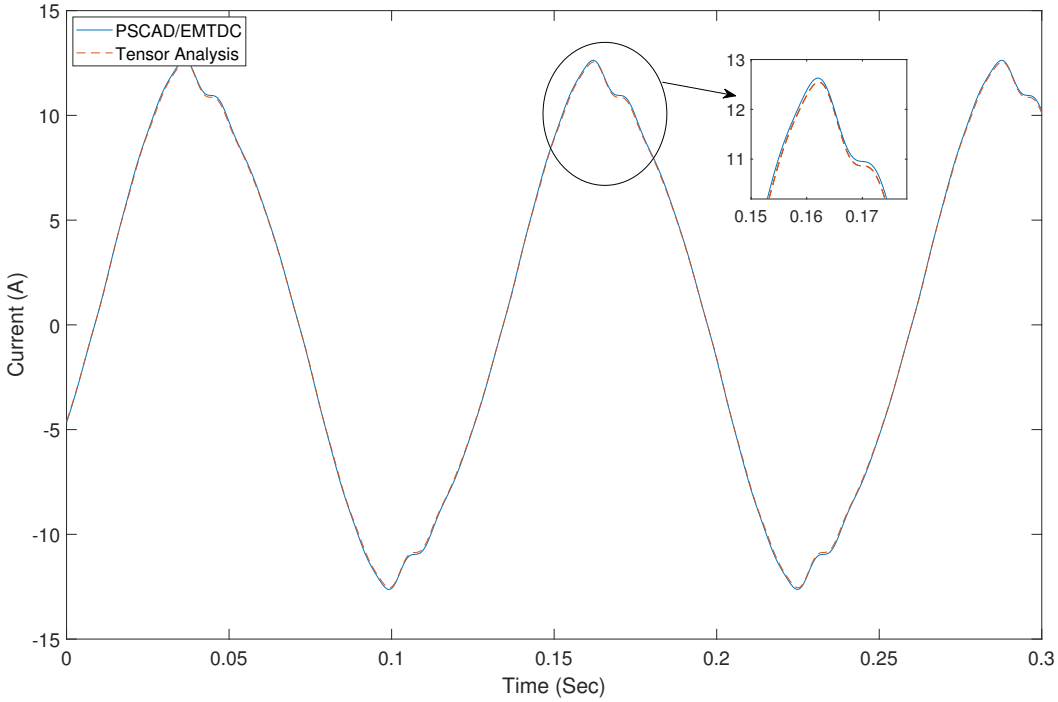

Figure 4.21 Tensors and Time-domain comparison for House 2

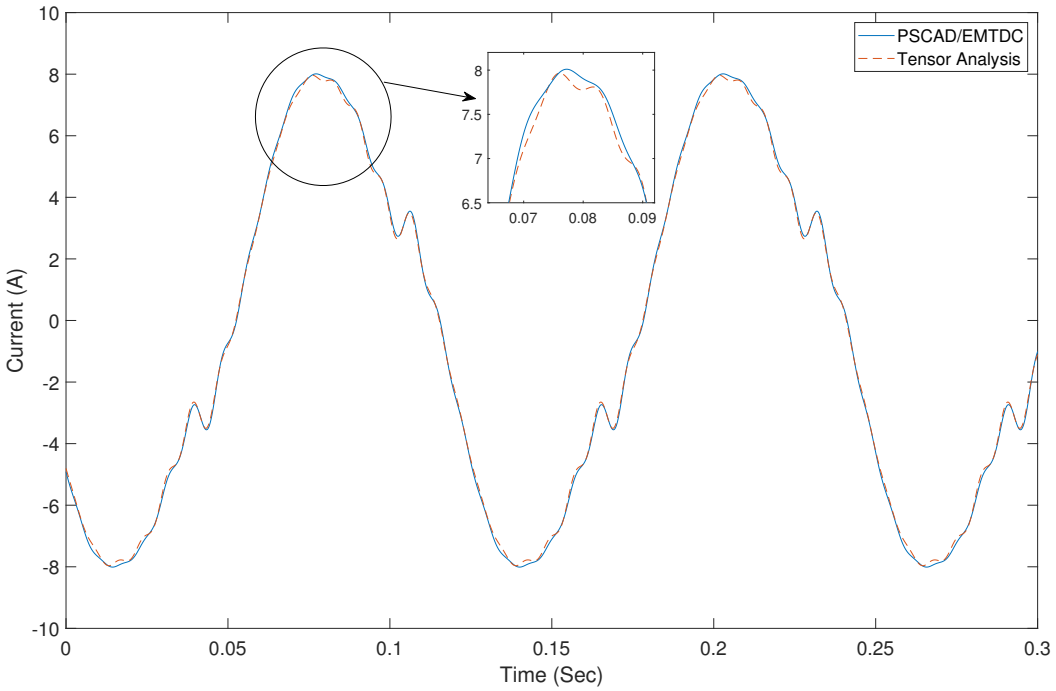

Figure 4.22 Tensors and Time-domain comparison for House 3

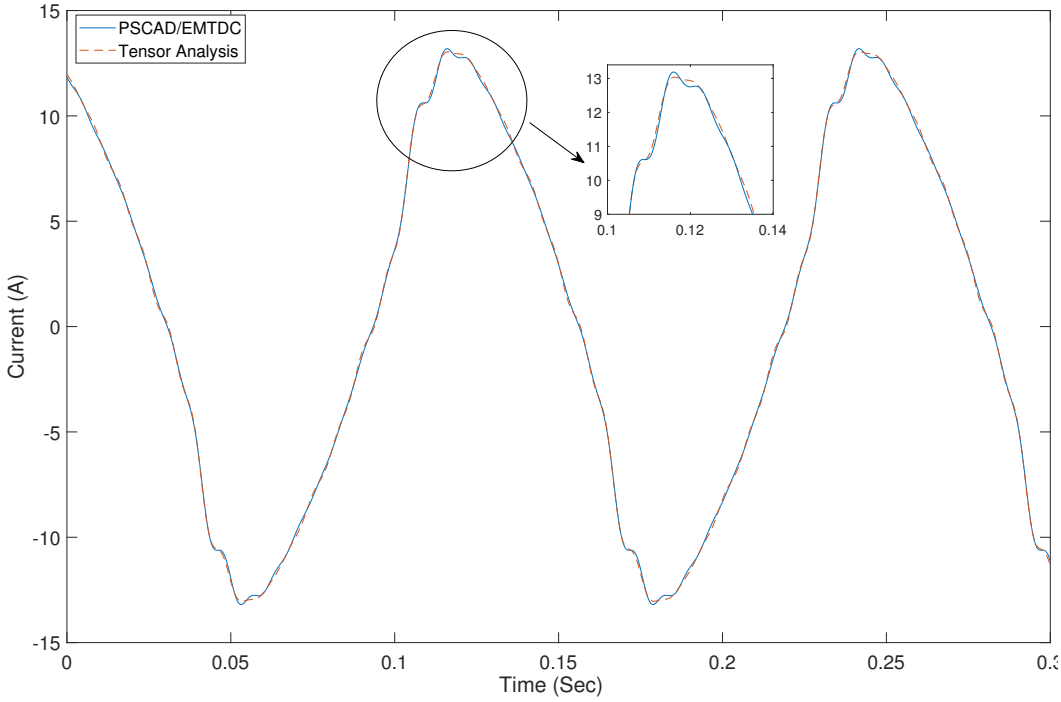

Figure 4.23 Tensors and Time-domain comparison for House 4

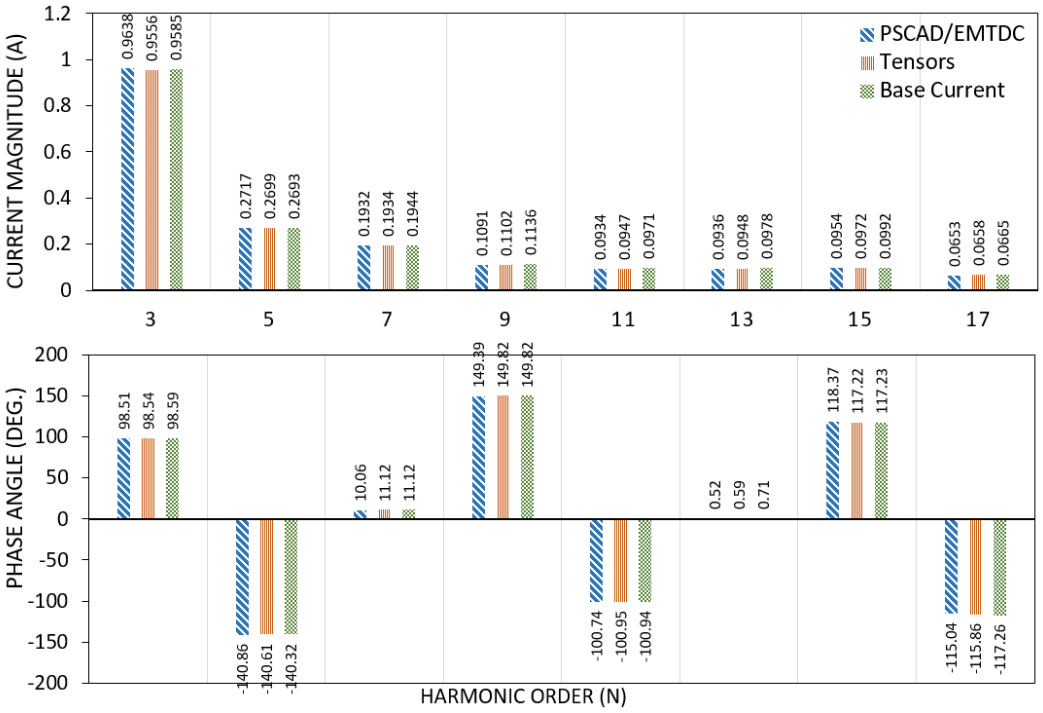

Figure 4.24 Current Magnitude and Phases of House 1

houses connected far from the a.c. source, therefore, the contribution of harmonic current increases. The interpreted results showed a difference for houses 2, 3 and 4, especially when compared to the CI method. The difference gets prominent for higher harmonics because, in the CI method, the non-linear devices are represented by fixed current sources. The harmonic CI method does not consider the harmonic interaction with the AC electrical network. Therefore, the CI model exhibits under or overestimation of the current magnitudes and phase angles compared to tensor and PSCAD/EMTDC results. There is strong agreement between the tensor approach and PSCAD/EMTDC. This new approach is expected to replace the CI method when accurate harmonic studies are needed.

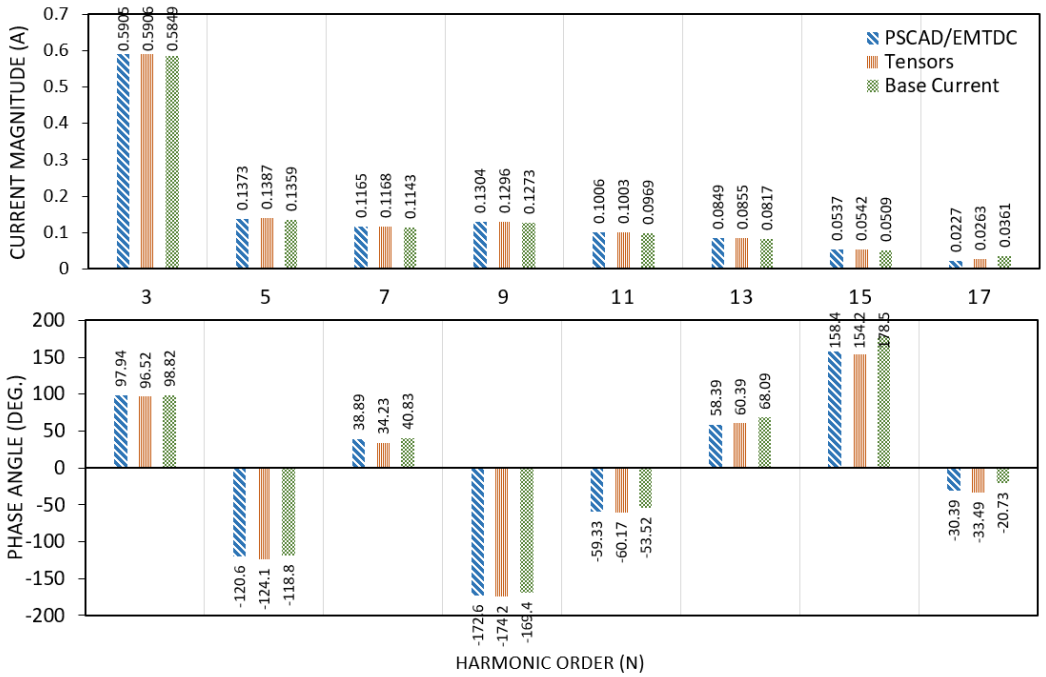

Figure 4.25 Current Magnitude and Phases of House 2

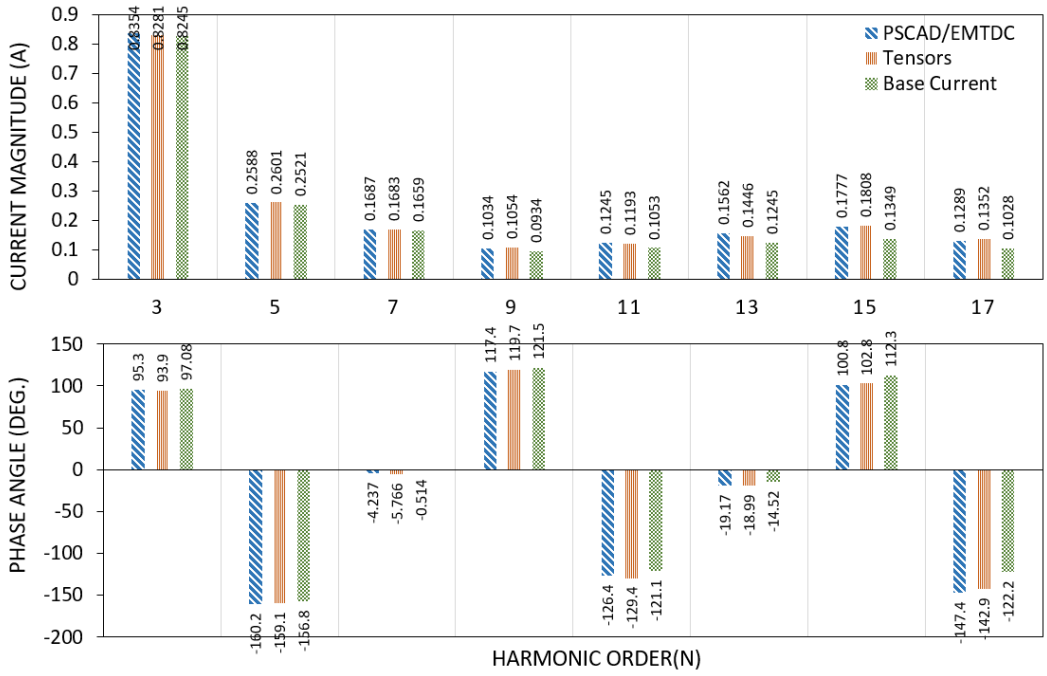

Figure 4.26 Current Magnitude and Phases of House 3

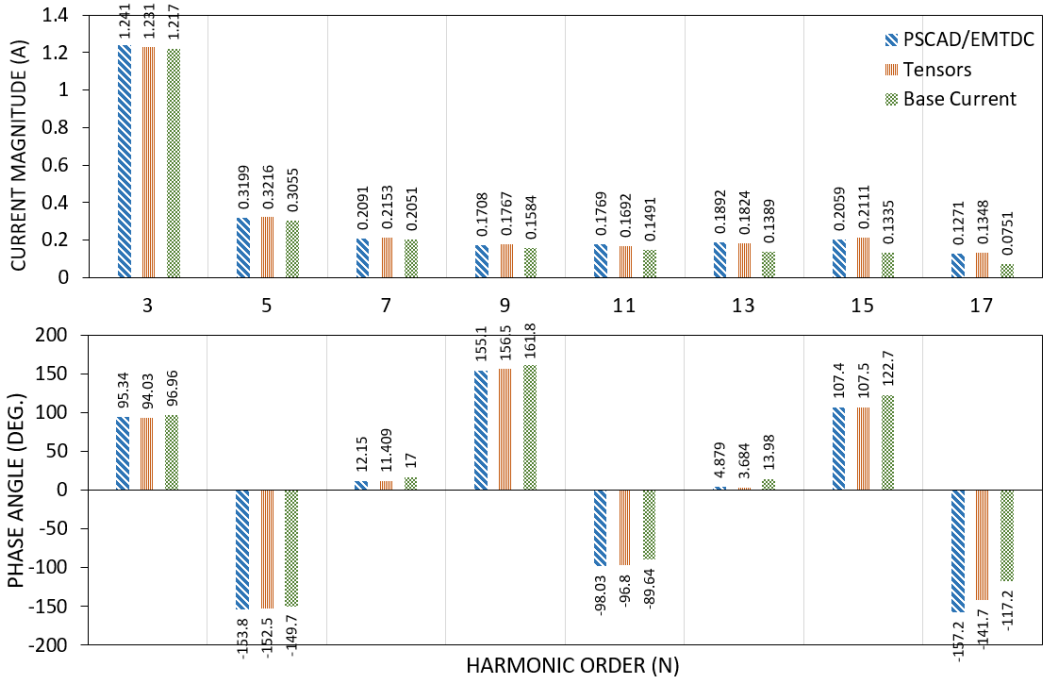

Figure 4.27 Current Magnitude and Phases of House 4

Chapter 5

APPLICATION TO DISTRIBUTION SYSTEMS

Harmonic analysis of distribution networks is becoming important as a large number of non-linear devices are being installed into the system. The detailed modelling of LV networks will help to provide a more accurate assessment of harmonic levels. Hence, the harmonic modelling of distribution networks is important to ensure that no adverse effects will be encountered. In this study, the tensor-based harmonic spectrum library of commonly used non-linear household appliances (built in chapter 4) is utilised. This chapter will extend the work of chapter 4 by evaluating distribution network harmonics.

Moreover, due to residential and commercial load fluctuations, different loading scenarios and demand patterns are investigated. Loading fluctuates throughout the day in response to demand patterns i.e. some appliances are switched OFF during the day, however, they have high penetration during peak times. Due to the time-varying nature of the non-linear devices, multiple loading scenarios are developed.

The previous chapter presented a tensor representation of a distribution feeder for the verification against the CI method and the time-domain simulation. In this chapter, the tensor representation of different distribution networks is obtained, and the results are compared with the CI method.

5.1 DISTRIBUTION NETWORK MODELLING

The whole purpose of this research is to demonstrate the use of tensor to analyse distribution networks. There are 10,558 11kV/415V transformers within one exemplar medium-sized distribution system in New Zealand [Watson et al. 2016],[Watson et al. 2014]. These 10,558 LV networks have been classified based on their characteristics and fall into four categories city, urban, industrial and commercial. Each customer is identified by an ICP number. In this research, two LV systems are selected from the overall network. The first system is a central city area, and the second system is an urban area. The following systems are modelled:

- 52-node (52×3) city LV network (Figure 5.1)
- 369-node (369×3) urban LV network (Figure 5.11)

5.1.1 Modelling of Residential and Commercial Customers

For an accurate understanding of the impact of non-linear loads on the distribution network, it is essential to consider the loading profiles of devices. That is demand over time due to its usage. Every device has a distinct load profile which impacts the network variably throughout the day. As an example, kitchen loads related to cooking activities exhibit a similar switching ON pattern every day. Similarly, luminaries, TV, and heat-pump regularly operate during evenings between 18:00 to 22:00. Also, these load profiles could be periodic like fridges or intermittent like microwaves. Authors in [Walker and Pokoski 1985],[Richardson et al. 2010], [Diao et al. 2017],[Foteinaki et al. 2019],[Liu and Cheng 2017] have developed probabilistic scenarios to supply the time window of the switched ON/OFF state of various non-linear and linear (modelled as a resistive loads) devices. According to [Walker and Pokoski 1985], there is a probability that loads are switched randomly throughout the day, but these loads follow a statistical switching pattern. In [Richardson et al. 2010] load profiles are developed for each load type to forecast the ON/OFF condition during a day.

Three scenarios with different proportion of non-linear loads were considered. These were 30%, 60% and 90% of the power being consumed by non-linear loads.

5.2 CASE STUDY 1 - CITY LV NETWORK

In the first case study, a city LV distribution system is modelled, and the single-line diagram is shown in Figure 5.1. A three-phase LV network of 156 (52×3) nodes is connected to 11/0.415 kV delta/wye transformer with a rating of 300 kVA. This network has 51 single phase customers connected on different phases at different nodes through the network.

As previously mentioned, various scenarios are analysed (three are represented in this thesis), and the complete LV network is solved using tensor analysis, and the harmonic current magnitudes and angles of the 3^{rd} to 17^{th} harmonics for all ICPs obtained. Due to the size of the system and the volume of output results, the comparison between tensor representation and CI method will be displayed at a few selected nodes (ICPs). These are selected to show the results near the supply point and further from the supply point. Two groups of nodes are selected from the city network are $Node_2$ to $Node_9$ and $Node_{36}$ to $Node_{45}$. Note that $Node_{36}$ is the furthest

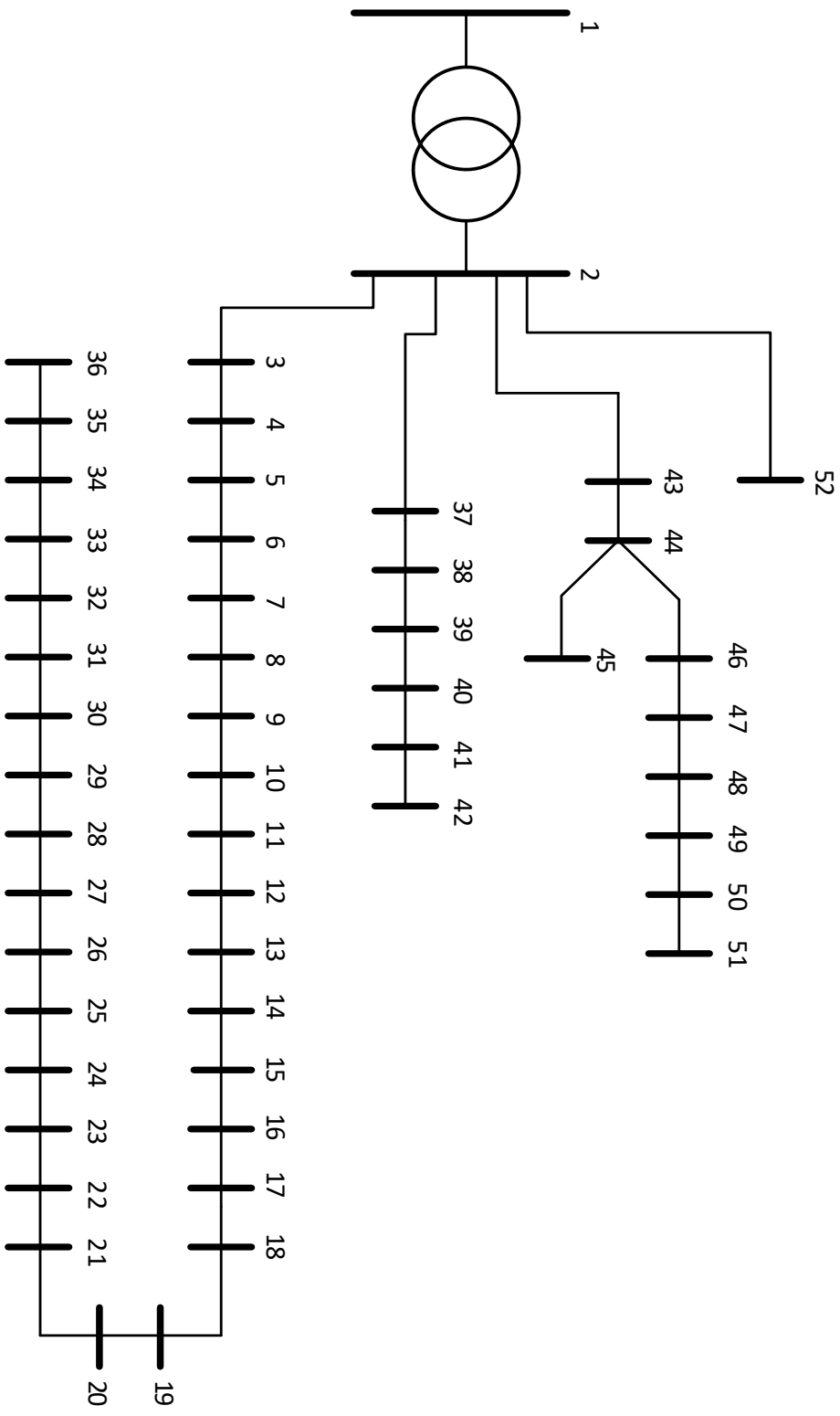

Figure 5.1 City LV Distribution Network New Zealand

from the supply point electrically and the $Node_{37}$ is the nearest to the supply point as it is connected to another feeder.

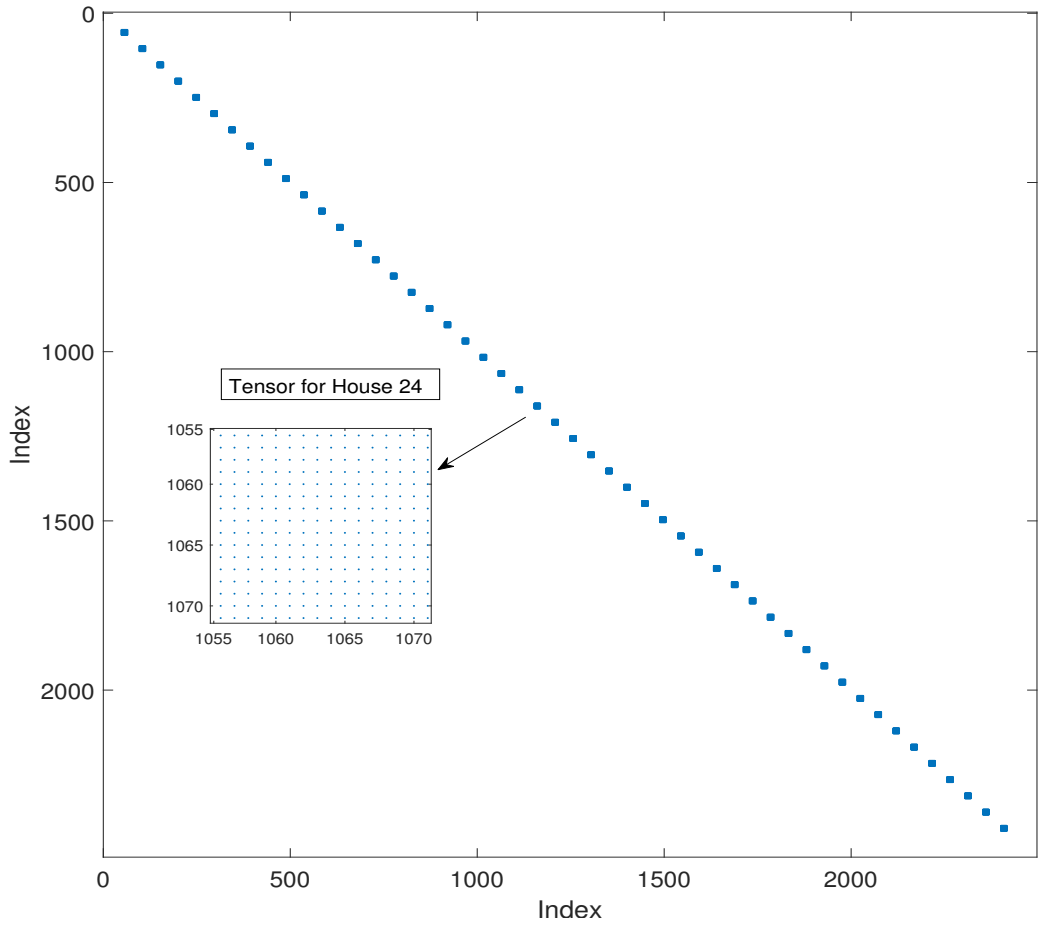

Figure 5.2 Resultant Tensors for 51 Customers Connected at Different Nodes

5.2.1 Scenario A (90% of the total load is non-linear)

This scenario considered 90% of total operating devices are non-linear. The harmonic injection is expected to increase due to the operation of a higher proportion of non-linear appliances. Various types of non-linear loads are modelled to achieve 90% of the loading. The combination of the devices for customer 1 comprises four types of lighting equipment, a TV, two PCs, two laptop chargers, an induction stove, a microwave oven, and a fridge for each customer connected at each node. Therefore, 12 tensors are automatically selected from the library of tensors. The addition of tensors is performed, and the resultant tensors for all 51 customers connected at different nodes, as represented in Figure 5.2. The dimension for index is $51 \times 3 \times 2 \times 8$ (51-nodes, 3-phase, 2 by 2 tensor form, and 3^{rd} to 17^{th} odd harmonics). The system admittance in the tensor form is calculated for the complete distribution system and a spy view

look down at the structure of the admittance matrix is presented in Figure 5.3.

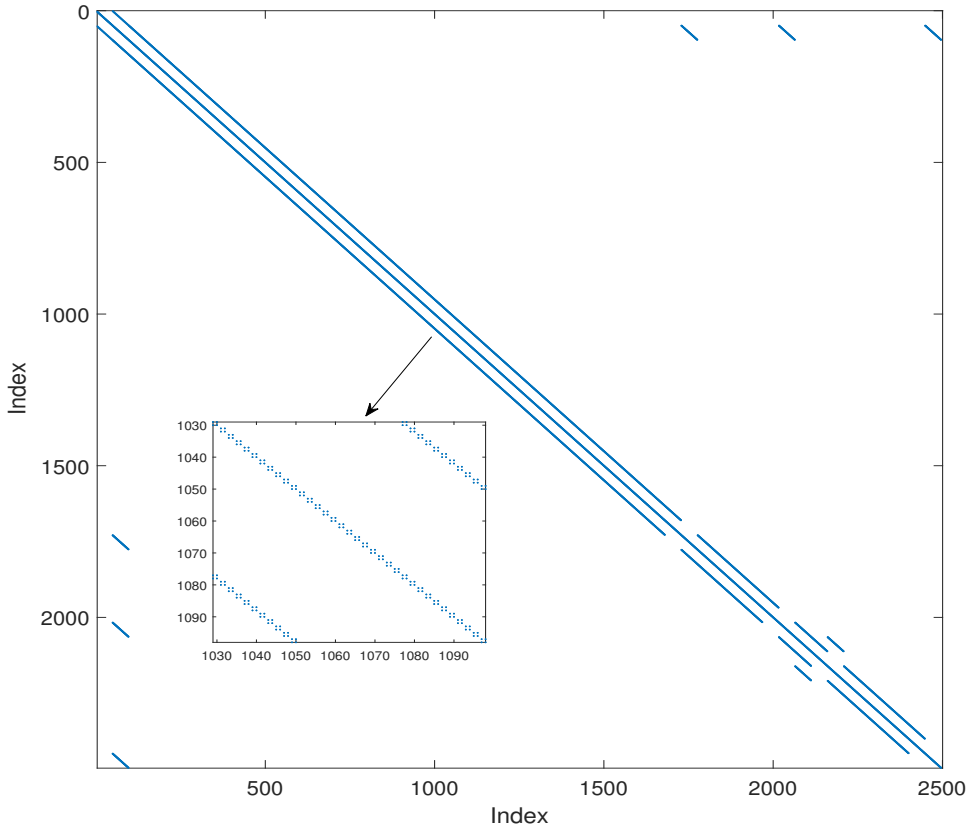

Figure 5.3 System Admittance Y_{sys} of 156-nodes System in Tensor Form

Two branches, $Node_2$ to $Node_9$ and $Node_{36}$ to $Node_{45}$, were selected to be looked at in more details. The results for the first branch, $Node_2$ to $Node_9$, is shown in Figure 5.4. For $Node_2$, the current magnitudes and phase angles are the same for both tensor and CI methods. This is because the customer connected to the $Node_2$, is closer to the supply transformer and has the least distortion. Therefore, the contribution of harmonic current through the Norton equivalent circuit is the smallest (see Figure 1.1b). However, the difference is more noteworthy from $Node_3$ to the higher nodes as the voltage distortion increases for customers connected further from the a.c. source. This difference gets prominent because, in the CI method, the non-linear devices are represented by fixed current sources, and it does not consider the harmonic interaction with the AC electrical network. Therefore, the CI model exhibits under or overestimation of the current magnitudes and phase angles compared to the tensor representation.

Similarly, Figure 5.5 shows the comparison for the second branch, ranging from $Node_{36}$ to $Node_{45}$. For $Node_{36}$, a significant difference can be seen as it is the last node of the feeder with the highest voltage distortion. This node is selected in this

group to show that the difference gets greater for nodes further down the feeder. This also can be seen in results for $Node_{37}$ to $Node_{45}$ and for $Node_2$ to $Node_9$. The results for all other connected customers are given in Appendix A.1.

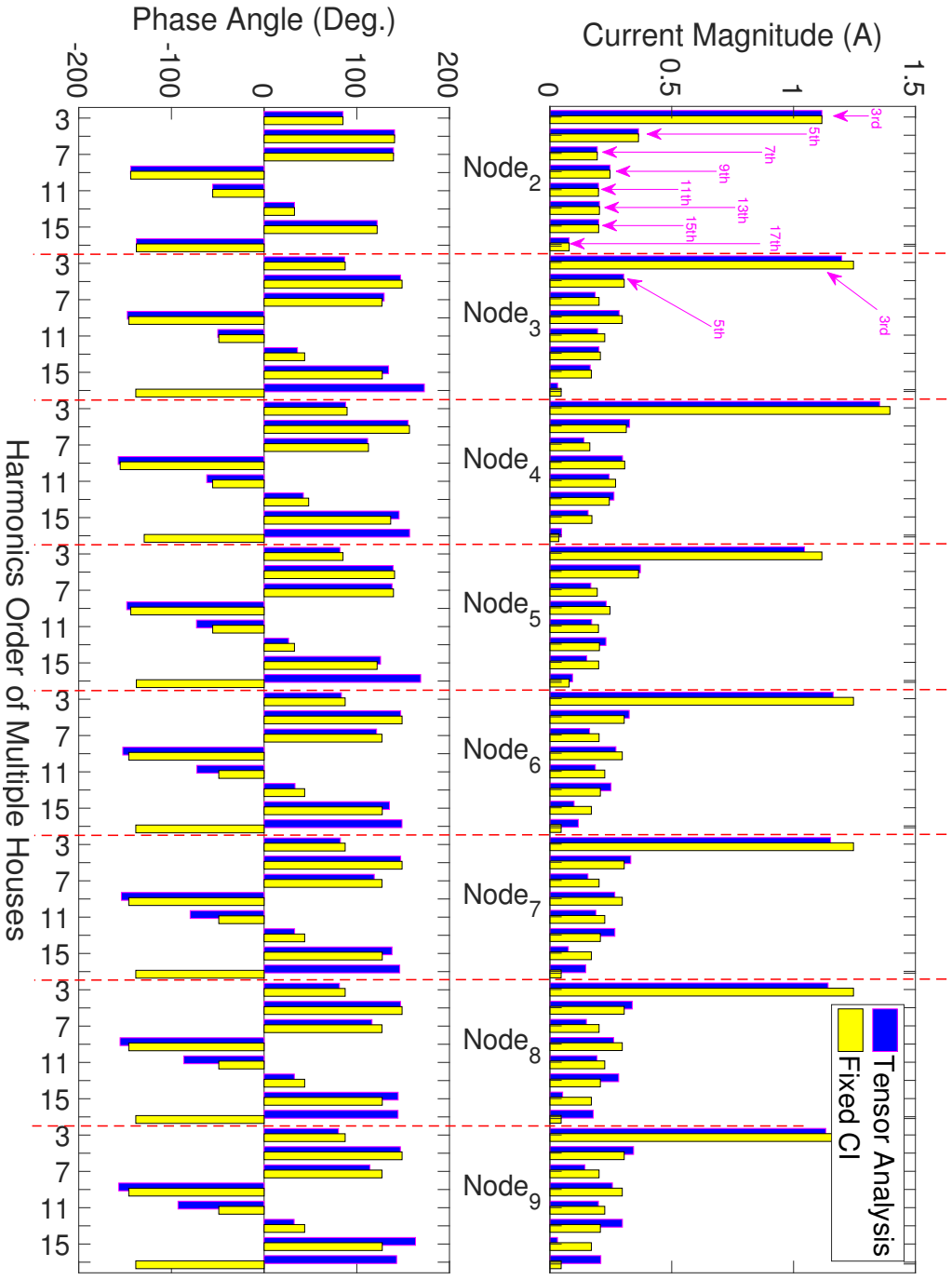

Figure 5.4 City LV Network (Scenario A) - Current Magnitude and Phase Angles for Customers Connected at $Node_2$ to $Node_9$

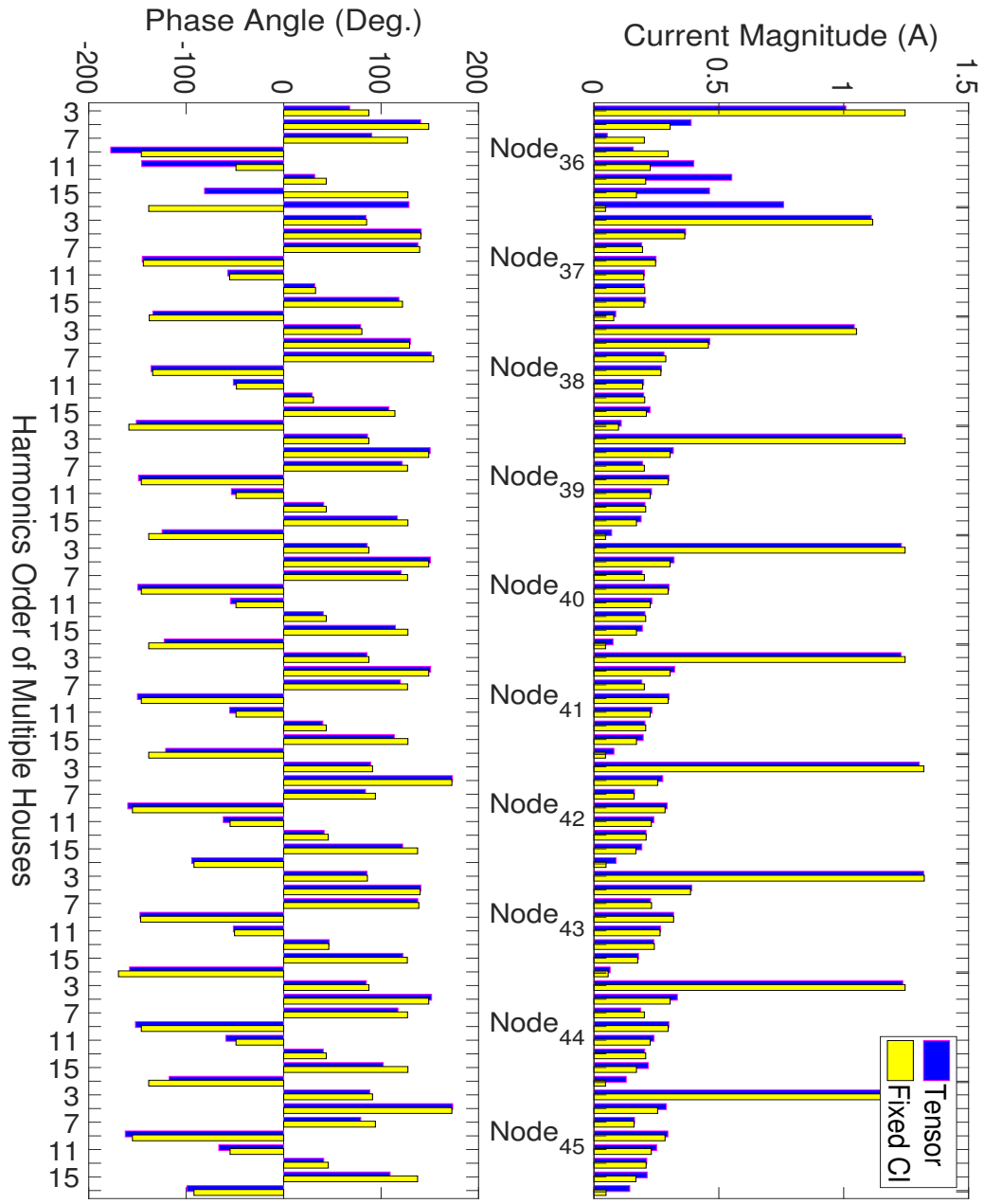

Figure 5.5 City LV Network (Scenario A) - Current Magnitude and Phase Angles for Customers Connected at $Node_{36}$ to $Node_{45}$

5.2.2 Scenario B (60% of the total load is non-linear)

In this scenario 60% of electrical loads are considered to be non-linear devices. Various non-linear devices are selected from the tensor library to represent non-linear loads in the premises and the remaining 40% loads represent the linear loads. The comparison of tensor and CI methods is shown in Figure 5.6 and Figure 5.7. Due to 40% of

linear loads, the difference between the tensor analysis and CI method has decreased relative to scenario A. Similarly to the previous scenario, the CI method shows a high difference in current magnitudes and phase angles for higher frequencies comparing to tensors. This difference also increases for the nodes located at the end of the feeders. $Node_{36}$ in Figure 5.5 and Figure 5.7 show a dramatic change in the mismatch between the CI and tensor analysis. The results for all other nodes are given in Appendix A.2.

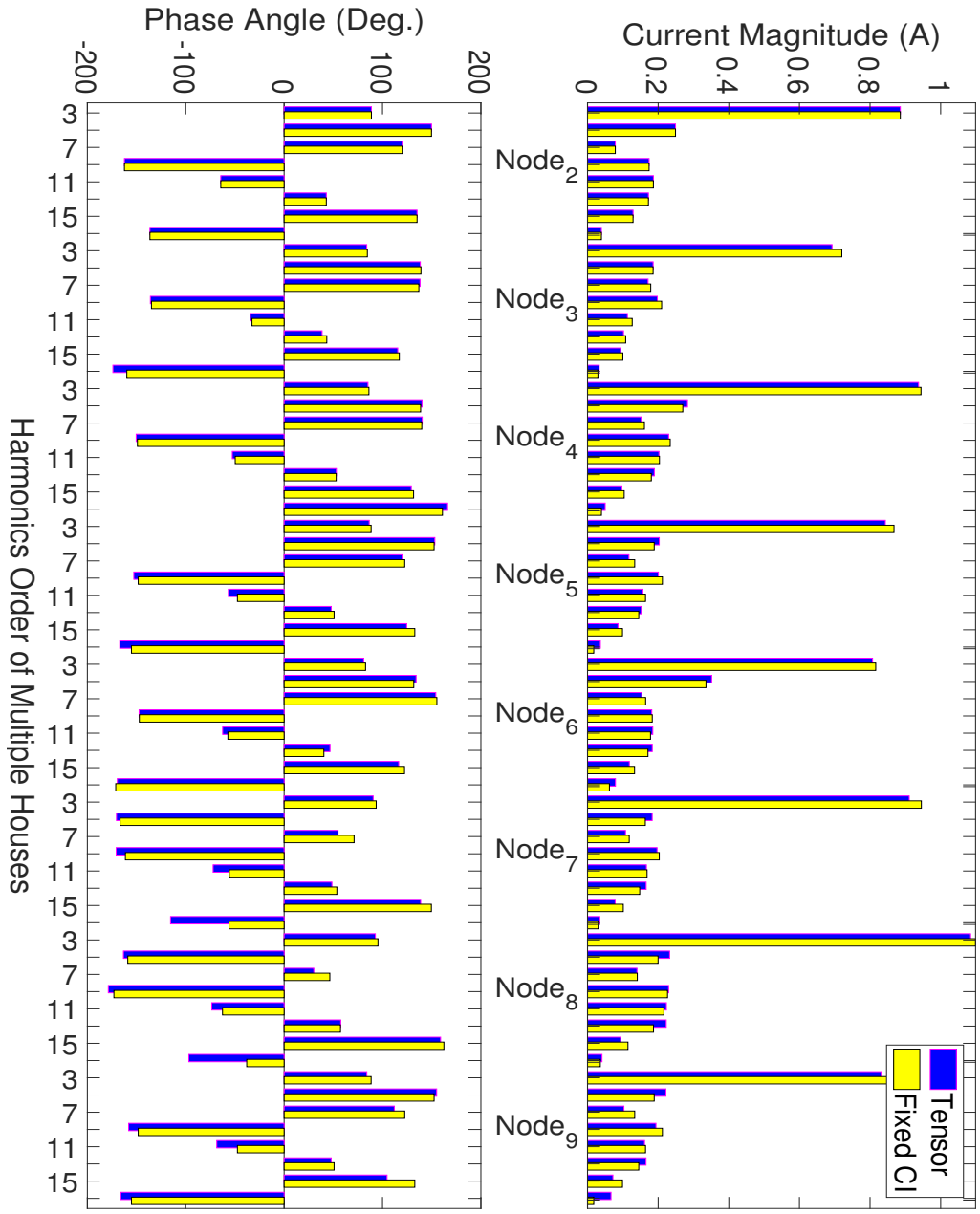

Figure 5.6 City LV Network (Scenario B) - Current Magnitude and Phase Angles for Customers Connected at $Node_2$ to $Node_9$

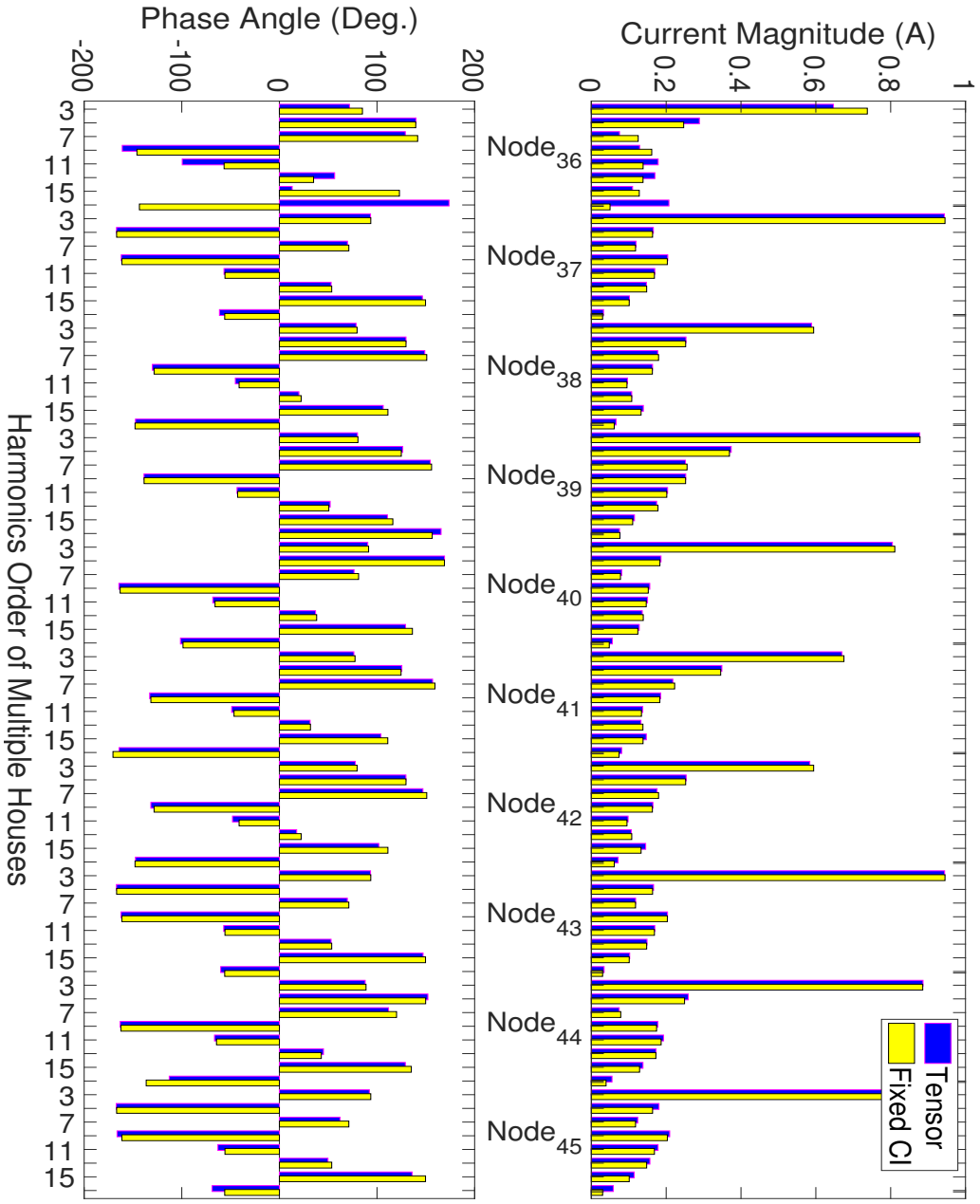

Figure 5.7 City LV Network (Scenario B) - Current Magnitude and Phase Angles for Customers Connected at $Node_{36}$ to $Node_{45}$

5.2.3 Scenario C (30% of the total load is non-linear)

Most of the non-linear devices are not operated as only 30% of the loading is non-linear loads. It is evident from Figure 5.8 and Figure 5.9 that the tensor analysis and CI method give similar results. This is because of the dominating effect of linear loads which is 70%. The results for all other customers are given in Appendix A.3.

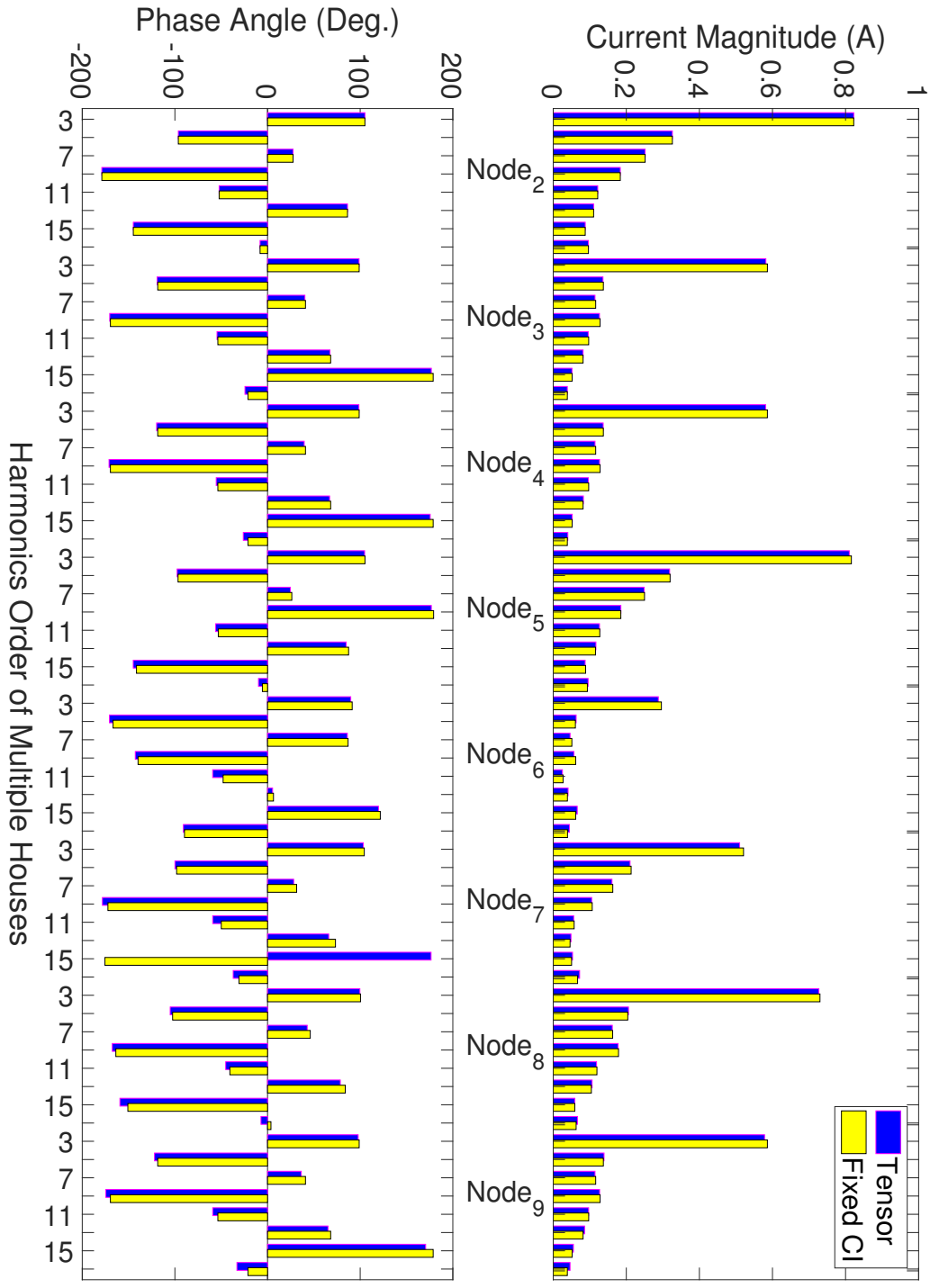

Figure 5.8 City LV Network (Scenario C) - Current Magnitude and Phase Angles for Customers Connected at $Node_2$ to $Node_9$

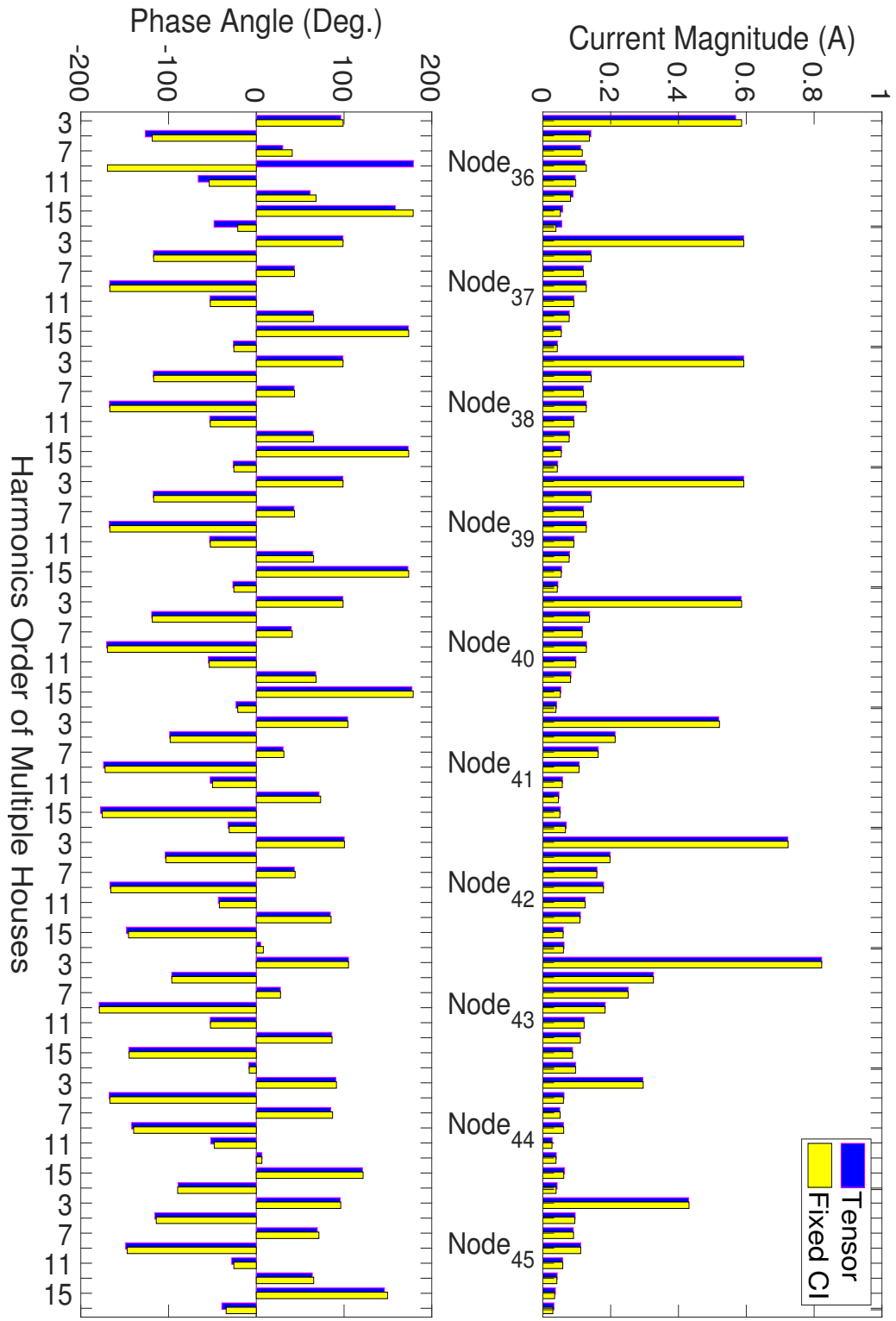

Figure 5.9 City LV Network (Scenario C) - Current Magnitude and Phase Angles for Customers Connected at $Node_{36}$ to $Node_{45}$

The tensor analysis has been taken as the benchmark to calculate the error of the CI analysis. The calculated error of the CI analysis is shown in Figure 5.10 for the first eight harmonics. Figure 5.10 (a) represents 90% of the loading as non-linear loads. As the feeder progresses from $Node_2$ to $Node_{36}$, the harmonics error percentage increases for all harmonics. It is seen that, 3^{rd} and 5^{th} harmonics have the lowest difference between the CI method and tensor representation. A significant change is seen for the higher harmonics especially 17^{th} harmonics. The customer connected at $Node_{37}$ has the lowest harmonics because it is nearest to the supply transformer and having lowest voltage distortion. From $Node_{42}$ to $Node_{51}$, the error gradually increases for all harmonics.

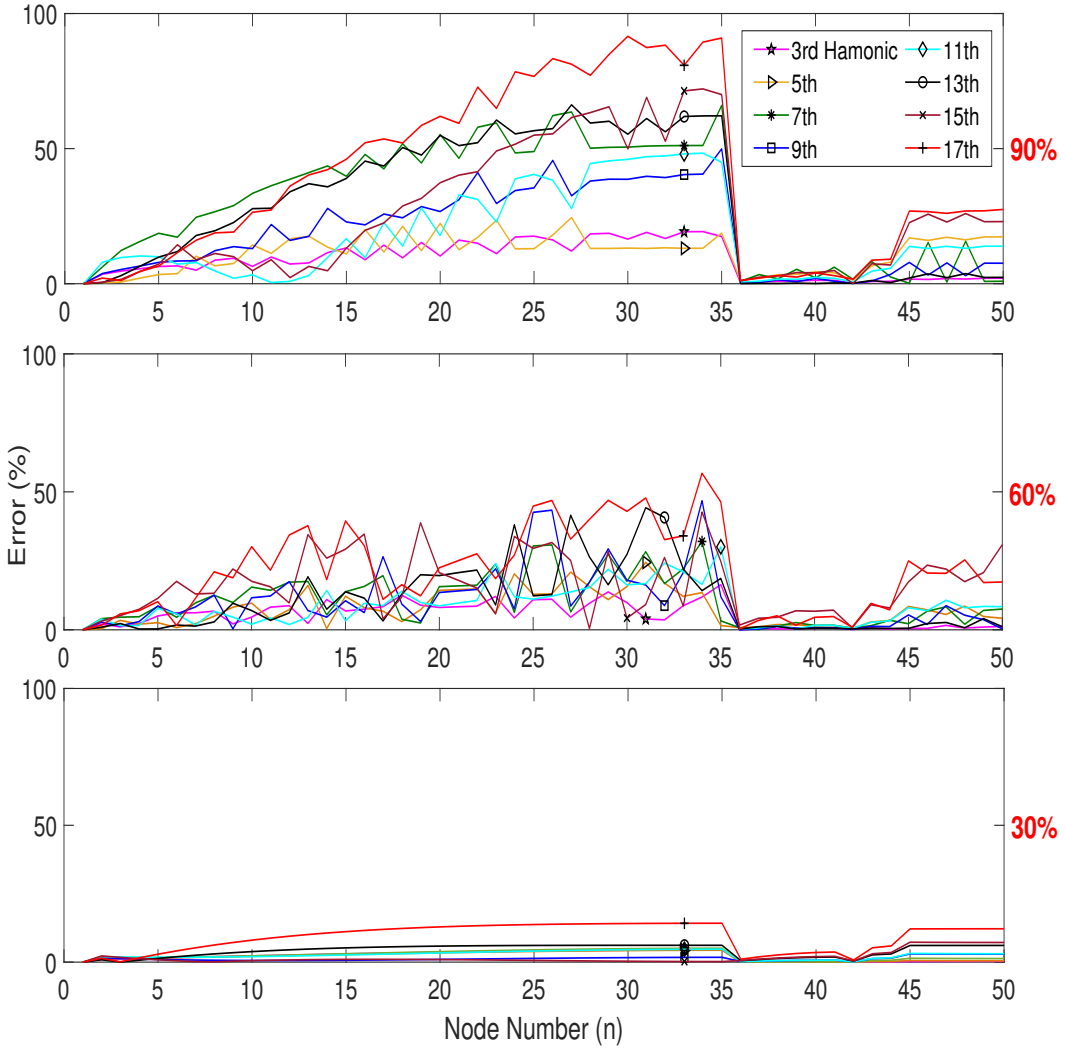

Figure 5.10 Error Estimation (%) between the CI and Tensor Representation for Different Percentages of Non-linear Loads of the Total Loading (a) 90% (b) 60% (c) 30%

Figures 5.10 (b) and (c) are showing the error for Scenario B and Scenario C,

respectively. For both cases, error is lower due to having fewer non-linear loads and a higher number of linear loads. Figure 5.10 (c) has the lowest error because of the dominating effects of linear loadings. A smooth change has occurred for $Node_2$ to $Node_{36}$, and there is no significant fluctuation compared to Scenario A and Scenario B.

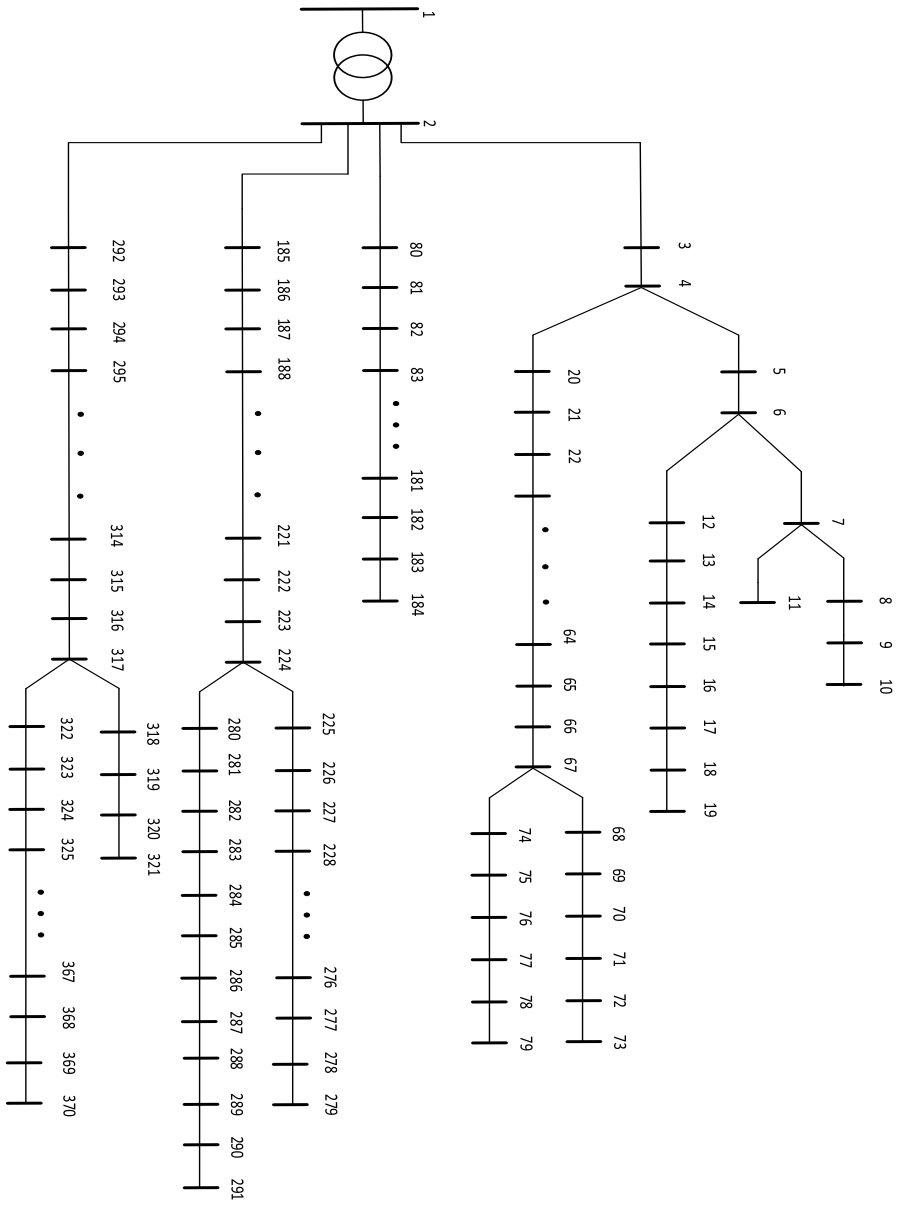

Figure 5.11 Urban LV Distribution Network New Zealand

5.3 CASE STUDY 2 - URBAN LV NETWORK

The LV urban network of 1110 (370×3) nodes connected with 11/0.415 kV delta/wye transformer and 300 kVA rating, is represented using tensors. This network is associated with 369 single phase customers connected on different phases at different nodes throughout the network. A schematic of this system is given in Figure 5.11. The urban LV networks were identified by clustering and typically have a larger distance between ICPs when compared with the city LV networks. Therefore, the comparison between the CI and the tensor analysis is more dramatic.

Again, the tensors of customer's appliances are added together, and the resultant tensors for all 369 customers distributed at different nodes are used to populate the system admittance matrix as shown in Figure 5.12. The system admittance in tensor form is shown in Figure 5.13. Similarly to the city network, three scenarios non-linear loading is performed; 90%, 60%, and 30% non-linear devices of the total loading.

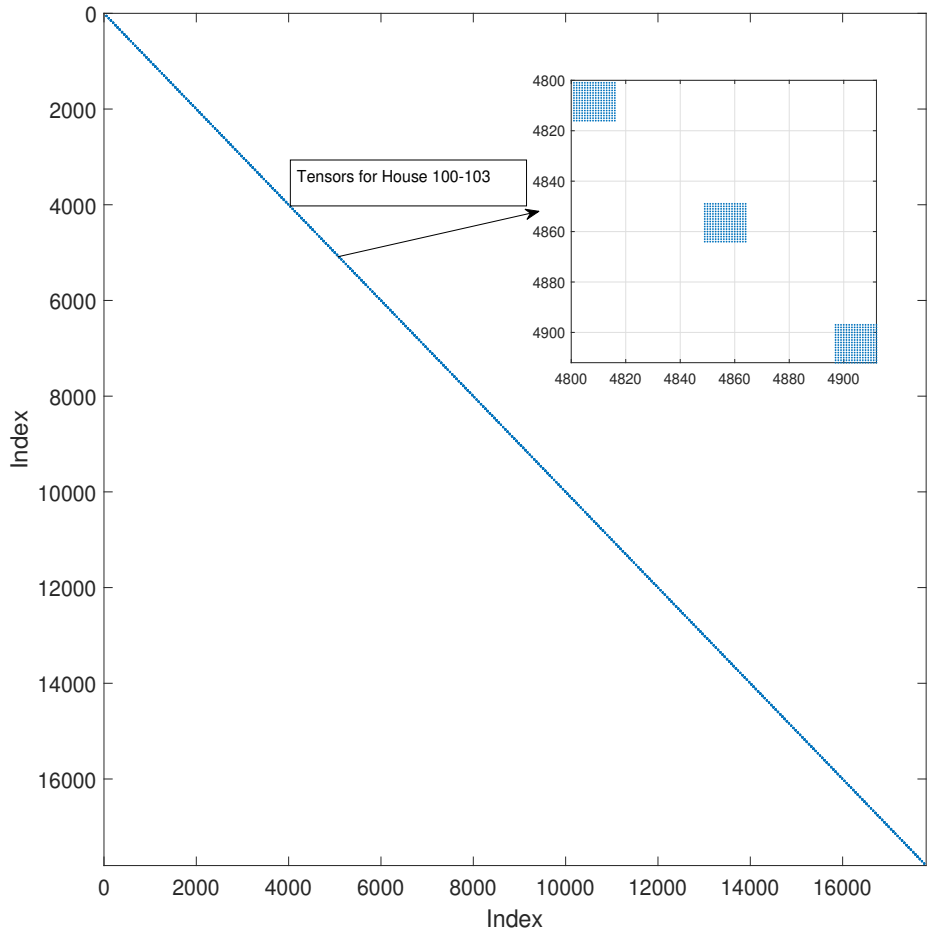

Figure 5.12 Resultant Tensors for 368 Customers Connected at Different Nodes

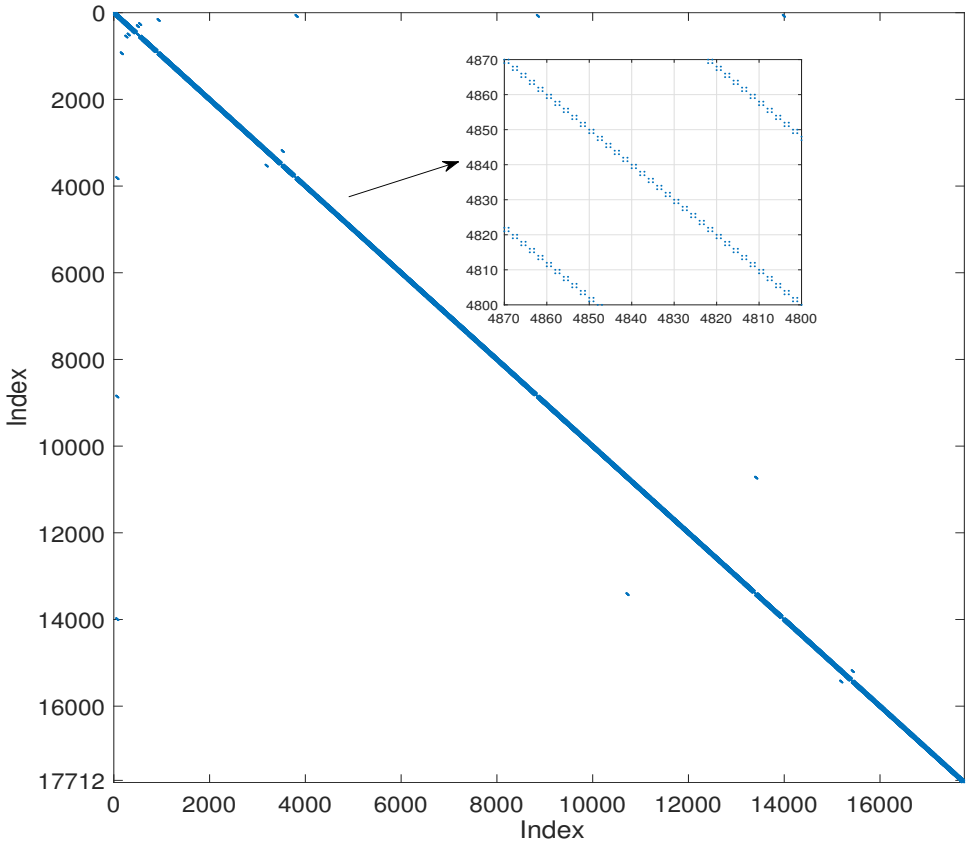

Figure 5.13 System Admittance Y_{sys} of 1107-nodes System in Tensor Form

5.3.1 Scenario A (90% of the total load is non-linear)

In this scenario, non-linear devices that compose 90% of the total load are considered. Similarly, like the city network, two groups of nodes $Node_2$ to $Node_{10}$ and $Node_{181}$ to $Node_{190}$, are considered to compare the tensor and the CI method as shown in Figure 5.14 and Figure 5.15, respectively.

There is no mismatch between the tensor analysis and the CI method for the ICPs connected near the supply voltage such as $Node_2$ to $Node_3$. The difference became larger for higher nodes further from the supply point. The CI model exhibited under or overestimation of the current magnitudes and phase angles compared to the tensor representation. A large mismatch can be seen for the ICPs connected at $Node_{181}$ to $Node_{184}$ because these are the last four nodes of the feeder (see $Node_{80}$ to $Node_{184}$ in Figure 5.11). For these ICPs, the CI model exhibited a large under or overestimation for all harmonics from 3^{rd} to 17^{th} harmonics. However, the highest mismatch was seen for the higher harmonics 15^{th} and 17^{th}. The difference between the tensor analysis

and the CI method dropped for the $Node_{185}$ as it is the first node of another feeder. The mismatch increased for ICPs connected further from the supply point such as $Node_{186}$ to $Node_{190}$ as shown in Figure 5.15. Note that the comparison between the CI and the tensor analysis was more dramatic when compared to city LV network because there is a larger distance between ICPs in urban LV network.

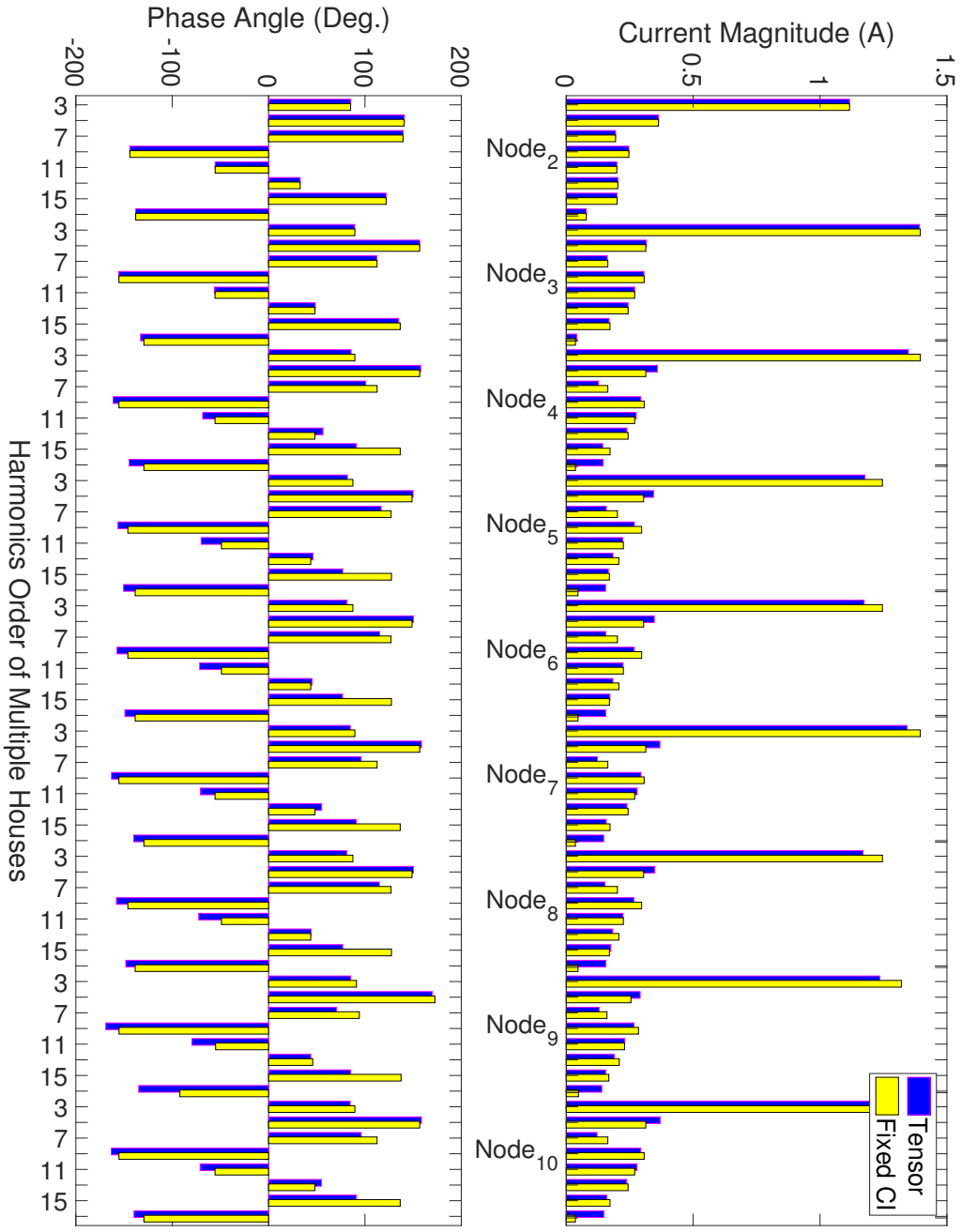

Figure 5.14 Urban LV Network (Scenario A) - Current Magnitude and Phase Angles for Customers Connected at $Node_2$ to $Node_{10}$

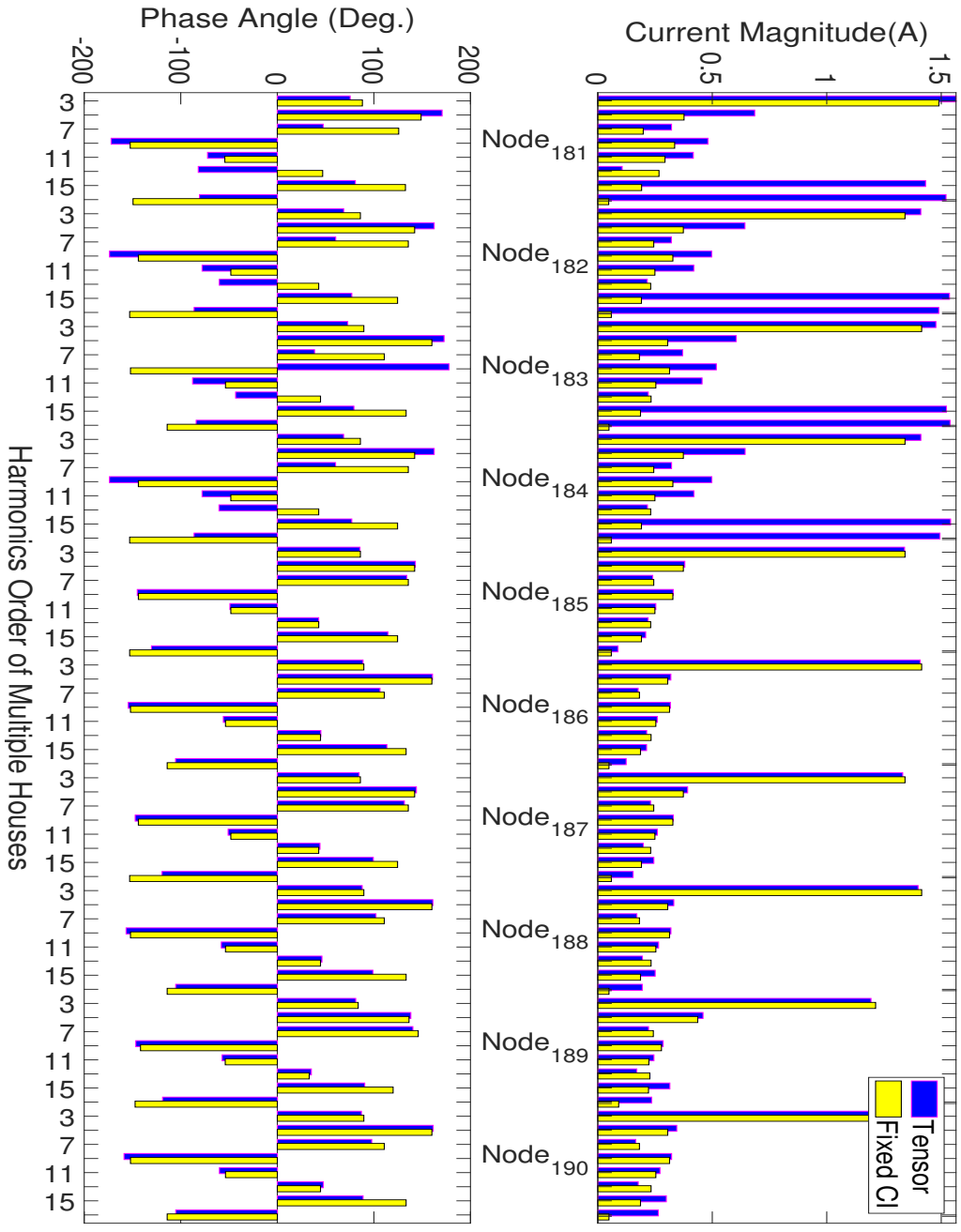

Figure 5.15 Urban LV Network (Scenario A) - Current Magnitude and Phase Angles for Customers Connected at $Node_{181}$ to $Node_{190}$

5.3.2 Scenario B (60% of the total load is non-linear)

The percentages of non-linear and linear loads considered in this scenario were 60% and 40%, respectively. The results for $Node_2$ to $Node_{10}$ and $Node_{181}$ to $Node_{190}$ are shown in Figure 5.16 and Figure 5.17, respectively. Because the non-linear loadings is

decreased and the linear loading is increased, the mismatch has decreased compared to Scenario A (see Figure 5.14 and Figure 5.15). However, still there is a significant differences for higher nodes such as $Node_{181}$ to $Node_{184}$ shown in Figure 5.17.

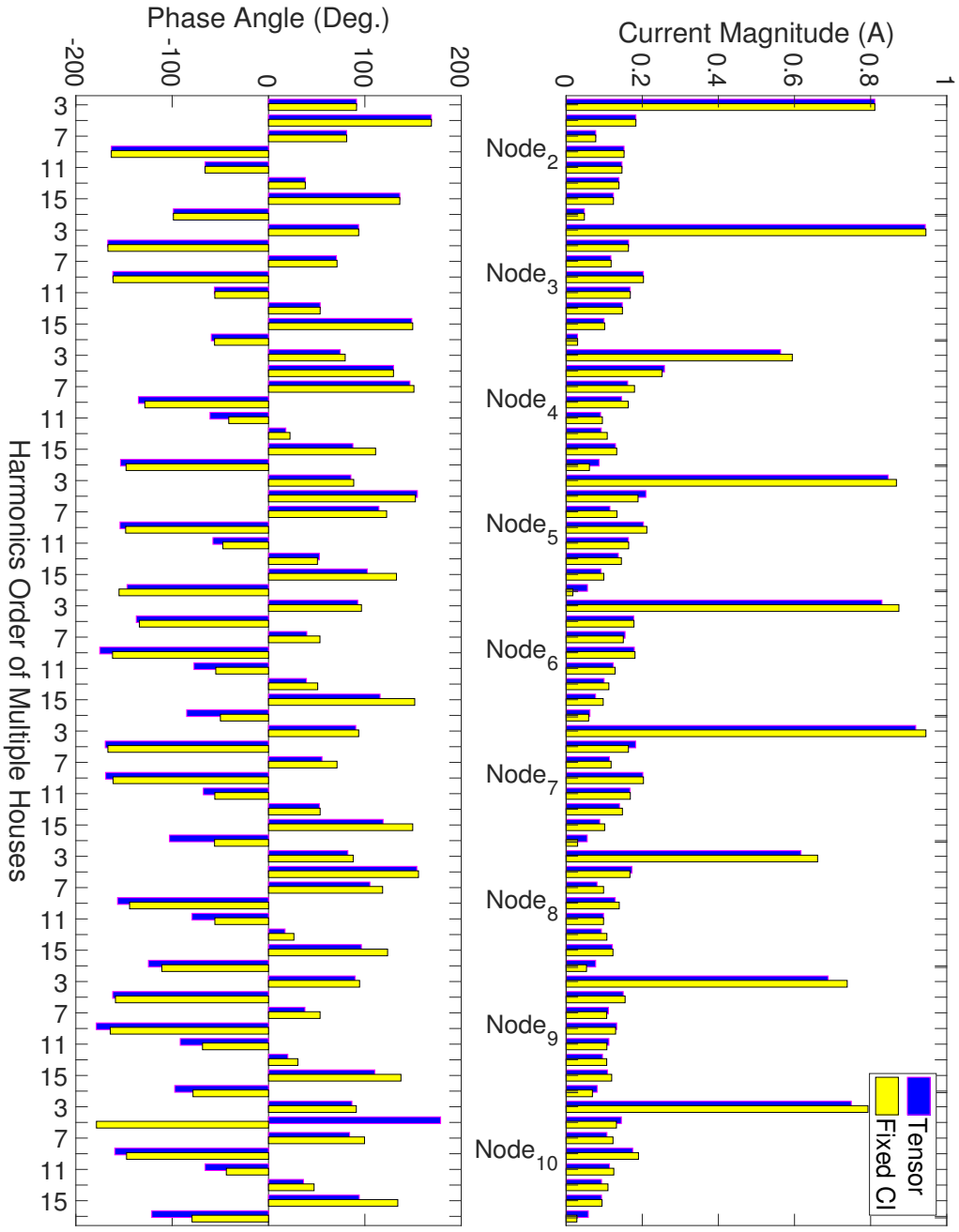

Figure 5.16 Urban LV Network (Scenario B) - Current Magnitude and Phase Angles for Customers Connected at $Node_2$ to $Node_{10}$

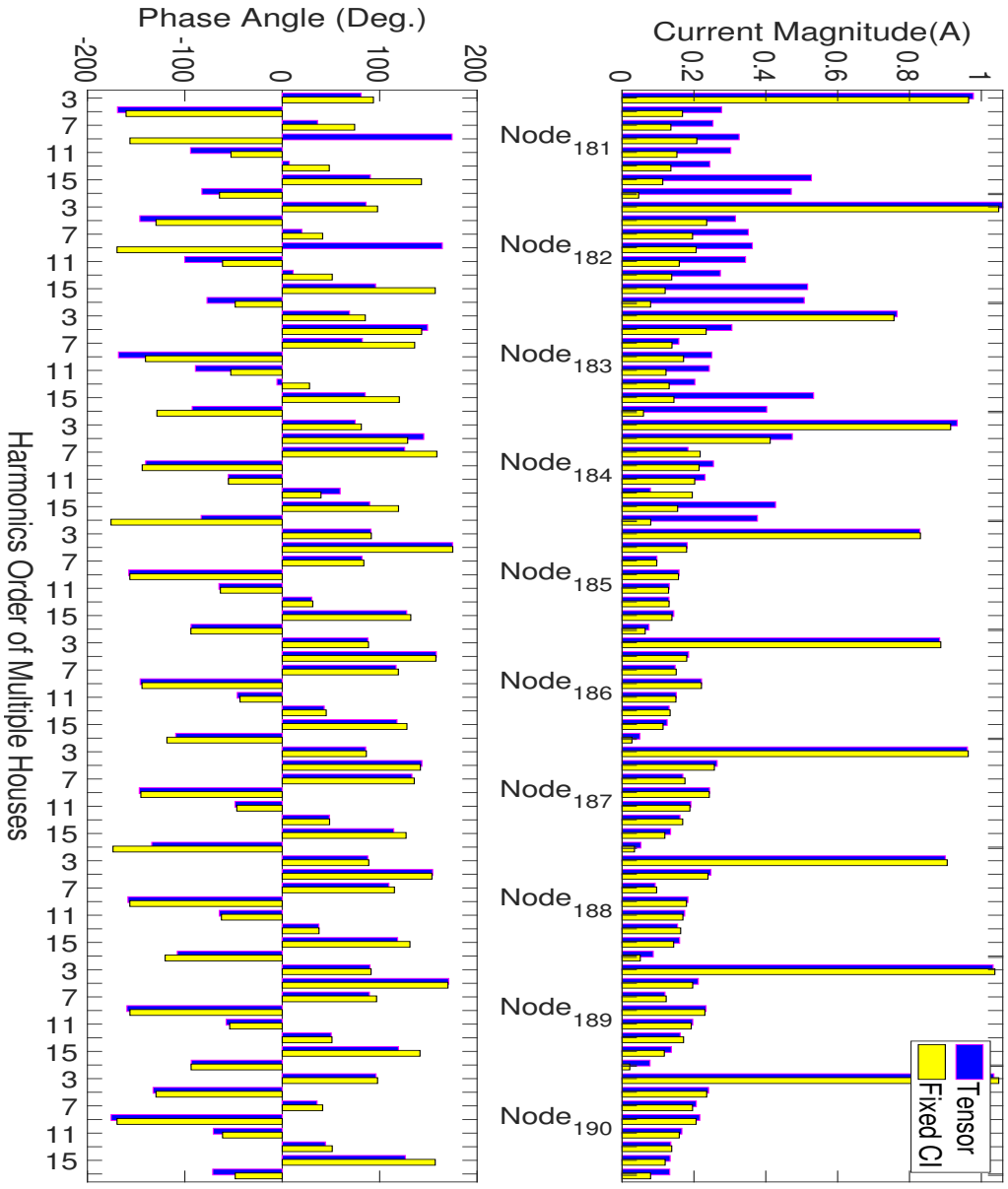

Figure 5.17 Urban LV Network (Scenario B) - Current Magnitude and Phase Angles for Customers Connected at $Node_{181}$ to $Node_{190}$

5.3.3 Scenario C (30% of the total load is non-linear)

In this scenario, the majority of the loading were composed of linear devices. Most of the non-linear devices are not considered as operating condition. Figure 5.18 and Figure 5.19 shows the result for $Node_2$ to $Node_{10}$ and $Node_{181}$ to $Node_{190}$. As the non-linear loading decreased, the mismatch between the tensor analysis and the CI method is very low even for higher nodes such as $Node_{181}$ to $Node_{184}$.

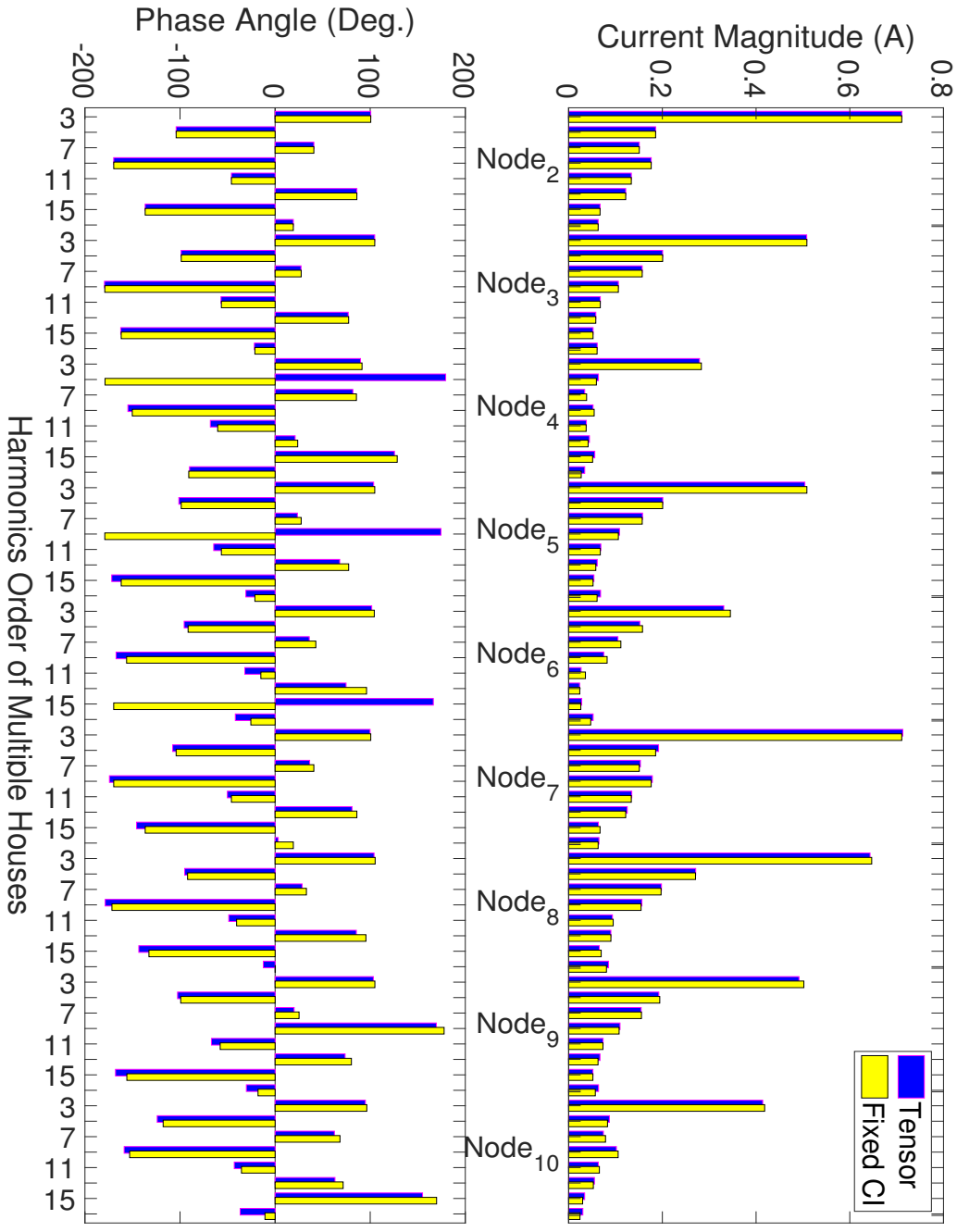

Figure 5.18 Urban LV Network (Scenario C) - Current Magnitude and Phase Angles for Customers Connected at $Node_2$ to $Node_{10}$

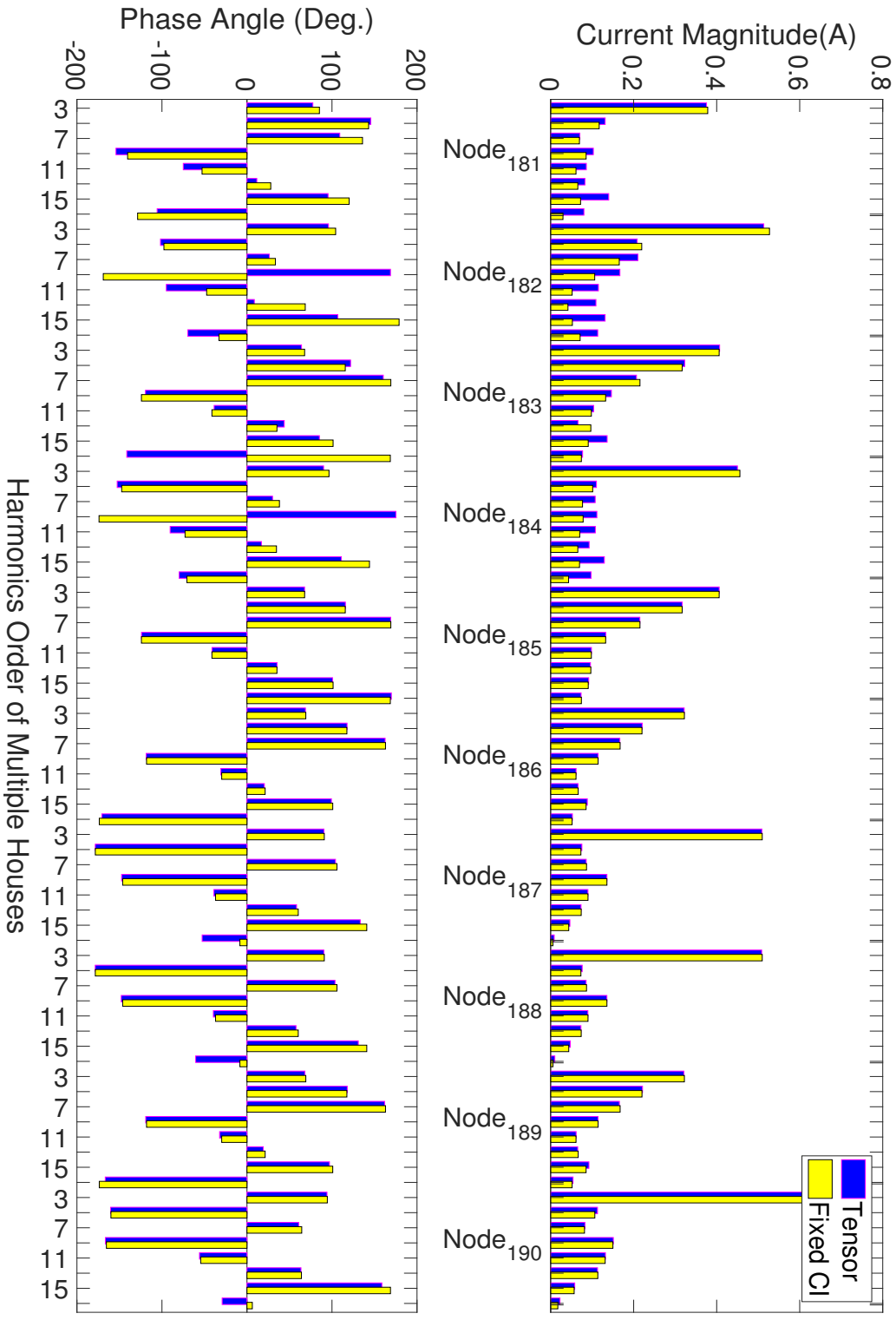

Figure 5.19 Urban LV Network (Scenario C) - Current Magnitude and Phase Angles for Customers Connected at $Node_{181}$ to $Node_{190}$

5.4 SUMMARY

This chapter has demonstrated two different test systems using the tensor analysis, and the results were compared against the CI method. City and urban LV networks were identified by clustering. Urban networks have a larger distance between the ICPs than the city networks. Therefore, the urban network showed a dramatic mismatch between the CI and the tensor analysis compared to the city network. The mismatch is greater for the higher frequencies of higher nodes connected far from the source. This is because there is a high level of distiotion for higher nodes. Secondly, each node is connected with a house and there can be a resonance. The coupling and the resonance into the system can cause dramatic mismatch for the higher frequencies.

It is evident from the comparison that there has been a significant difference between the results obtained from the tensor analysis and the CI method. This is because, for the given selection of devices the current injection would be the same regardless of the network. It is a fixed CI for each device and they add up to a nominal CI that would be the same and will not considered any interaction. However, in the tensor representation the harmonic current the device injects into the network will be different depending on the network structure. These differences could be important if an accurate harmonic analysis is required. Moreover, the tensor analysis is capable of analysing large distribution systems unlike the time-domain such as PSCAD/EMTDC tool.

Chapter 6

CONCLUSION & FUTURE WORK

6.1 SUMMARY & KEY ACHIEVEMENTS

The key contribution of this work is the tensor representation of distribution networks. In the previous work, tensor representation was used on an HVDC link, however, the present work has extended tensors for the modelling of distribution systems with a large number of non-linear devices. The development of tensors is explained and demonstrated. This involves linearisation around an operating point. It can be viewed as a Norton equivalent where the parallel admittance is a 2×2 tensor. The key achievements of this research are:

1. For an accurate approximation of tensors, different optimisation techniques were tested. A comparison between FD and AAL showed that tensors obtained through AAL are more accurate than FD. Therefore, throughout this research work, AAL technique is considered because of its higher accuracy.

2. For the validation of tensors, a successful laboratory experiment is performed.

3. A linearity region for different values of smoothing capacitors, inductors, and loads for different distortion levels was obtained.

4. A tensor representation of a test feeder is implemented to compare the proposed method against the time-domain PSCAD/EMTDC and CI method. A strong agreement is seen between the tensor approach and PSCAD/EMTDC.

5. The combination of individual tensors to produce tensors for a large part of the network has been demonstrated for the first time.

6. Tensor representation is acquired for different appliances. A successful assessment of the city and urban distribution system is achieved, and the results are compared with the existing CI method.

At first, the harmonic perturbation analysis was performed with various levels of voltage distortions. The purpose was to get one tensor to represent the device for all realistic distortion levels. The experimental results show that the admittance loci are not double traced for higher voltage distortion i.e. they lose their linearity in the frequency-domain above a certain distortion level. There were differences in the shapes of tensors that were not exactly the same for all distortion levels and so must be approximated. Hence, AAL is implemented in this research which produced one tensor for all realistic voltage distortions accurately. In addition, a laboratory experiment was carried out for the validation of the tensors. The optimisation approaches are performed on the data collected from both laboratory experiment and computer-based simulations.

A large number of PSCAD/EMTDC runs were performed to obtain the linearity region in the latter stage. For the tensor representation, the non-linear devices were linearised around the operating point by perturbation analysis. The linearity region is defined. After defining the linearity region, an extensive number of runs were performed in PSCAD/EMTDC to build a library of tensors for different non-linear devices such as modern TVs, advanced air conditioning systems, lighting equipment (LED and CFLs), VSDs systems, and appliances with VSDs such as fridges and freezers. Admittance tensor matrices of various non-linear devices were developed in this work to describe the harmonic interaction between voltage and current components.

The tensors library has been used to model a test feeder, and the results were evaluated in comparison to the PSCAD/EMTDC and the CI method. A successful validation was obtained by evaluating the effect of non-linear devices on a distribution network to assess their harmonic impact. The results were verified and compared against the PSCAD/EMTDC in two ways. At first, the tensor analysis results were converted to time waveforms and were compared with PSCAD/EMTDC waveforms to demonstrate the accuracy. There was a good agreement between tensor time waveform and PSCAD/EMTDC. However, the slight differences in the current waveforms were due to the harmonics spectra's truncation used in the tensor analysis (limited number of harmonic considered). Secondly, the FFT block in PSCAD/EMTDC was used to measure the magnitudes and phase angles of the harmonic voltages and currents. These also agreed well.

In this research, two LV systems were selected from the overall extensive network of New Zealand. The first system was a central city LV network, while the second system was an urban LV network. Multiple loading scenarios were developed due to the time-varying nature of loads. Three different scenarios were examined by considering different percentage of non-linear loads of the total loading. These investigations led to a prediction of the potential impact of different load types on the LV feeders, and

consequently, allows a proper network design of the networks. A comparison between tensors with the CI method was performed. The CI method is a fixed current source which neither evaluates the interaction between non-linear devices and a.c. system nor interaction between multiple non-linear devices. Therefore, has been demonstrated that the CI model exhibited under- or over-estimation of the current magnitudes and phase angles compared to the tensor analysis and have also incorrectly estimated the voltage distortion. This under- and over-estimation was low for the houses connected at the start of the feeder. This is because the voltage distortion is smallest and therefore, the smallest incremental harmonic current due to terminal voltage distortion. The voltage distortion increases as customers move far from the supply point, which results in a high contribution of harmonic current from the terminal voltage distortion. The reason of the frequency-domain approach using tensor analysis is important because it has the ability to model very large electrical networks which are impractical to model using a time-domain tool such as PSCAD/EMTDC.

6.2 FUTURE WORK

This research work can be extended by the following:

1. Developing a larger database of tensors for equipment in use. The present work has demonstrated the procedure and applicability of the technique but has not developed a comprehensive database.

2. More work enable the linear region to be predicted based on the class of circuit used. The work present demonstrated the region of linearity but did not produce guidelines to enable prediction of the region based on circuit types and parameters.

3. Error analysis of the tensors and the overall error in the harmonic assessment.

    - dependence on frequency
    - propagation of error from tensor to final solution
    - effect of selection of harmonics

Appendix A

CITY LV NETWORK

A.1 CITY LV NETWORK - SCENARIO A

A.2 CITY LV NETWORK - SCENARIO B

A.3 CITY LV NETWORK - SCENARIO C

Table A.1 City LV Network (Scenario A) - Current Magnitude and Phase Angles for Customers

		Current Magnitudes								Phase Angles							
Harmonic Order		h_3	h_5	h_7	h_9	h_{11}	h_{13}	h_{15}	h_{17}	h_3	h_5	h_7	h_9	h_{11}	h_{13}	h_{15}	h_{17}
ICP																	
1	Tensors	1.321	0.255	0.16	0.285	0.23	0.209	0.168	0.048	91.21	172.623	94.147	-155.175	-54.978	45.801	137.46	-92.045
	Fixed CI	1.321	0.255	0.16	0.285	0.23	0.209	0.168	0.048	91.21	172.623	94.15	-155.174	-54.976	45.801	137.462	-92.04
2	Tensors	1.362	0.317	0.147	0.299	0.244	0.245	0.179	0.02	88.891	154.986	115.784	-156.438	-56.955	41.602	143.178	173.838
	Fixed CI	1.395	0.313	0.164	0.307	0.27	0.244	0.172	0.036	89.545	156.837	112.602	-155.278	-55.565	48.095	136.598	-129.384
3	Tensors	1.257	0.256	0.134	0.268	0.194	0.224	0.154	0.018	89.48	169.88	89.802	-159.441	-65.483	35.463	145.872	177.919
	Fixed CI	1.321	0.255	0.16	0.285	0.23	0.209	0.168	0.048	91.21	172.623	94.15	-155.174	-54.976	45.801	137.462	-92.04
4	Tensors	1.176	0.319	0.169	0.274	0.185	0.24	0.13	0.08	84.529	147.422	125.069	-150.851	-65.936	33.094	136.242	151.436
	Fixed CI	1.246	0.305	0.202	0.297	0.225	0.207	0.17	0.046	87.469	148.875	127.135	-146.051	-48.908	43.747	127.495	-138.456
5	Tensors	1.165	0.325	0.161	0.268	0.184	0.258	0.109	0.108	83.436	147.415	122.732	-152.467	-73.768	32.407	138.774	147.264
	Fixed CI	1.246	0.305	0.202	0.297	0.225	0.207	0.17	0.046	87.469	148.875	127.135	-146.051	-48.908	43.747	127.495	-138.456
6	Tensors	1.223	0.272	0.121	0.261	0.2	0.28	0.101	0.1	86.342	167.836	75.328	-165.526	-88	32.5	160.39	142.438
	Fixed CI	1.321	0.255	0.16	0.285	0.23	0.209	0.168	0.048	91.21	172.623	94.15	-155.174	-54.976	45.801	137.462	-92.04
7	Tensors	1.016	0.385	0.148	0.217	0.185	0.28	0.093	0.159	78.3	138.634	134.744	-151.784	-94.983	26.762	132.614	149.574
	Fixed CI	1.116	0.364	0.194	0.247	0.199	0.203	0.2	0.079	85.123	140.776	139.6	-144.003	-55.477	32.744	121.96	-137.897
8	Tensors	1.32	0.367	0.106	0.281	0.251	0.363	0.093	0.18	84.216	155.974	96.278	-161.639	-87.369	42.172	-172.97	143.106
	Fixed CI	1.395	0.313	0.164	0.307	0.27	0.244	0.172	0.036	89.545	156.837	112.602	-155.278	-55.565	48.095	136.598	-129.384
9	Tensors	1.313	0.373	0.1	0.278	0.257	0.382	0.092	0.21	83.552	155.872	93.169	-162.309	-91.564	42.385	-157.464	141.891
	Fixed CI	1.395	0.313	0.164	0.307	0.27	0.244	0.172	0.036	89.545	156.837	112.602	-155.278	-55.565	48.095	136.598	-129.384
10	Tensors	0.989	0.395	0.131	0.205	0.213	0.323	0.033	0.243	75.15	137.802	131.461	-155.005	-110.453	28.104	178.819	141.052
	Fixed CI	1.116	0.364	0.194	0.247	0.199	0.203	0.2	0.079	85.123	140.776	139.6	-144.003	-55.477	32.744	121.96	-137.897
11	Tensors	1.172	0.289	0.11	0.246	0.246	0.363	0.093	0.258	81.891	164.252	53.618	-173.91	-114.57	31.206	-119.744	135.044
	Fixed CI	1.321	0.255	0.16	0.285	0.23	0.209	0.168	0.048	91.21	172.623	94.15	-155.174	-54.976	45.801	137.462	-92.04
12	Tensors	1.163	0.291	0.109	0.243	0.258	0.378	0.112	0.291	81.112	163.54	49.768	-175.334	-118.235	31.243	-109.262	134.136
	Fixed CI	1.321	0.255	0.16	0.285	0.23	0.209	0.168	0.048	91.21	172.623	94.15	-155.174	-54.976	45.801	137.462	-92.04
13	Tensors	1.154	0.293	0.108	0.239	0.269	0.393	0.136	0.325	80.373	162.803	46.194	-176.663	-121.467	31.35	-102.081	133.336
	Fixed CI	1.321	0.255	0.16	0.285	0.23	0.209	0.168	0.048	91.21	172.623	94.15	-155.174	-54.976	45.801	137.462	-92.04
14	Tensors	1.086	0.366	0.107	0.222	0.26	0.4	0.144	0.395	75.451	145.131	105.727	-164.284	-120.802	31.984	-86.691	134.075
	Fixed CI	1.246	0.305	0.202	0.297	0.225	0.207	0.17	0.046	87.469	148.875	127.135	-146.051	-48.908	43.747	127.495	-138.456
15	Tensors	1.417	0.509	0.089	0.29	0.331	0.567	0.208	0.411	81.157	150.539	119.921	-154.02	-96.001	53.003	-110.064	141.264
	Fixed CI	1.471	0.388	0.183	0.329	0.31	0.279	0.177	0.045	88.049	146.537	128.753	-155.369	-56.003	49.812	135.778	-170.176
16	Tensors	1.129	0.296	0.106	0.23	0.302	0.432	0.212	0.425	78.386	160.567	36.822	179.924	-129.249	31.773	-91.218	131.374
	Fixed CI	1.321	0.255	0.16	0.285	0.23	0.209	0.168	0.048	91.21	172.623	94.15	-155.174	-54.976	45.801	137.462	-92.04
17	Tensors	1.065	0.372	0.095	0.208	0.292	0.438	0.226	0.492	73.512	143.868	101.918	-166.855	-128.304	32.583	-82.107	132.057
	Fixed CI	1.246	0.305	0.202	0.297	0.225	0.207	0.17	0.046	87.469	148.875	127.135	-146.051	-48.908	43.747	127.495	-138.456
18	Tensors	0.89	0.515	0.202	0.174	0.278	0.414	0.193	0.514	63.041	127.464	145.709	-141.964	-128.993	32.578	-72.826	132.439
	Fixed CI	1.051	0.458	0.288	0.268	0.195	0.203	0.21	0.098	80.263	129.249	153.852	-134.435	-48.476	30.585	114.164	-158.817
19	Tensors	1.198	0.494	0.122	0.236	0.313	0.538	0.278	0.557	74.837	142.256	130.708	-152.259	-114.708	45.451	-88.39	135.289
	Fixed CI	1.323	0.387	0.23	0.319	0.265	0.242	0.175	0.057	85.924	140.06	138.717	-146.786	-50.42	46.354	126.916	-169.481
20	Tensors	0.921	0.414	0.094	0.163	0.316	0.44	0.248	0.532	67.479	134.146	127.831	-161.742	-135.504	32.349	-81.345	129.945
	Fixed CI	1.116	0.364	0.194	0.247	0.199	0.203	0.2	0.079	85.123	140.776	139.6	-144.003	-55.477	32.744	121.96	-137.897
21	Tensors	1.095	0.298	0.103	0.214	0.349	0.487	0.337	0.573	75.776	157.328	24.025	175.61	-138.112	32.325	-86.259	128.845
	Fixed CI	1.321	0.255	0.16	0.285	0.23	0.209	0.168	0.048	91.21	172.623	94.15	-155.174	-54.976	45.801	137.462	-92.04
22	Tensors	0.991	0.478	0.163	0.178	0.318	0.487	0.341	0.666	66.185	132.934	134.782	-152.606	-133.693	34.25	-76.28	130.261
	Fixed CI	1.177	0.39	0.283	0.316	0.223	0.206	0.177	0.069	83.269	133.623	145.133	-137.845	-42.667	41.66	118.068	-169.028
23	Tensors	1.033	0.381	0.074	0.184	0.345	0.501	0.371	0.656	70.582	141.777	96.33	-170.95	-137.95	33.441	-81.442	128.933
	Fixed CI	1.246	0.305	0.202	0.297	0.225	0.207	0.17	0.046	87.469	148.875	127.135	-146.051	-48.908	43.747	127.495	-138.456
24	Tensors	1.081	0.299	0.102	0.207	0.373	0.515	0.401	0.645	74.592	155.864	17.431	173.353	-141.644	32.594	-85.859	127.595
	Fixed CI	1.321	0.255	0.16	0.285	0.23	0.209	0.168	0.048	91.21	172.623	94.15	-155.174	-54.976	45.801	137.462	-92.04
25	Tensors	1.025	0.383	0.068	0.177	0.36	0.519	0.409	0.699	69.882	141.217	95.119	-172.105	-140.039	33.617	-81.849	128.142
	Fixed CI	1.246	0.305	0.202	0.297	0.225	0.207	0.17	0.046	87.469	148.875	127.135	-146.051	-48.908	43.747	127.495	-138.456

Continued on next page

Table A.1 (continued) City LV Network (Scenario A) - Current Magnitude and Phase Angles for Customers

		Current Magnitudes								Phase Angles							
Harmonic Order		h_3	h_5	h_7	h_9	h_{11}	h_{13}	h_{15}	h_{17}	h_3	h_5	h_7	h_9	h_{11}	h_{13}	h_{15}	h_{17}
ICP																	
26	Tensors	1.022	0.384	0.066	0.174	0.366	0.527	0.426	0.717	69.584	140.95	94.679	-172.62	-140.903	33.695	-82.043	127.806
	Fixed CI	1.246	0.305	0.202	0.297	0.225	0.207	0.17	0.046	87.469	148.875	127.135	-146.051	-48.908	43.747	127.495	-138.456
27	Tensors	1.069	0.299	0.102	0.2	0.392	0.538	0.452	0.702	73.709	154.625	12.167	171.49	-144.136	32.796	-85.907	126.65
	Fixed CI	1.321	0.255	0.16	0.285	0.23	0.209	0.168	0.048	91.21	172.623	94.15	-155.174	-54.976	45.801	137.462	-92.04
28	Tensors	1.226	0.422	0.044	0.218	0.378	0.639	0.465	0.717	76.267	150.971	42.755	-166.815	-128.798	45.122	-90.853	130.908
	Fixed CI	1.395	0.313	0.164	0.307	0.27	0.244	0.172	0.036	89.545	156.837	112.602	-155.278	-55.565	48.095	136.598	-129.384
29	Tensors	1.224	0.423	0.043	0.216	0.381	0.646	0.477	0.731	76.132	150.776	41.077	-166.773	-129.415	45.132	-90.755	130.701
	Fixed CI	1.395	0.313	0.164	0.307	0.27	0.244	0.172	0.036	89.545	156.837	112.602	-155.278	-55.565	48.095	136.598	-129.384
30	Tensors	1.011	0.385	0.059	0.165	0.385	0.549	0.478	0.776	68.722	140.011	93.937	-173.837	-143.462	33.868	-82.518	126.857
	Fixed CI	1.246	0.305	0.202	0.297	0.225	0.207	0.17	0.046	87.469	148.875	127.135	-146.051	-48.908	43.747	127.495	-138.456
31	Tensors	1.009	0.385	0.058	0.163	0.387	0.552	0.487	0.785	68.59	139.824	93.976	-173.876	-143.947	33.842	-82.568	126.708
	Fixed CI	1.246	0.305	0.202	0.297	0.225	0.207	0.17	0.046	87.469	148.875	127.135	-146.051	-48.908	43.747	127.495	-138.456
32	Tensors	0.885	0.42	0.073	0.134	0.382	0.517	0.428	0.728	63.56	131.393	133.541	-164.602	-145.186	33.862	-82.936	125.545
	Fixed CI	1.116	0.364	0.194	0.247	0.199	0.203	0.2	0.079	85.123	140.776	139.6	-144.003	-55.477	32.744	121.96	-137.897
33	Tensors	1.056	0.297	0.1	0.191	0.41	0.559	0.508	0.767	72.811	152.948	7.08	170.178	-147.065	32.769	-85.846	125.723
	Fixed CI	1.321	0.255	0.16	0.285	0.23	0.209	0.168	0.048	91.21	172.623	94.15	-155.174	-54.976	45.801	137.462	-92.04
34	Tensors	1.055	0.297	0.1	0.191	0.411	0.56	0.512	0.771	72.761	152.815	6.865	170.163	-147.25	32.763	-85.808	125.681
	Fixed CI	1.321	0.255	0.16	0.285	0.23	0.209	0.168	0.048	91.21	172.623	94.15	-155.174	-54.976	45.801	137.462	-92.04
35	Tensors	0.848	0.527	0.181	0.13	0.366	0.517	0.429	0.77	57.66	125.304	148.06	-139.274	-143.006	34.997	-79.192	126.172
	Fixed CI	1.051	0.458	0.288	0.268	0.195	0.203	0.21	0.098	80.263	129.249	153.852	-134.435	-48.476	30.585	114.164	-158.817
36	Tensors	1.241	0.31	0.198	0.297	0.227	0.208	0.178	0.055	86.891	149.467	125.204	-147.283	-51.217	42.365	123.394	-130.055
	Fixed CI	1.246	0.305	0.202	0.297	0.225	0.207	0.17	0.046	87.469	148.875	127.135	-146.051	-48.908	43.747	127.495	-138.456
37	Tensors	1.189	0.458	0.224	0.27	0.243	0.233	0.218	0.093	82.677	135.798	147.336	-145.877	-58.239	36.848	116.96	-145.94
	Fixed CI	1.194	0.451	0.231	0.268	0.239	0.236	0.205	0.086	83.564	134.69	149.562	-145.043	-56.057	36.969	121.602	-157.704
38	Tensors	1.234	0.318	0.193	0.297	0.229	0.209	0.193	0.07	86.007	150.36	122.271	-149.175	-54.699	40.29	117.979	-120.638
	Fixed CI	1.246	0.305	0.202	0.297	0.225	0.207	0.17	0.046	87.469	148.875	127.135	-146.051	-48.908	43.747	127.495	-138.456
39	Tensors	1.388	0.334	0.156	0.31	0.276	0.245	0.195	0.069	88.238	158.908	105.193	-157.9	-60.038	46.507	126.61	-104.505
	Fixed CI	1.395	0.313	0.164	0.307	0.27	0.244	0.172	0.036	89.545	156.837	112.602	-155.278	-55.565	48.095	136.598	-129.384
40	Tensors	1.305	0.275	0.158	0.289	0.239	0.215	0.196	0.089	89.338	173.181	84.604	-160.126	-62.977	40.7	124.379	-89.961
	Fixed CI	1.321	0.255	0.16	0.285	0.23	0.209	0.168	0.048	91.21	172.623	94.15	-155.174	-54.976	45.801	137.462	-92.04
41	Tensors	1.304	0.277	0.158	0.29	0.239	0.215	0.198	0.092	89.24	173.214	84.09	-160.376	-63.348	40.447	123.8	-89.802
	Fixed CI	1.321	0.255	0.16	0.285	0.23	0.209	0.168	0.048	91.21	172.623	94.15	-155.174	-54.976	45.801	137.462	-92.04
42	Tensors	1.32	0.391	0.227	0.319	0.267	0.241	0.177	0.064	85.557	140.696	137.604	-147.389	-51.658	46.752	122.929	-160.997
	Fixed CI	1.323	0.387	0.23	0.319	0.265	0.242	0.175	0.057	85.924	140.06	138.717	-146.786	-50.42	46.354	126.916	-169.481
43	Tensors	1.102	0.381	0.182	0.253	0.221	0.201	0.232	0.133	82.262	142.333	130.639	-149.294	-65.233	31.676	102.779	-127.882
	Fixed CI	1.116	0.364	0.194	0.247	0.199	0.203	0.2	0.079	85.123	140.776	139.6	-144.003	-55.477	32.744	121.96	-137.897
44	Tensors	1.234	0.333	0.191	0.303	0.245	0.208	0.209	0.116	84.647	151.541	115.767	-152.278	-60.299	40.635	102.04	-122.845
	Fixed CI	1.246	0.305	0.202	0.297	0.225	0.207	0.17	0.046	87.469	148.875	127.135	-146.051	-48.908	43.747	127.495	-138.456
45	Tensors	1.386	0.385	0.159	0.322	0.319	0.244	0.243	0.2	85.245	162.645	84.638	-163.952	-69.857	52.751	92.757	-110.695
	Fixed CI	1.395	0.313	0.164	0.307	0.27	0.244	0.172	0.036	89.545	156.837	112.602	-155.278	-55.565	48.095	136.598	-129.384
46	Tensors	1.158	0.444	0.247	0.314	0.271	0.199	0.301	0.21	76.871	140.106	128.435	-149.74	-65.251	39.144	77.116	-132.378
	Fixed CI	1.177	0.39	0.283	0.316	0.223	0.206	0.177	0.069	83.269	133.623	145.133	-137.845	-42.667	41.66	118.068	-169.028
47	Tensors	1.222	0.365	0.184	0.308	0.279	0.21	0.278	0.203	81.41	153.803	102.589	-159.736	-71.625	39.444	82.259	-121.181
	Fixed CI	1.246	0.305	0.202	0.297	0.225	0.207	0.17	0.046	87.469	148.875	127.135	-146.051	-48.908	43.747	127.495	-138.456
48	Tensors	1.311	0.451	0.197	0.323	0.311	0.233	0.263	0.203	81.268	147.978	119.596	-154.625	-64.751	53.333	84.952	-123.113
	Fixed CI	1.323	0.387	0.23	0.319	0.265	0.242	0.175	0.057	85.924	140.06	138.717	-146.786	-50.42	46.354	126.916	-169.481
49	Tensors	1.293	0.316	0.18	0.312	0.291	0.221	0.258	0.205	85.454	173.176	65.931	-169.866	-77.647	39.652	88.228	-109.695
	Fixed CI	1.321	0.255	0.16	0.285	0.23	0.209	0.168	0.048	91.21	172.623	94.15	-155.174	-54.976	45.801	137.462	-92.04
50	Tensors	1.311	0.451	0.196	0.323	0.311	0.233	0.263	0.204	81.235	147.99	119.557	-154.685	-64.841	53.384	84.761	-123.214
	Fixed CI	1.323	0.387	0.23	0.319	0.265	0.242	0.175	0.057	85.924	140.06	138.717	-146.786	-50.42	46.354	126.916	-169.481
51	Tensors	1.111	0.364	0.192	0.247	0.199	0.2	0.201	0.083	84.828	140.84	138.936	-144.467	-56.219	32.419	119.775	-137.481
	Fixed CI	1.116	0.364	0.194	0.247	0.199	0.203	0.2	0.079	85.123	140.776	139.6	-144.003	-55.477	32.744	121.96	-137.897

Table A.2 City LV Network (Scenario B) - Current Magnitudes and Phase Angles for Customers

		Current Magnitudes								Phase Angles							
Harmonic Order		h_3	h_5	h_7	h_9	h_{11}	h_{13}	h_{15}	h_{17}	h_3	h_5	h_7	h_9	h_{11}	h_{13}	h_{15}	h_{17}
ICP																	
1	Tensors	0.793	0.132	0.123	0.19	0.125	0.11	0.094	0.028	91.111	-178.614	99.641	-147.359	-43.794	47.288	134.16	-79.415
	Fixed CI	0.793	0.132	0.123	0.19	0.125	0.11	0.094	0.028	91.112	-178.614	99.642	-147.358	-43.792	47.289	134.162	-79.411
2	Tensors	0.632	0.165	0.091	0.131	0.088	0.101	0.115	0.049	87.244	154.399	119.832	-145.884	-59.985	22.072	122.509	-119.817
	Fixed CI	0.661	0.168	0.098	0.14	0.098	0.107	0.123	0.054	87.876	155.665	118.428	-144.211	-55.707	26.349	123.599	-110.713
3	Tensors	0.921	0.169	0.108	0.197	0.16	0.149	0.09	0.023	92.391	-169.131	65.857	-164.833	-61.435	50.66	146.151	-88.738
	Fixed CI	0.945	0.164	0.118	0.203	0.169	0.148	0.101	0.03	93.597	-166.744	71.12	-161.336	-55.753	53.589	149.675	-56.025
4	Tensors	0.681	0.194	0.163	0.19	0.108	0.107	0.089	0.055	81.764	139.185	135.006	-139.548	-45.411	35.199	99.606	-175.603
	Fixed CI	0.72	0.186	0.179	0.21	0.127	0.108	0.1	0.029	84.619	139.076	136.954	-134.844	-32.65	43.378	117.077	-159.898
5	Tensors	0.65	0.357	0.209	0.173	0.133	0.138	0.124	0.099	74.19	126.017	157.378	-133.592	-57.127	35.056	97.509	-174.23
	Fixed CI	0.675	0.346	0.223	0.183	0.134	0.138	0.138	0.074	77.476	124.608	159.363	-131.653	-46.491	31.817	111.027	-170.469
6	Tensors	0.705	0.261	0.108	0.153	0.14	0.144	0.107	0.077	81.298	140.452	138.547	-150.834	-70.771	37.607	107.214	-158.329
	Fixed CI	0.738	0.247	0.125	0.161	0.138	0.138	0.128	0.05	85.063	139.682	141.647	-145.913	-56.645	34.997	122.961	-143.396
7	Tensors	0.833	0.217	0.108	0.195	0.16	0.159	0.072	0.068	84.593	154.202	114.547	-156.067	-65.163	48.738	104.422	-168.691
	Fixed CI	0.868	0.189	0.134	0.212	0.164	0.145	0.099	0.018	88.441	152.457	122.593	-148.328	-47.45	50.786	132.812	-155.174
8	Tensors	0.83	0.222	0.104	0.193	0.161	0.163	0.069	0.077	84.013	154.531	112.857	-157.301	-67.984	48.868	98.269	-169.05
	Fixed CI	0.868	0.189	0.134	0.212	0.164	0.145	0.099	0.018	88.441	152.457	122.593	-148.328	-47.45	50.786	132.812	-155.174
9	Tensors	0.827	0.226	0.101	0.191	0.163	0.166	0.067	0.085	83.462	154.8	111.261	-158.482	-70.637	49.005	91.841	-169.497
	Fixed CI	0.868	0.189	0.134	0.212	0.164	0.145	0.099	0.018	88.441	152.457	122.593	-148.328	-47.45	50.786	132.812	-155.174
10	Tensors	0.789	0.174	0.152	0.177	0.138	0.136	0.048	0.057	89.613	-141.783	29.749	173.858	-100.326	29.48	100.533	-136.904
	Fixed CI	0.874	0.178	0.15	0.181	0.129	0.112	0.097	0.059	96.456	-134.055	53.398	-161.918	-54.758	51.056	151.741	-49.955
11	Tensors	0.97	0.232	0.196	0.214	0.189	0.187	0.051	0.061	92.561	-141.213	16.085	169.61	-92.27	48.184	147.275	-120.338
	Fixed CI	1.029	0.222	0.185	0.205	0.176	0.151	0.111	0.065	97.943	-132.928	36.788	-174.781	-63.486	56.286	164.601	-40.568
12	Tensors	0.751	0.205	0.064	0.15	0.168	0.164	0.073	0.088	84.389	165.705	46.663	-176.607	-93.294	42.551	102.748	-149.634
	Fixed CI	0.811	0.183	0.078	0.152	0.147	0.139	0.124	0.048	91.373	169.065	81.116	-163.149	-65.912	38.155	136.251	-98.747
13	Tensors	0.683	0.277	0.09	0.143	0.158	0.158	0.087	0.121	76.953	141.364	133.867	-156.509	-85.854	44.296	76.925	-168.361
	Fixed CI	0.738	0.247	0.125	0.161	0.138	0.138	0.128	0.05	85.063	139.682	141.647	-145.913	-56.645	34.997	122.961	-143.396
14	Tensors	0.882	0.203	0.107	0.192	0.182	0.187	0.036	0.098	86.649	-174.491	36.423	-179.645	-90.013	49.572	76.192	-162.155
	Fixed CI	0.945	0.164	0.118	0.203	0.169	0.148	0.101	0.03	93.597	-166.744	71.12	-161.336	-55.753	53.589	149.675	-56.025
15	Tensors	0.81	0.244	0.086	0.179	0.175	0.181	0.066	0.137	80.684	155.213	103.548	-164.32	-82.856	51.517	46.111	-176.01
	Fixed CI	0.868	0.189	0.134	0.212	0.164	0.145	0.099	0.018	88.441	152.457	122.593	-148.328	-47.45	50.786	132.812	-155.174
16	Tensors	0.995	0.278	0.069	0.212	0.232	0.256	0.028	0.13	85.737	166.956	63.025	-168.872	-77.246	64.101	79.69	-166.367
	Fixed CI	1.018	0.202	0.104	0.225	0.209	0.184	0.105	0.006	91.143	164.76	97.264	-160.869	-56.366	55.138	147.763	-132.946
17	Tensors	1.068	0.261	0.145	0.226	0.239	0.265	0.02	0.111	89.747	-167.54	14.298	177.503	-84.95	63	156.299	-154.572
	Fixed CI	1.099	0.2	0.141	0.227	0.216	0.187	0.114	0.036	95.391	-158.923	46.461	-173.022	-62.645	57.29	162.396	-38.006
18	Tensors	0.67	0.285	0.083	0.137	0.168	0.164	0.085	0.154	74.647	141.261	131.944	-159.057	-91.873	49.561	49.531	-175.396
	Fixed CI	0.738	0.247	0.125	0.161	0.138	0.138	0.128	0.05	85.063	139.682	141.647	-145.913	-56.645	34.997	122.961	-143.396
19	Tensors	0.866	0.208	0.107	0.188	0.189	0.193	0.05	0.139	84.966	-176.5	29.563	177.196	-96.295	51.713	18.929	-172.585
	Fixed CI	0.945	0.164	0.118	0.203	0.169	0.148	0.101	0.03	93.597	-166.744	71.12	-161.336	-55.753	53.589	149.675	-56.025
20	Tensors	0.619	0.233	0.116	0.136	0.135	0.124	0.143	0.202	69.584	140.316	120.938	-163.585	-104.178	28.389	16.686	171.173
	Fixed CI	0.72	0.186	0.179	0.21	0.127	0.108	0.1	0.029	84.619	139.076	136.954	-134.844	-32.65	43.378	117.077	-159.898
21	Tensors	0.987	0.29	0.065	0.208	0.237	0.269	0.04	0.172	84.671	166.415	56.63	-169.173	-80.012	67.132	16.036	-171.486
	Fixed CI	1.018	0.202	0.104	0.225	0.209	0.184	0.105	0.006	91.143	164.76	97.264	-160.869	-56.366	55.138	147.763	-132.946
22	Tensors	0.792	0.257	0.077	0.17	0.182	0.186	0.1	0.197	78.457	154.6	97.788	-167.532	-89.958	55.917	11.817	178.041
	Fixed CI	0.868	0.189	0.134	0.212	0.164	0.145	0.099	0.018	88.441	152.457	122.593	-148.328	-47.45	50.786	132.812	-155.174
23	Tensors	0.496	0.283	0.127	0.097	0.133	0.105	0.153	0.206	58.781	127.712	139.591	-154.115	-114.685	20.615	22.599	171.19
	Fixed CI	0.594	0.252	0.18	0.163	0.095	0.108	0.133	0.061	79.585	129.689	150.927	-128.344	-41.283	22.298	111.152	-147.867
24	Tensors	0.611	0.392	0.178	0.141	0.169	0.16	0.135	0.224	64.127	129.542	150.585	-138.448	-85.723	58.455	25.915	175.454
	Fixed CI	0.675	0.346	0.223	0.183	0.134	0.138	0.138	0.074	77.476	124.608	159.363	-131.653	-46.491	31.817	111.027	-170.469
25	Tensors	0.581	0.503	0.283	0.164	0.171	0.157	0.17	0.262	54.152	123.131	155.796	-121.281	-75.995	63.048	24.428	172.135
	Fixed CI	0.627	0.458	0.328	0.213	0.134	0.138	0.153	0.106	68.535	116.548	166.027	-120.921	-36.011	28.636	101.082	177.131

Continued on next page

Table A.2 (continued) City LV Network (Scenario B) - Current Magnitude and Phase Angles for Customers

		Current Magnitudes								Phase Angles							
Harmonic Order		h_3	h_5	h_7	h_9	h_{11}	h_{13}	h_{15}	h_{17}	h_3	h_5	h_7	h_9	h_{11}	h_{13}	h_{15}	h_{17}
ICP																	
26	Tensors	0.656	0.162	0.084	0.145	0.156	0.125	0.144	0.206	75.738	167.327	52.085	171.886	-120.669	26.065	2.098	171.415
	Fixed CI	0.793	0.132	0.123	0.19	0.125	0.11	0.094	0.028	91.112	-178.614	99.642	-147.358	-43.792	47.289	134.162	-79.411
27	Tensors	0.784	0.263	0.072	0.165	0.184	0.187	0.121	0.223	77.465	154.344	95.22	-168.812	-92.932	57.725	3.766	176.497
	Fixed CI	0.868	0.189	0.134	0.212	0.164	0.145	0.099	0.018	88.441	152.457	122.593	-148.328	-47.45	50.786	132.812	-155.174
28	Tensors	0.652	0.294	0.074	0.13	0.175	0.167	0.109	0.203	71.885	140.88	130.563	-160.645	-97.57	56.525	19.483	178.614
	Fixed CI	0.738	0.247	0.125	0.161	0.138	0.138	0.128	0.05	85.063	139.682	141.647	-145.913	-56.645	34.997	122.961	-143.396
29	Tensors	0.979	0.301	0.061	0.205	0.238	0.28	0.068	0.212	83.642	165.797	49.688	-169.301	-82.534	69.138	-2.26	-174.208
	Fixed CI	1.018	0.202	0.104	0.225	0.209	0.184	0.105	0.006	91.143	164.76	97.264	-160.869	-56.366	55.138	147.763	-132.946
30	Tensors	0.712	0.157	0.161	0.176	0.179	0.133	0.125	0.183	82.051	-148.921	10.74	155.328	-131.725	22.052	-6.967	174.793
	Fixed CI	0.874	0.178	0.15	0.181	0.129	0.112	0.097	0.059	96.456	-134.055	53.398	-161.918	-54.758	51.056	151.741	-49.955
31	Tensors	0.711	0.157	0.161	0.175	0.179	0.132	0.127	0.185	81.945	-149.041	10.347	155.081	-132.348	21.667	-7.18	174.762
	Fixed CI	0.874	0.178	0.15	0.181	0.129	0.112	0.097	0.059	96.456	-134.055	53.398	-161.918	-54.758	51.056	151.741	-49.955
32	Tensors	0.649	0.295	0.071	0.129	0.174	0.165	0.114	0.208	71.437	140.9	130.858	-160.693	-98.701	57.115	17.123	178.448
	Fixed CI	0.738	0.247	0.125	0.161	0.138	0.138	0.128	0.05	85.063	139.682	141.647	-145.913	-56.645	34.997	122.961	-143.396
33	Tensors	0.914	0.223	0.202	0.21	0.2	0.195	0.075	0.172	87.733	-147.348	1.341	161.82	-112.959	51.007	-17.895	-173.605
	Fixed CI	1.029	0.222	0.185	0.205	0.176	0.151	0.111	0.065	97.943	-132.928	36.788	-174.781	-63.486	56.286	164.601	-40.568
34	Tensors	0.486	0.287	0.119	0.087	0.136	0.093	0.172	0.231	55.96	127.763	139.624	-157.093	-121.39	20.888	13.206	169.347
	Fixed CI	0.594	0.252	0.18	0.163	0.095	0.108	0.133	0.061	79.585	129.689	150.927	-128.344	-41.283	22.298	111.152	-147.867
35	Tensors	0.52	0.185	0.047	0.101	0.156	0.104	0.142	0.197	67.137	143.852	74.493	172.386	-131.064	16.866	10.606	172.421
	Fixed CI	0.661	0.168	0.098	0.14	0.098	0.107	0.123	0.054	87.876	155.665	118.428	-144.211	-55.707	26.349	123.599	-110.713
36	Tensors	0.944	0.167	0.119	0.204	0.17	0.149	0.104	0.035	93.286	-166.877	69.304	-162.32	-57.262	52.567	147.031	-58.813
	Fixed CI	0.945	0.164	0.118	0.203	0.169	0.148	0.101	0.03	93.597	-166.744	71.12	-161.336	-55.753	53.589	149.675	-56.025
37	Tensors	0.735	0.25	0.122	0.162	0.14	0.139	0.134	0.053	84.383	140.33	139.918	-146.986	-58.911	34.2	120.201	-135.913
	Fixed CI	0.738	0.247	0.125	0.161	0.138	0.138	0.128	0.05	85.063	139.682	141.647	-145.913	-56.645	34.997	122.961	-143.396
38	Tensors	0.942	0.172	0.119	0.205	0.171	0.151	0.109	0.043	92.826	-167.075	66.665	-163.756	-59.442	51.111	143.268	-62.041
	Fixed CI	0.945	0.164	0.118	0.203	0.169	0.148	0.101	0.03	93.597	-166.744	71.12	-161.336	-55.753	53.589	149.675	-56.025
39	Tensors	0.864	0.197	0.129	0.212	0.166	0.147	0.11	0.026	87.468	154.122	118.81	-150.57	-51.532	48.326	125.898	-121.116
	Fixed CI	0.868	0.189	0.134	0.212	0.164	0.145	0.099	0.018	88.441	152.457	122.593	-148.328	-47.45	50.786	132.812	-155.174
40	Tensors	0.941	0.174	0.12	0.205	0.172	0.152	0.111	0.047	92.576	-167.189	65.275	-164.51	-60.601	50.321	141.182	-63.717
	Fixed CI	0.945	0.164	0.118	0.203	0.169	0.148	0.101	0.03	93.597	-166.744	71.12	-161.336	-55.753	53.589	149.675	-56.025
41	Tensors	0.732	0.252	0.12	0.162	0.142	0.139	0.14	0.057	83.774	140.863	138.322	-147.925	-60.854	33.489	117.736	-130.287
	Fixed CI	0.738	0.247	0.125	0.161	0.138	0.138	0.128	0.05	85.063	139.682	141.647	-145.913	-56.645	34.997	122.961	-143.396
42	Tensors	0.872	0.178	0.151	0.181	0.129	0.113	0.097	0.06	96.156	-134.32	52.454	-163.038	-56.987	49.18	148.327	-52.72
	Fixed CI	0.874	0.178	0.15	0.181	0.129	0.112	0.097	0.059	96.456	-134.055	53.398	-161.918	-54.758	51.056	151.741	-49.955
43	Tensors	0.816	0.341	0.16	0.184	0.183	0.168	0.139	0.068	81.982	133.486	152.982	-146.724	-59.131	43.362	116.076	-155.816
	Fixed CI	0.816	0.335	0.165	0.183	0.178	0.171	0.133	0.062	82.787	131.772	155.274	-147.207	-57.162	40.393	122.371	-171.161
44	Tensors	0.733	0.252	0.121	0.163	0.145	0.139	0.14	0.064	83.481	140.455	136.846	-148.153	-62.836	33.566	112.77	-135.032
	Fixed CI	0.738	0.247	0.125	0.161	0.138	0.138	0.128	0.05	85.063	139.682	141.647	-145.913	-56.645	34.997	122.961	-143.396
45	Tensors	0.624	0.466	0.32	0.212	0.144	0.13	0.189	0.126	64.603	118.594	160.731	-122.593	-47.476	28.989	84.278	-167.947
	Fixed CI	0.627	0.458	0.328	0.213	0.134	0.138	0.153	0.106	68.535	116.548	166.027	-120.921	-36.011	28.636	101.082	177.131
46	Tensors	1.023	0.233	0.1	0.223	0.218	0.188	0.118	0.059	89.51	168.775	82.454	-163.553	-63.552	57.436	126.214	-101.618
	Fixed CI	1.018	0.202	0.104	0.225	0.209	0.184	0.105	0.006	91.143	164.76	97.264	-160.869	-56.366	55.138	147.763	-132.946
47	Tensors	0.948	0.294	0.146	0.228	0.212	0.181	0.122	0.062	84.528	144.793	132.586	-150.591	-56.164	56.86	110.444	-139.322
	Fixed CI	0.944	0.27	0.161	0.234	0.204	0.181	0.104	0.039	86.199	138.749	139.928	-149.115	-49.698	52.912	131.587	160.936
48	Tensors	0.668	0.355	0.213	0.183	0.147	0.134	0.17	0.099	73.74	126.677	152.884	-134.955	-58.898	31.079	92.31	-153.406
	Fixed CI	0.675	0.346	0.223	0.183	0.134	0.138	0.138	0.074	77.476	124.608	159.363	-131.653	-46.491	31.817	111.027	-170.469
49	Tensors	0.799	0.194	0.086	0.162	0.168	0.145	0.146	0.081	88.23	168.85	66.381	-168.97	-78.519	34.726	114.579	-102.826
	Fixed CI	0.811	0.183	0.078	0.152	0.147	0.139	0.124	0.048	91.373	169.065	81.116	-163.149	-65.912	38.155	136.251	-98.747
50	Tensors	0.799	0.194	0.086	0.162	0.167	0.145	0.146	0.081	88.221	168.842	66.357	-168.978	-78.546	34.715	114.525	-102.843
	Fixed CI	0.811	0.183	0.078	0.152	0.147	0.139	0.124	0.048	91.373	169.065	81.116	-163.149	-65.912	38.155	136.251	-98.747
51	Tensors	0.797	0.276	0.213	0.23	0.164	0.142	0.105	0.05	82.173	129.859	147.723	-137.245	-39.453	47.828	115.621	168.654
	Fixed CI	0.799	0.276	0.215	0.231	0.163	0.143	0.105	0.05	82.336	129.622	148.106	-136.899	-38.886	47.883	116.619	168.271

Table A.3 City LV Network (Scenario C) - Current Magnitude and Phase Angles for Customers

		Current Magnitudes								Phase Angles							
Harmonic Order		h_3	h_5	h_7	h_9	h_{11}	h_{13}	h_{15}	h_{17}	h_3	h_5	h_7	h_9	h_{11}	h_{13}	h_{15}	h_{17}
ICP																	
1	Tensors	0.296	0.061	0.051	0.061	0.027	0.039	0.062	0.039	91.363	-166.745	86.939	-139.771	-47.953	6.417	121.705	-89.654
	Fixed CI	0.296	0.061	0.051	0.061	0.027	0.039	0.062	0.039	91.363	-166.745	86.939	-139.77	-47.952	6.417	121.705	-89.655
2	Tensors	0.653	0.281	0.201	0.154	0.085	0.076	0.06	0.081	104.806	-92.302	35.301	-168.063	-35.558	94.531	-142.546	-10.502
	Fixed CI	0.659	0.284	0.204	0.157	0.087	0.078	0.061	0.082	104.92	-91.938	35.947	-167.022	-34.431	96.014	-140.911	-8.252
3	Tensors	0.819	0.325	0.251	0.184	0.121	0.111	0.087	0.098	104.825	-97.03	26.485	179.404	-54.179	83.992	-147.449	-11.233
	Fixed CI	0.822	0.326	0.252	0.184	0.122	0.111	0.088	0.096	105.095	-96.312	27.581	-178.866	-52.259	86.317	-144.91	-8.075
4	Tensors	0.581	0.137	0.114	0.127	0.096	0.083	0.053	0.042	98.414	-120.464	38.804	-171.882	-56.065	66.678	174.247	-28.6
	Fixed CI	0.586	0.137	0.116	0.128	0.097	0.082	0.052	0.039	98.916	-118.547	40.952	-169.621	-53.641	68.135	178.788	-21.138
5	Tensors	0.511	0.21	0.16	0.105	0.056	0.048	0.052	0.071	103.594	-99.832	28.689	-177.099	-56.938	67.505	177.635	-36.78
	Fixed CI	0.521	0.213	0.163	0.107	0.057	0.046	0.05	0.067	104.436	-98.143	31.424	-172.318	-49.93	73.33	-175.526	-30.871
6	Tensors	0.649	0.28	0.201	0.154	0.083	0.078	0.059	0.085	104.016	-93.882	32.85	-171.942	-40.672	89.651	-149.479	-16.635
	Fixed CI	0.659	0.284	0.204	0.157	0.087	0.078	0.061	0.082	104.92	-91.938	35.947	-167.022	-34.431	96.014	-140.911	-8.252
7	Tensors	0.589	0.145	0.119	0.128	0.092	0.081	0.058	0.051	98.067	-119.835	39.948	-170.75	-56.752	61.116	167.343	-35.13
	Fixed CI	0.593	0.142	0.119	0.128	0.091	0.078	0.054	0.043	98.87	-117.006	43.581	-166.877	-52.45	65.278	173.667	-25.559
8	Tensors	0.647	0.28	0.201	0.154	0.083	0.078	0.059	0.087	103.679	-94.546	31.802	-173.605	-42.922	87.561	-152.415	-19.134
	Fixed CI	0.659	0.284	0.204	0.157	0.087	0.078	0.061	0.082	104.92	-91.938	35.947	-167.022	-34.431	96.014	-140.911	-8.252
9	Tensors	0.647	0.279	0.201	0.154	0.082	0.078	0.059	0.088	103.525	-94.847	31.319	-174.373	-43.983	86.588	-153.781	-20.278
	Fixed CI	0.659	0.284	0.204	0.157	0.087	0.078	0.061	0.082	104.92	-91.938	35.947	-167.022	-34.431	96.014	-140.911	-8.252
10	Tensors	0.506	0.209	0.16	0.106	0.057	0.051	0.055	0.077	102.615	-101.55	25.947	178.114	-64.019	62.472	171.788	-41.358
	Fixed CI	0.521	0.213	0.163	0.107	0.057	0.046	0.05	0.067	104.436	-98.143	31.424	-172.318	-49.93	73.33	-175.526	-30.871
11	Tensors	0.715	0.2	0.156	0.176	0.122	0.113	0.057	0.064	99.124	-107.697	38.664	-171.808	-48.583	79.793	-159.325	-10.567
	Fixed CI	0.724	0.198	0.159	0.179	0.125	0.109	0.06	0.061	100.409	-103.123	44.256	-165.729	-42.095	85.251	-145.625	8.03
12	Tensors	0.806	0.319	0.251	0.19	0.129	0.122	0.087	0.103	103.888	-99.706	21.562	172.209	-60.951	80.408	-152.207	-17.873
	Fixed CI	0.816	0.32	0.25	0.185	0.127	0.116	0.089	0.093	105.178	-96.595	26.191	179.281	-53.175	87.496	-141.485	-5.577
13	Tensors	0.714	0.2	0.156	0.176	0.122	0.114	0.056	0.065	98.941	-108.3	37.88	-172.667	-49.554	79.007	-161.426	-13.079
	Fixed CI	0.724	0.198	0.159	0.179	0.125	0.109	0.06	0.061	100.409	-103.123	44.256	-165.729	-42.095	85.251	-145.625	8.03
14	Tensors	0.587	0.148	0.118	0.128	0.093	0.084	0.062	0.057	97.418	-121.86	37.016	-173.854	-60.372	57.767	162.415	-41.399
	Fixed CI	0.593	0.142	0.119	0.128	0.091	0.078	0.054	0.043	98.87	-117.006	43.581	-166.877	-52.45	65.278	173.667	-25.559
15	Tensors	0.587	0.148	0.118	0.128	0.093	0.084	0.062	0.058	97.346	-122.082	36.696	-174.185	-60.776	57.366	161.748	-42.197
	Fixed CI	0.593	0.142	0.119	0.128	0.091	0.078	0.054	0.043	98.87	-117.006	43.581	-166.877	-52.45	65.278	173.667	-25.559
16	Tensors	0.587	0.148	0.118	0.128	0.093	0.085	0.062	0.058	97.278	-122.292	36.392	-174.498	-61.155	56.997	161.133	-42.934
	Fixed CI	0.593	0.142	0.119	0.128	0.091	0.078	0.054	0.043	98.87	-117.006	43.581	-166.877	-52.45	65.278	173.667	-25.559
17	Tensors	0.574	0.141	0.113	0.126	0.097	0.088	0.057	0.053	96.875	-125.12	32.49	-178.31	-63.055	63.09	162.727	-43.603
	Fixed CI	0.586	0.137	0.116	0.128	0.097	0.082	0.052	0.039	98.916	-118.547	40.952	-169.621	-53.641	68.135	178.788	-21.138
18	Tensors	0.639	0.277	0.199	0.152	0.079	0.078	0.056	0.091	102.509	-96.786	28.084	-179.495	-51.357	79.851	-163.7	-28.412
	Fixed CI	0.659	0.284	0.204	0.157	0.087	0.078	0.061	0.082	104.92	-91.938	35.947	-167.022	-34.431	96.014	-140.911	-8.252
19	Tensors	0.888	0.255	0.208	0.212	0.166	0.153	0.086	0.088	100.335	-111.266	26.496	177.249	-59.912	73.286	-161.232	-14.896
	Fixed CI	0.886	0.244	0.203	0.204	0.162	0.144	0.086	0.075	101.401	-106.959	32.097	-176.497	-53.913	80.284	-148.258	5.193
20	Tensors	0.411	0.095	0.074	0.097	0.048	0.046	0.049	0.047	92.462	-126.606	62.43	-157.967	-44.148	50.46	129.168	-65.5
	Fixed CI	0.431	0.094	0.091	0.112	0.059	0.041	0.035	0.03	96.249	-114.025	71.367	-147.124	-25.627	65.392	149.602	-34.339
21	Tensors	0.497	0.206	0.157	0.105	0.056	0.053	0.058	0.082	101.312	-103.728	22.159	171.749	-74.261	55.181	162.512	-48.631
	Fixed CI	0.521	0.213	0.163	0.107	0.057	0.046	0.05	0.067	104.436	-98.143	31.424	-172.318	-49.93	73.33	-175.526	-30.871
22	Tensors	0.801	0.318	0.251	0.191	0.128	0.123	0.084	0.106	103.265	-101.108	19.304	168.928	-64.87	76.911	-158.055	-24.175
	Fixed CI	0.816	0.32	0.25	0.185	0.127	0.116	0.089	0.093	105.178	-96.595	26.191	179.281	-53.175	87.496	-141.485	-5.577
23	Tensors	0.496	0.206	0.157	0.104	0.056	0.054	0.058	0.083	101.17	-103.965	21.719	171.042	-75.484	54.31	161.345	-49.559
	Fixed CI	0.521	0.213	0.163	0.107	0.057	0.046	0.05	0.067	104.436	-98.143	31.424	-172.318	-49.93	73.33	-175.526	-30.871
24	Tensors	0.571	0.142	0.111	0.125	0.096	0.089	0.058	0.055	96.461	-126.389	30.749	-179.978	-65.01	61.908	158.756	-48.199
	Fixed CI	0.586	0.137	0.116	0.128	0.097	0.082	0.052	0.039	98.916	-118.547	40.952	-169.621	-53.641	68.135	178.788	-21.138
25	Tensors	0.495	0.205	0.157	0.104	0.056	0.054	0.058	0.083	101.051	-104.151	21.36	170.451	-76.532	53.568	160.359	-50.328
	Fixed CI	0.521	0.213	0.163	0.107	0.057	0.046	0.05	0.067	104.436	-98.143	31.424	-172.318	-49.93	73.33	-175.526	-30.871

Continued on next page

Table A.3 (continued) City LV Network (Scenario C) - Current Magnitude and Phase Angles for Customers

		Current Magnitudes								Phase Angles							
Harmonic Order		h_3	h_5	h_7	h_9	h_{11}	h_{13}	h_{15}	h_{17}	h_3	h_5	h_7	h_9	h_{11}	h_{13}	h_{15}	h_{17}
ICP																	
26	Tensors	0.57	0.142	0.111	0.125	0.096	0.089	0.058	0.056	96.379	-126.628	30.414	179.691	-65.417	61.676	158.011	-49.04
	Fixed CI	0.586	0.137	0.116	0.128	0.097	0.082	0.052	0.039	98.916	-118.547	40.952	-169.621	-53.641	68.135	178.788	-21.138
27	Tensors	0.8	0.318	0.251	0.191	0.127	0.123	0.083	0.106	103.094	-101.475	18.669	168.011	-66.026	75.903	-159.758	-25.969
	Fixed CI	0.816	0.32	0.25	0.185	0.127	0.116	0.089	0.093	105.178	-96.595	26.191	179.281	-53.175	87.496	-141.485	-5.577
28	Tensors	0.273	0.072	0.032	0.045	0.025	0.045	0.078	0.061	84.791	-179.825	82.865	-153.051	-90.66	2.737	113.441	-96.259
	Fixed CI	0.296	0.061	0.051	0.061	0.027	0.039	0.062	0.039	91.363	-166.745	86.939	-139.77	-47.952	6.417	121.705	-89.655
29	Tensors	0.408	0.094	0.071	0.093	0.045	0.046	0.051	0.049	91.81	-128.682	61.045	-159.719	-47.77	47.579	125.334	-70.348
	Fixed CI	0.431	0.094	0.091	0.112	0.059	0.041	0.035	0.03	96.249	-114.025	71.367	-147.124	-25.627	65.392	149.602	-34.339
30	Tensors	0.569	0.142	0.11	0.124	0.095	0.089	0.059	0.057	96.255	-126.989	29.893	179.168	-66.049	61.353	157.125	-50.042
	Fixed CI	0.586	0.137	0.116	0.128	0.097	0.082	0.052	0.039	98.916	-118.547	40.952	-169.621	-53.641	68.135	178.788	-21.138
31	Tensors	0.493	0.204	0.156	0.104	0.056	0.054	0.059	0.084	100.786	-104.584	20.564	169.126	-78.753	52.212	158.874	-51.517
	Fixed CI	0.521	0.213	0.163	0.107	0.057	0.046	0.05	0.067	104.436	-98.143	31.424	-172.318	-49.93	73.33	-175.526	-30.871
32	Tensors	0.889	0.256	0.209	0.212	0.166	0.154	0.085	0.09	100.075	-112.228	25.106	175.719	-61.537	71.495	-164.748	-19.578
	Fixed CI	0.886	0.244	0.203	0.204	0.162	0.144	0.086	0.075	101.401	-106.959	32.097	-176.497	-53.913	80.284	-148.258	5.193
33	Tensors	0.584	0.15	0.117	0.127	0.093	0.086	0.065	0.064	96.656	-124.195	33.554	-177.392	-64.778	53.639	155.865	-49.141
	Fixed CI	0.593	0.142	0.119	0.128	0.091	0.078	0.054	0.043	98.87	-117.006	43.581	-166.877	-52.45	65.278	173.667	-25.559
34	Tensors	0.815	0.328	0.255	0.192	0.124	0.117	0.087	0.114	103.166	-101.131	20.213	169.864	-65.722	70.291	-163.877	-27.626
	Fixed CI	0.822	0.326	0.252	0.184	0.122	0.111	0.088	0.096	105.095	-96.312	27.581	-178.866	-52.259	86.317	-144.91	-8.075
35	Tensors	0.815	0.328	0.255	0.193	0.124	0.117	0.087	0.115	103.161	-101.144	20.195	169.838	-65.752	70.264	-163.894	-27.631
	Fixed CI	0.822	0.326	0.252	0.184	0.122	0.111	0.088	0.096	105.095	-96.312	27.581	-178.866	-52.259	86.317	-144.91	-8.075
36	Tensors	0.296	0.061	0.051	0.061	0.027	0.039	0.062	0.04	91.198	-167.04	86.517	-140.268	-48.82	6.463	121.585	-89.501
	Fixed CI	0.296	0.061	0.051	0.061	0.027	0.039	0.062	0.039	91.363	-166.745	86.939	-139.77	-47.952	6.417	121.705	-89.655
37	Tensors	0.52	0.213	0.163	0.107	0.058	0.047	0.051	0.068	104.26	-98.499	30.923	-173.206	-50.992	72.57	-176.668	-31.777
	Fixed CI	0.521	0.213	0.163	0.107	0.057	0.046	0.05	0.067	104.436	-98.143	31.424	-172.318	-49.93	73.33	-175.526	-30.871
38	Tensors	0.52	0.213	0.164	0.108	0.058	0.047	0.051	0.069	104.193	-98.638	30.732	-173.559	-51.417	72.284	-177.017	-32.05
	Fixed CI	0.521	0.213	0.163	0.107	0.057	0.046	0.05	0.067	104.436	-98.143	31.424	-172.318	-49.93	73.33	-175.526	-30.871
39	Tensors	0.723	0.199	0.16	0.179	0.125	0.11	0.06	0.062	100.221	-103.814	43.432	-166.574	-42.861	84.733	-147.461	5.273
	Fixed CI	0.724	0.198	0.159	0.179	0.125	0.109	0.06	0.061	100.409	-103.123	44.256	-165.729	-42.095	85.251	-145.625	8.03
40	Tensors	0.658	0.284	0.205	0.158	0.088	0.079	0.062	0.085	104.644	-92.531	35.089	-168.413	-36.065	94.555	-143.262	-10.39
	Fixed CI	0.659	0.284	0.204	0.157	0.087	0.078	0.061	0.082	104.92	-91.938	35.947	-167.022	-34.431	96.014	-140.911	-8.252
41	Tensors	0.429	0.095	0.09	0.111	0.059	0.042	0.037	0.032	95.825	-115.502	69.98	-148.56	-27.548	64.426	147.96	-37.769
	Fixed CI	0.431	0.094	0.091	0.112	0.059	0.041	0.035	0.03	96.249	-114.025	71.367	-147.124	-25.627	65.392	149.602	-34.339
42	Tensors	0.52	0.213	0.163	0.107	0.057	0.046	0.051	0.067	104.355	-98.298	31.192	-172.737	-50.497	72.902	-176.1	-31.314
	Fixed CI	0.521	0.213	0.163	0.107	0.057	0.046	0.05	0.067	104.436	-98.143	31.424	-172.318	-49.93	73.33	-175.526	-30.871
43	Tensors	0.43	0.095	0.09	0.111	0.059	0.043	0.037	0.033	95.701	-115.736	69.497	-149.015	-28.423	63.758	147.432	-38.48
	Fixed CI	0.431	0.094	0.091	0.112	0.059	0.041	0.035	0.03	96.249	-114.025	71.367	-147.124	-25.627	65.392	149.602	-34.339
44	Tensors	0.824	0.328	0.255	0.187	0.124	0.114	0.09	0.102	104.869	-96.956	26.796	179.848	-53.617	84.487	-147.211	-10.118
	Fixed CI	0.822	0.326	0.252	0.184	0.122	0.111	0.088	0.096	105.095	-96.312	27.581	-178.866	-52.259	86.317	-144.91	-8.075
45	Tensors	0.658	0.285	0.208	0.16	0.089	0.081	0.062	0.09	104.075	-93.613	33.459	-171.129	-39.946	91.144	-148.76	-14.528
	Fixed CI	0.659	0.284	0.204	0.157	0.087	0.078	0.061	0.082	104.92	-91.938	35.947	-167.022	-34.431	96.014	-140.911	-8.252
46	Tensors	0.586	0.141	0.119	0.131	0.1	0.085	0.056	0.046	98.219	-120.673	37.984	-172.66	-56.513	67.007	173.848	-28.111
	Fixed CI	0.586	0.137	0.116	0.128	0.097	0.082	0.052	0.039	98.916	-118.547	40.952	-169.621	-53.641	68.135	178.788	-21.138
47	Tensors	0.429	0.097	0.089	0.111	0.058	0.044	0.041	0.038	95.009	-117.795	67.145	-151.422	-32.045	61.622	144.444	-43.143
	Fixed CI	0.431	0.094	0.091	0.112	0.059	0.041	0.035	0.03	96.249	-114.025	71.367	-147.124	-25.627	65.392	149.602	-34.339
48	Tensors	0.586	0.141	0.119	0.131	0.1	0.085	0.056	0.046	98.21	-120.706	37.942	-172.702	-56.56	66.981	173.75	-28.254
	Fixed CI	0.586	0.137	0.116	0.128	0.097	0.082	0.052	0.039	98.916	-118.547	40.952	-169.621	-53.641	68.135	178.788	-21.138
49	Tensors	0.519	0.214	0.166	0.111	0.06	0.05	0.055	0.075	103.404	-100.012	28.71	-177.364	-56.811	68.483	178.023	-35.316
	Fixed CI	0.521	0.213	0.163	0.107	0.057	0.046	0.05	0.067	104.436	-98.143	31.424	-172.318	-49.93	73.33	-175.526	-30.871
50	Tensors	0.585	0.141	0.119	0.131	0.1	0.085	0.056	0.046	98.205	-120.721	37.924	-172.721	-56.582	66.968	173.705	-28.317
	Fixed CI	0.586	0.137	0.116	0.128	0.097	0.082	0.052	0.039	98.916	-118.547	40.952	-169.621	-53.641	68.135	178.788	-21.138
51	Tensors	0.586	0.137	0.116	0.128	0.097	0.082	0.052	0.039	98.881	-118.655	40.804	-169.781	-53.84	68.029	178.482	-21.572
	Fixed CI	0.586	0.137	0.116	0.128	0.097	0.082	0.052	0.039	98.916	-118.547	40.952	-169.621	-53.641	68.135	178.788	-21.138

Appendix B

ADMITTANCES LOCI OF 3^{RD} TO 17^{TH} HARMONICS

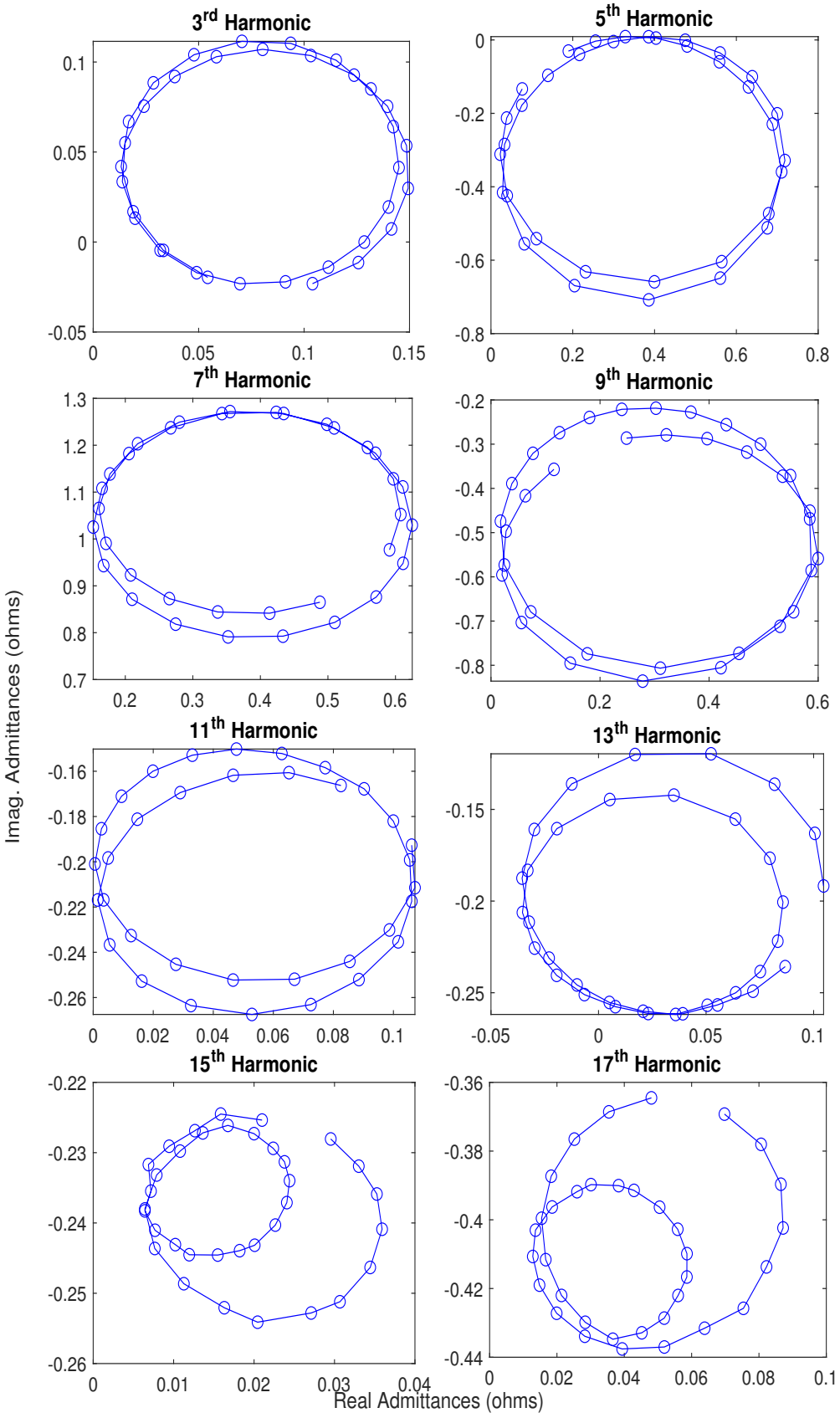
3rd Harmonic
5th Harmonic
7th Harmonic
9th Harmonic
11th Harmonic
13th Harmonic
15th Harmonic
17th Harmonic
Imag. Admittances (ohms)
Real Admittances (ohms)

Appendix C

LIST OF PUBLICATIONS

The following journal papers are prepared and in the process of submission.

Paper 01: Comparison of Assessment Methods for Tensors of Non-Linear Devices

Paper 02: Aggregation of Tensors for Harmonic Analysis of Distribution System

REFERENCES

61000.2.2, A. (2003), 'Electromagnetic compatibility (emc) - part 2.2: Environment—compatibility levels for low-frequency conducted disturbances and signalling in public low-voltage power supply systems', .

Acha, E. and Madrigal, M. (2001), *Power System Harmonics: computer modelling and analysis*, John Wiley.

Ahmed, N.A., Miyatake, M. and Al-Othman, A. (2008), 'Power fluctuations suppression of stand-alone hybrid generation combining solar photovoltaic/wind turbine and fuel cell systems', *Energy Conversion and Management*, Vol. 49, No. 10, pp. 2711–2719.

Aprille, T. and Trick, T. (1972), 'A computer algorithm to determine the steady-state response of nonlinear oscillators', *IEEE Transactions on Circuit Theory*, Vol. 19, No. 4, pp. 354–360.

Arrillaga, J. and Callaghan, C. (1989), 'Double-iterative algorithm for the analysis of power and harmonic flows at ac/dc convertor terminals', In *IEE Proceedings C (Generation, Transmission and Distribution)*, Vol. 136, IET, pp. 319–324.

Arrillaga, J. and Watson, N.R. (2004), *Power system harmonics*, John Wiley & Sons.

Arrillaga, J., Medina, A., Lisboa, M., Cavia, M. and Sanchez, P. (1995), 'The harmonic domain. a frame of reference for power system harmonic analysis', *IEEE Transactions on Power Systems*, Vol. 10, No. 1, pp. 433–440.

Arrillaga, J., Smith, B.C., Watson, N.R. and Wood, A.R. (1997), *Power system harmonic analysis*, John Wiley & Sons.

Arrillaga, J., Watson, N.R. and Bathurst, G.N. (2004), 'A multifrequency power flow of general applicability', *IEEE transactions on power delivery*, Vol. 19, No. 1, pp. 342–349.

BaSudan, O. and Hegazy, Y.G. (2001), 'Probabilistic modeling of distribution system loads for harmonic studies', In *Power Engineering Society Summer Meeting. Conference Proceedings (Cat. No. 01CH37262)*, Vol. 3, IEEE, pp. 1778–1781.

Bathurst, G.N., Smith, B.C., Watson, N.R. and Arillaga, J. (1998), 'A modular approach to the solution of the three-phase harmonic power-flow', In *8th*

International Conference on Harmonics and Quality of Power. Proceedings (Cat. No.98EX227), Vol. 2, pp. 653–659 vol.2.

Bathurst, G.N., Smith, B.C., Watson, N.R. and Arrillaga, J. (1999), 'Modelling of hvdc transmission systems in the harmonic domain', *IEEE Transactions on Power Delivery*, Vol. 14, No. 3, pp. 1075–1080.

Bathurst, G.N. (1999), *A Newton solution for the harmonic analysis of power systems with multiple non-linear devices*, Phd thesis, Department of Electrical and Computer Engineering, University of Canterbury, Christchurch, New Zealand.

Browne, N., Perera, S. and Ribeiro, P. (2007), 'Harmonic levels and television events', In *2007 IEEE Power Engineering Society General Meeting*, IEEE, pp. 1–6.

Carbone, R., Fantauzzi, M., Gagliardi, F. and Testa, A. (1993), 'Some considerations on the iterative harmonic analysis convergence', *IEEE transactions on power delivery*, Vol. 8, No. 2, pp. 487–493.

Chang, G., Chu, S. and Wang, H. (2007), 'An improved backward/forward sweep load flow algorithm for radial distribution systems', *IEEE Transactions on power systems*, Vol. 22, No. 2, pp. 882–884.

Collins, C.D. (2006), *FACTS device modelling in the harmonic domain*, Phd thesis, Department of Electrical and Computer Engineering, University of Canterbury, Christchurch, New Zealand.

Das, J. (2002), *Power system analysis: short-circuit load flow and harmonics*, Vol. 1, CRC press.

Densem, T. (1983), *Three phase power system harmonic penetration*, Phd thesis, Department of Electrical and Computer Engineering, University of Canterbury, Christchurch, New Zealand.

Densem, T., Bodger, P. and Arrillaga, J. (1984), 'Three phase transmisssion system modelling for harmonic penetration studies', *IEEE transactions on power apparatus and systems*, , No. 2, pp. 310–317.

Diao, L., Sun, Y., Chen, Z. and Chen, J. (2017), 'Modeling energy consumption in residential buildings: A bottom-up analysis based on occupant behavior pattern clustering and stochastic simulation', *Energy and Buildings*, Vol. 147, pp. 47–66.

Dommel, H.W. (1986), *Electromagnetic transients program reference manual: (EMTP) theory*, Boneville Power Administration.

Dommel, H.W. (1969), 'Digital computer solution of electromagnetic transients in single-and multiphase networks', *IEEE transactions on power apparatus and systems*, , No. 4, pp. 388–399.

Doroshin, A. and Neri, F. (2014), 'Open research issues on nonlinear dynamics, dynamical systems and processes', *WSEAS Transactions on Systems*, Vol. 13, pp. 644–647.

Elphick, S.T. (2011), *The modern domestic load and its impact on the electricity distribution network*, Master of engineering thesis, School of Electrical, Computer and Telecommunication, University of Wollongong, Wollongong, Australia.

European Commission (2010), 'Directive 2010/31/eu on the energy performance of buildings', *Off. J. Eur. Union*.

Fauri, M. (1997), 'Harmonic modelling of non-linear load by means of crossed frequency admittance matrix', *IEEE transactions on Power systems*, Vol. 12, No. 4, pp. 1632–1638.

Foteinaki, K., Li, R., Rode, C. and Andersen, R.K. (2019), 'Modelling household electricity load profiles based on danish time-use survey data', *Energy and Buildings*, Vol. 202, p. 109355.

Frater, L.P. (2015), *Light flicker and harmonic modelling of electrical lighting*, Phd thesis, Department of Electrical and Computer Engineering, University of Canterbury, Christchurch, New Zealand.

Gallo, D., Landi, C., Langella, R., Luiso, M., Testa, A. and Watson, N. (2017), 'On the measurement of power electronic devices' frequency coupling admittance', In *2017 IEEE International Workshop on Applied Measurements for Power Systems (AMPS)*, IEEE, pp. 1–6.

Gallo, D., Langella, R., Luiso, M., Testa, A. and Watson, N.R. (2018), 'A new test procedure to measure power electronic devices' frequency coupling admittance', *IEEE Transactions on Instrumentation and Measurement*, Vol. 67, No. 10, pp. 2401–2409.

Grady, W.M. and Santoso, S. (2001), 'Understanding power system hannonics', *IEEE Power Engineering Review*, Vol. 21, No. 11, pp. 8–11.

Hardie, S. and Watson, N. (2010), 'The effect of new residential appliances on power quality', In *2010 20th Australasian Universities Power Engineering Conference*, IEEE, pp. 1–6.

Hume, D.J., Wood, A.R., Smith, B.C. and Arrillaga, J. (1998), 'Linearised direct harmonic solution method for a back-to-back hvdc link', In *8th International Conference on Harmonics and Quality of Power. Proceedings (Cat. No.98EX227)*, Vol. 2, pp. 727–733 vol.2.

Hume, D.J. (2002), *Harmonic and interharmonic cross modulation in HVDC links*, Phd thesis, Department of Electrical and Computer Engineering, University of Canterbury, Christchurch, New Zealand.

Kazibwe, W.E., Ringlee, R.J., Woodzell, G.W. and Sendaula, H.M. (1990), 'Power quality: a review', *IEEE Computer Applications in Power*, Vol. 3, No. 1, pp. 39–42.

Langella, R., Testa, A., Caicedo, J.E., Romero, A.A., Zini, H.C., Meyer, J. and Watson, N.R. (2018), 'On the use of fourier descriptors for the assessment of

frequency coupling matrices of power electronic devices', In *2018 18th International Conference on Harmonics and Quality of Power (ICHQP)*, IEEE, pp. 1–6.

Larsen, E., Baker, D. and McIver, J. (1989), 'Low-order harmonic interactions on ac/dc systems', *IEEE Transactions on Power Delivery*, Vol. 4, No. 1, pp. 493–501.

Leitão, J., Fonseca, L., Lira, M., Soares, L. and Ribeiro, P. (2007), 'Harmonic distortion on a transmission system during games of the brazilian national team in the 2006 world cup', In *2007 IEEE Power Engineering Society General Meeting*, IEEE, pp. 1–2.

Lins, C., Williamson, L.E., Leitner, S. and Teske, S. (2014), 'The first decade: 2004—2014: 10 years of renewable energy progress', *Renewable Energy Policy Network for the 21st Century.*

Liu, E. and Cheng, P. (2017), 'Achieving privacy protection using distributed load scheduling: A randomized approach', *IEEE Transactions on Smart Grid*, Vol. 8, No. 5, pp. 2460–2473.

Medina, A., Segundo-Ramirez, J., Ribeiro, P., Xu, W., Lian, K., Chang, G., Dinavahi, V. and Watson, N. (2013), 'Harmonic analysis in frequency and time domain', *IEEE Transactions on Power Delivery*, Vol. 28, No. 3, pp. 1813–1821.

Nguyen, H.L. (1997), 'Newton-raphson method in complex form [power system load flow analysis]', *IEEE Transactions on Power Systems*, Vol. 12, No. 3, pp. 1355–1359.

Rawa, M.J.H., Thomas, D.W.P. and Sumner, M. (2011), 'Simulation of non-linear loads for harmonic studies', In *11th International Conference on Electrical Power Quality and Utilisation*, pp. 1–6.

Reeve, J. and Baron, J. (1971), 'Harmonic interaction between hvdc converters and ac power systems', *IEEE Transactions on Power Apparatus and Systems*, , No. 6, pp. 2785–2793.

Richardson, I., Thomson, M., Infield, D. and Clifford, C. (2010), 'Domestic electricity use: A high-resolution energy demand model', *Energy and buildings*, Vol. 42, No. 10, pp. 1878–1887.

Samal, P. and Ganguly, S. (2015), 'A modified forward backward sweep load flow algorithm for unbalanced radial distribution systems', In *2015 IEEE Power & Energy Society General Meeting*, IEEE, pp. 1–5.

Semlyen, A. and Iravani, M. (1993), 'Frequency domain modeling of external systems in an electro-magnetic transients program', *IEEE transactions on power systems*, Vol. 8, No. 2, pp. 527–533.

Semlyen, A. and Medina, A. (1995), 'Computation of the periodic steady state in systems with nonlinear components using a hybrid time and frequency domain methodology', *IEEE Transactions on Power Systems*, Vol. 10, No. 3, pp. 1498–1504.

Sharifian, M.B., Ali-Abbasi, K.B. and PourAzar, S. (2005), 'Study and testing of large non-linear loads effects on the distribution networks', In *UCTEA The Chamber of Electrical Engineers*, Kizilay, Ankara.

Smith, B.C. and Arrillaga, J. (1999), 'Power flow constrained harmonic analysis in ac-dc power systems', *IEEE Transactions on Power Systems*, Vol. 14, No. 4, pp. 1251–1261.

Smith, B.C., Watson, N.R., Wood, A.R. and Arrillaga, J. (1996), 'A newton solution for the harmonic phasor analysis of ac/dc converters', *IEEE Transactions on Power Delivery*, Vol. 11, No. 2, pp. 965–971.

Smith, B.C., Watson, N.R., Wood, A.R. and Arrillaga, J. (1997), 'A sequence components model of the ac/dc converter in the harmonic domain', *IEEE Transactions on Power Delivery*, Vol. 12, No. 4, pp. 1736–1743.

Smith, B.C., Arrillaga, J., Wood, A.R. and Watson, N.R. (1998a), 'A review of iterative harmonic analysis for ac-dc power systems', *IEEE Transactions on Power Delivery*, Vol. 13, No. 1, pp. 180–185.

Smith, B., Watson, N., Wood, A. and Arrillaga, J. (1998b), 'Harmonic tensor linearisation of hvdc converters', *IEEE transactions on power delivery*, Vol. 13, No. 4, pp. 1244–1250.

Smith, B.C. (1996), *A harmonic domain model for the interaction of the HVdc convertor with ac and dc systems*, Phd thesis, Department of Electrical and Computer Engineering, University of Canterbury, Christchurch, New Zealand.

Sun, Y., Zhang, G., Xu, W. and Mayordomo, J.G. (2007), 'A harmonically coupled admittance matrix model for ac/dc converters', *IEEE Transactions on Power Systems*, Vol. 22, No. 4, pp. 1574–1582.

Tolbert, L., King, T., Ozpineci, B., Campbell, J., Muralidharan, G., Rizy, D., Sabau, A., Zhang, H., Zhang, W. and Xu, Y. (2005), 'Power electronics for distributed energy systems and transmission and distribution applications', *ORNL/TM-2005/230, UT-Battelle, LLC, Oak Ridge National Laboratory*, Vol. 8.

Walker, C.F. and Pokoski, J.L. (1985), 'Residential load shape modelling based on customer behavior', *IEEE Transactions on Power Apparatus and Systems*, , No. 7, pp. 1703–1711.

Watson, J.D., Watson, N.R., Santos-Martin, D., Lemon, S., Wood, A. and Miller, A. (2014), 'Low voltage network modelling', In *EEA Conference & Exhibition 2014*, pp. 1–15.

Watson, J.D., Watson, N.R., Santos-Martin, D., Wood, A.R., Lemon, S. and Miller, A.J. (2016), 'Impact of solar photovoltaics on the low-voltage distribution network in new zealand', *IET Generation, Transmission & Distribution*, Vol. 10, No. 1, pp. 1–9.

Watson, N.R., Scott, T.L. and Hirsch, S.J.J. (2009a), 'Implications for distribution networks of high penetration of compact fluorescent lamps', *IEEE Transactions on Power Delivery*, Vol. 24, No. 3, pp. 1521–1528.

Watson, N., Arrillaga, J. and Arrillaga, J. (2018), *Power systems electromagnetic transients simulation, 2nd ed.*, IET.

Watson, N.R. (2010), 'Power quality state estimation', *European transactions on electrical power*, Vol. 20, No. 1, pp. 19–33.

Watson, N.R., Scott, T.L. and Hirsch, S.J. (2009b), 'Implications for distribution networks of high penetration of compact fluorescent lamps', *IEEE transactions on power delivery*, Vol. 24, No. 3, pp. 1521–1528.

Wei, Z., Watson, N. and Frater, L. (2008), 'Modelling of compact fluorescent lamps', In *2008 13th International Conference on Harmonics and Quality of Power*, IEEE, pp. 1–6.

Wei, Z.J. (2009), *Compact Fluorescent Lamps phase dependency modelling and harmonic assessment of their widespread use in distribution systems*, Master of engineering thesis, Department of Electrical and Computer Engineering, University of Canterbury, Christchurch, New Zealand.

Wood, A.R. (1993), *An analysis of non-ideal HVDC convertor behaviour in the frequency domain, and a new control proposal.*, Phd thesis, Department of Electrical and Computer Engineering, University of Canterbury, Christchurch, New Zealand.

Woodford, D., Gole, A. and Menzies, R. (1983), 'Digital simulation of dc links and ac machines', *IEEE Transactions on Power Apparatus and Systems*, , No. 6, pp. 1616–1623.

Xu, W., Marti, J.R. and Dommel, H.W. (1991), 'A multiphase harmonic load flow solution technique', *IEEE Transactions on Power systems*, Vol. 6, No. 1, pp. 174–182.

Zahn, C.T. and Roskies, R.Z. (1972), 'Fourier descriptors for plane closed curves', *IEEE Transactions on computers*, Vol. 100, No. 3, pp. 269–281.

Zimmer, V., Tenfen, D., Decker, I.C. and Lemos, F.A.B. (2013), 'Three-phase newton raphson power flow considering microgeneration', In *2013 IEEE PES Conference on Innovative Smart Grid Technologies (ISGT Latin America)*, pp. 1–7.